An improved liquid ^{3}helium/ ^{4}helium diode heat switch

by Kenneth Joel Katz

A thesis submitted in partial fulfillment of the requirements for the degree of

Master of Science (Mechanical Engineering)

at the

University of Wisconsin – Madison 2019

Abstract

The heat switch is an essential part of an adiabatic demagnetization refrigerator (ADR). During the ADR refrigeration cycle a paramagnetic salt pill must be repeatedly thermally joined to and disconnected from a heat sink. ADRs are used in space-based research instruments that require subkelvin cooling and so passive heat switches with no moving parts are desirable. The passive gas gap heat switch (PGGHS) is now used successfully, but is complex in design and construction. Below the lambda point ^{4}He has ultra-high thermal conductivity, while ^{3}He does not. A passive heat diode using a weak solution of ^{3}He in ^{4}He was successfully used in the 1950s. In a thin capillary between large and small end volumes normal fluid ^{4}He sweeps ^{3}He in the direction of thermal flow ('heat flush'). In the heat diode's ON state all ^{3}He is swept out of the capillary into a larger end volume; the column is highly conductive. In the diode's OFF state ^{3}He is swept into the capillary, cannot all enter the small volume, and forms a thermally insulating plug in the capillary – the column is up to 10,000 times less conductive. The effect fails when the diode's end temperatures differ by more than $\Delta T = 1.3$ K. Following the 'two-fluid' model of superfluid helium by which normal ^{4}He moves with heat flow, superfluid ^{4}He flows the opposite way , the reason for this failure appears to be that with increasing ΔT at some point the normal/superfluid counter-flow exceeds the 'critical velocity'. Quantum vortices form and cause the ^{3}He to diffuse through the capillary in the OFF state, destroying the 'insulating plug.' Addition of a second capillary that is a superleak (only admits superfluid) between the diode's end volumes is expected to cause ^{4}He to circulate such that the critical velocity is never reached. The diode should then function without interruption with increasing ΔT . A simple, passive, easy to fabricate heat switch would be added to the ensemble of available tools for ADR refrigeration.

ACKNOWLEDGEMENTS

Thanks to my advisor, Prof. Franklin K. Miller, for introducing me to the study of thermodynamics and heat transfer, and for his lectures on statistical thermal physics. He is a teacher who is always crystal clear, and keen that his subject be understood. I thank him also for posing to me the problem addressed in this thesis. It is an absorbing problem that has required patient and detailed work in thermodynamics and heat transfer, computer programming and instrumentation, machining and brazing, pumps, oils, powders, metals, dealing with manufacturers and suppliers. When brought to conclusion it should illuminate a corner of physics and engineering, and maybe add a useful tool to low temperature engineering. Franklin provided expert assistance and personal instruction on all of these topics, often with an instructive story from his work at NASA or in cryogenics in general. I could not have asked for a better project with which to learn.

I also thank Prof. John Pfotenhauer for introducing me to the subject of cryogenics and teaching me thermodynamics. His teaching is also of exemplary clarity and thoroughness. Two particular things he taught I keep in mind. The first is an interest in how what we know was discovered; the patience and exactness shown by the great men in this field to build up what we know, what we can try to demonstrate, the wrong turns and wrong theories required to find the right ones. The second is the quiet awe at the thought that cryogenics allows a person to approach very closely to one of the mysterious limits of nature, where the Kelvin scale ends, and do it right here in Madison. I thank John also for giving me the opportunity to work in China, something which I hope I can continue.

I thank Prof. Greg Nellis for teaching me heat transfer, and for his textbooks, which are good friends and guides. He is also a teacher of great clarity in a subject full of intricacies. Among many things his course was an education in thinking carefully about which terms can be overlooked, which must be included. He was also lucid on the very interesting concept of boundary layers, a profound subject.

Prof. Matt Hitchman, in the Department of Atmospheric and Oceanic Sciences, enlarged my understanding of fluid dynamics teaching the fluid dynamics of earth's atmosphere. His homework assignment about looking for von Karman vortices in the plumes from a small smoke bomb memorably clarified some book problems.

You have all been the best teachers one can imagine. Also, from time to time one of you would make a remark, or in Franklin's case use a technique in the lab to resolve a problem, that alerted me that what I heard in class showed you all working at perhaps ten percent of your actual capacities. I thank you again for your enormous patience teaching at my level. It has been a privilege to be your student. I hope that my future work will be a credit to all of you.

Thanks to my friend Prof. Peter Timbie of the Physics Department for loaning his ADR, which he personally had built, and working with me to adjust a suspension system to hold the paramagnetic salt canister in proper alignment with the magnet. I am pleased that we are returning the favor – we established that after many years sitting neglected in a box somewhere in California the FAA salt crystal is intact and the unit still functions.

I thank the Instrument Maker machinists in the College of Engineering TEAMLab, formerly the Student Shop. Charles Allhands, Jay Bowe, Eric Ellefsen, Paul Kijak, Jeff Rappe, and their student assistants patiently applied their ingenuity and good advice to guide me in machining copper parts. John Pfotenhauer asked me that this thesis not be a 'travelogue' so I have omitted from it any description of the more than 100 hours I spent with these good people.

Yanan Wang, a visiting scholar from Beijing, China worked with me to make the superleaks. Her work was essential in validating the method developed to make them. Her technical skills are excellent. We also worked closely devising techniques to silver braze very thin steel capillaries to copper parts, often requiring two people to hold simultaneously a MAP gas canister and an acetylene torch. I hope we will have an opportunity to continue to work on this project.

Another 'travelogue' topic omitted from the thesis is the very many days spent with rotary vane pumps and their oils. Xia Ming, a visiting scholar from Kunming, China shared with me the job of cleaning the inside of the large Alcatel 2063 rotary vane pump (one of three rotary vane pumps I disassembled and serviced) which had not been run for perhaps ten years. He assisted with rewiring it. He is also a very good man to work with. Lindsey Thomas, an undergraduate student, was able to fix the dry diaphragm pump, well done.

Anne Glorioso, Science and Engineering Librarian, assisted me in locating papers not held in the UW collection, and in obtaining unpublished dissertations.

All of the graduate student colleagues in the SEL are great people to work with, and one could always interrupt any of them for a quick query on any detail of our work – information, computing, a lab procedure. All of their SEL presentations and thesis or dissertation defenses were always of great interest. I thank in particular Zhiyi Jiang for teaching me how to use the helium leak detector; Uzo Mmeje for help with LabView; Jake Boxleitner for working with me to make photomicrographs, and for help lifting rotary vane pumps; Jen Detlor for sharing information and experience about acetylene torch work and vacuum parts; and Jeff Maskalunas, Tyler Hanzlik, Yanan Wang, and Lindsey Thomas for photographs included in this thesis.

This thesis is dedicated to the memory of my Father, Arthur J. Katz, 1927 – 2018, an electrical and electronics engineer and my first teacher in mathematics and physical sciences.

TABLE OF CONTENTS

Table of figures

List of Tables

1. INTRODUCTION

An adiabatic demagnetization refrigerator (ADR) is a device that can produce temperatures between approximately 1.2 K and 50 mK. The main parts of an ADR are a magnet,

a paramagnetic salt, a heat sink, and a heat switch. This thesis is about an improved design for an ADR heat switch.

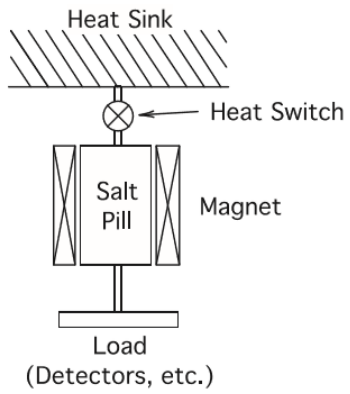

Figure 1 – A schematic drawing of an adiabatic demagnetization refrigerator (ADR). *The heat switch functions to thermally connect or disconnect a paramagnetic salt from a heat sink [1].*

1.1 Adiabatic Demagnetization Refrigerators (ADRs) – Origins, Operating Principles, Uses

1.1.1 Origins

Before the invention of the ADR the lowest temperatures that had been reached were achieved by evaporative cooling of liquid helium. Thermal energy transferred into a liquid causes more energized molecules to leave the liquid's surface -- evaporation. By removing these more energetic evaporated molecules – 'pumping on the liquid' – the temperature can be kept low. 'Vapor pressure' is defined as the pressure at which evaporation and condensation are in equilibrium. By pumping on a liquid the pressure at the liquid's surface is lowered below the vapor pressure and more liquid molecules will evaporate and be pumped away, lowering the liquid's temperature.

But vapor pressure falls with temperature; vapor pressure has a negative exponential dependence on temperature (Figure 2). This places a practical lower limit to the temperatures that can be reached by evaporative cooling. At some low temperature the rate at which vapor can be pumped and pressure can be lowered yields such a small drop in temperature that this evaporative cooling cannot compete with inevitable heat leaks into any cryogenic system. This thermal energy leaks in from warmer parts of the system by conduction through structural parts, electrical or gas feed lines, or an attached experiment; or by radiation. When the ADR was conceived in the 1920's the only known isotope of helium was ^{4}He for which the practical lower limit for evaporative cooling is 1.2K. With ^{3}He, discovered in 1933 and used for evaporative cooling only in the 1950's, evaporative cooling with modest pumping systems can reach 0.3K [2]. The isotopes of helium will be discussed in Section 2.

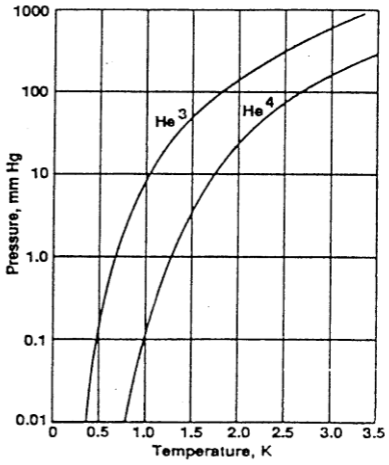

Figure 2 – Vapor pressure of helium at low temperatures. *For ^{4}He, the only isotope known in the early 20th century, evaporative cooling becomes impractical below a temperature of about 1.2 K. For ^{3}He the practical low temperature is 0.3 K. Below those temperatures decreases in pressure yield relatively little temperature reduction [3].*

In 1922 Kamerlingh Onnes used a battery of pumps attempting by means of evaporative cooling to reach a temperature at which he hoped helium would solidify. Addressing the Faraday Society he reported that

> …taking into account the uncertainty of the extrapolation [from observed temperature and vapor pressure data for helium down to 1.5 K] it will be better to say that the lowest temperature yet attained is some hundredths of a degree below 0.°9 K … one may say that if we could have gone further only 1/6 of a degree, we should have arrived at the limit obtainable in the ordinary way with helium… If it is considered that our knowledge of atomic structure renders improbable that another substance could be discovered, or obtained in another way, more volatile than helium, then the limit indicated, from which we are separated by only such a small amount, would seem an absolute one set to us in the obtaining of yet lower temperatures…

Onnes concluded with an encomium to Faraday who had been unable to liquefy hydrogen, and with the hope that progress toward lower temperatures might still come by "long and patient investigation of the properties of matter at the lowest temperature we can reach" [4].

"A refrigerator is a form of 'entropy squeezer'"[5]. Entropy is a function of both temperature and other physical parameters such as pressure and volume. Reduction in temperature can be achieved by altering a suitable parameter X in such a manner that entropy is also reduced. As early as 1924 W. F. Giauque had spoken with colleagues of the possibility of using the magnetic properties of the paramagnetic salt $Gd_2(SO_4)3\cdot 8H_2O$ for refrigeration.

> The reversible transfer of heat from one temperature to another requires a working substance which is capable of undergoing an isothermal entropy change at the temperatures concerned [around 1 K]… Compared to those of pressure, the effects ordinarily produced by obtainable electric and magnetic fields on the neutral states of matter are minute. However a critical consideration indicated that while the latter cannot compete with pressure in producing a change in entropy at ordinary temperatures, a magnetic field will produce large effects at very low temperatures. The important point is that the magnetic effects are large when pressure is no longer practicable as a means of producing a further drop in temperature [6].

In a footnote Giauque acknowledged that P. Debye had independently developed the same idea.

Six years were required to construct the required experimental apparatus. A short letter to the editor of the *American Physical Review* in April, 1933 communicated that starting at 3.4 K and using a field of 8000 Gauss (0.8 T) temperatures of 0.53 K, 0.34 K, and 0.25 K had been achieved "through preliminary experiments on the adiabatic demagnetization of $Gd_2(SO_4)_3 \cdot 8H_2O$" [7].

Casimir succinctly described the process we refer to as adiabatic demagnetization refrigeration.

> If a substance is at a temperature T and a field is applied, then heat is developed. If this heat is carried away there results a state of lower entropy than the initial state. If then the field is switched off and no heat is supplied the entropy will remain constant. There will result a state in zero field with lower entropy than the initial state and therefore a state of lower temperature [8].

1.1.2 Operating Principles and Uses

The process of adiabatic demagnetization refrigeration is described in detail in several standard works [9]. The following discussion makes reference to the paramagnetic salt FAA (ferric ammonium alum, $NH_4Fe(SO_4)_2 \cdot 12H_2O$) which will be used for the ADR described later in this thesis.

The entropy of a paramagnetic salt is the sum of entropy from the crystal lattice, conduction electrons, and magnetic entropy. At very low temperatures the magnetic entropy is much larger than the other two. Each ion in a paramagnetic salt has a magnetic moment resulting from unfilled electron shells – in the case of FAA from the transition metal iron. This imparts an electronic (as opposed to nuclear) angular momentum (designated J) to each ion. Initially the dipoles of each ion have no preferred orientation. When a magnetic field B is

applied, with respect to the direction of the applied field the magnetic moment of a given ion will point in one of (2J + 1) quantized directions. From statistical mechanics it is possible to derive the dependency of the magnetic entropy – the significant entropy in the low temperature regime – from the partition function. The magnetic ions are separated from one another in FAA by water molecules, ensuring the rough independence of the magnetic moments of each ion from one another.

Under these conditions it is possible to write an expression for the reduced magnetic entropy, *S/R* (*R* is the gas constant, 8.314 J/mol-K) of a low temperature paramagnetic salt that contains *n* ions, and to plot the relationship between reduced entropy and temperature for that salt for a range of magnetic fields,

$$\frac{S}{R} = nk\left(\ln\frac{\sinh(2J+1)\frac{x}{2}}{\sinh\frac{x}{2}}\right) + \frac{x}{2}\coth\frac{x}{2} - \frac{x}{2}(2J+1)\coth(2J+1)\frac{x}{2} \quad (1.1)$$

with

$$x = \frac{\mu_B g B}{2kT} \quad (1.2)$$

and

$$B = \sqrt{B_{app}^2 + B_{int}^2} \quad (1.3).$$

B_{int} denotes a material-dependent factor, the field internal to the salt that results from mutual interactions of the dipoles and interactions between magnetic moments of electrons and nuclei. μ_B is the Bohr magneton ($9.27 \times 10^{-24}\, J/T$), *k* is the Boltzmann constant ($1.38 \times 10^{-23}\, J/K$) and *g* is the Landé splitting factor. The Landé splitting factor relates spin angular momentum (S, but a different S than that used for magnetic entropy in Equation (1.1) and the discussion there),

electron orbital angular momentum L, and overall angular momentum J. The Landé splitting factor g is defined as

$$g = 1 + \frac{J(J+1)+S(S+1)-L(L+1)}{2J(J+1)} \quad (1.4).$$

For FAA $g \cong 2$ and $J = 5/2$.

Typical plots of Equation (1.1) are shown in Figure 3 for a 'high temperature' paramagnetic salt FAA, and in Figure 4 for a 'low temperature' paramagnetic salt CMN (cerous magnesium nitrate $2Ce(NO_3)_3 \cdot 3Mg(NO_3)_2 \cdot 24H_2O$, $J = 1/2$).

Figure 3 and figure 4 also introduce the states in the ADR refrigeration cycle. These cycles vary slightly in the two figures shown. Consider Figure 3. At the start of the cycle the ADR has been cooled to a starting temperature of 2.4 K. A heat switch between the paramagnetic salt and a thermal reservoir is closed (ON state), and a magnetic field B is applied, ramping from 0 T to 3 T. The magnetic moments of the ions in each salt line up—iron in FAA, the rare earth element cerium in CMN -- and their entropy is reduced, transferring the heat of magnetization to the thermal reservoir. The ADR state travels down the vertical (isothermal) line A-B in Figure 3. The thermal reservoir must absorb the energy

$$q_{hot} = T_{hot}\,(S_A - S_B) = T_{hot}\Delta S_{hot} \quad (1.5).$$

At point B there is a pause for the system to reach thermal equilibrium, and then the thermal link with the reservoir is broken by opening the heat switch (OFF state). The magnetic field is adiabatically decreased and the temperature of the salt falls. The ADR moves from state B toward C. The adiabatic demagnetization of the salt continues until the salt reaches a desired temperature at C. The applied magnetic field is then reduced at a rate such that cooling balances

parasitic heat loads. The temperature can be maintained in this manner for a period of hours. Eventually the state of the system moves isothermally along line C-D until the applied field is at 0. During this isothermal stage the salt absorbs heat

$$q_{cold} = T_{cold}\,(S_D - S_C) = T_{cold}\Delta S_{cold} \tag{1.6}$$

The cycle may then be repeated.

The properties of a particular ADR are determined by the starting temperature and magnetic field, the salt chosen, and the heat leaks in an ADR system from structures or electrical lines.

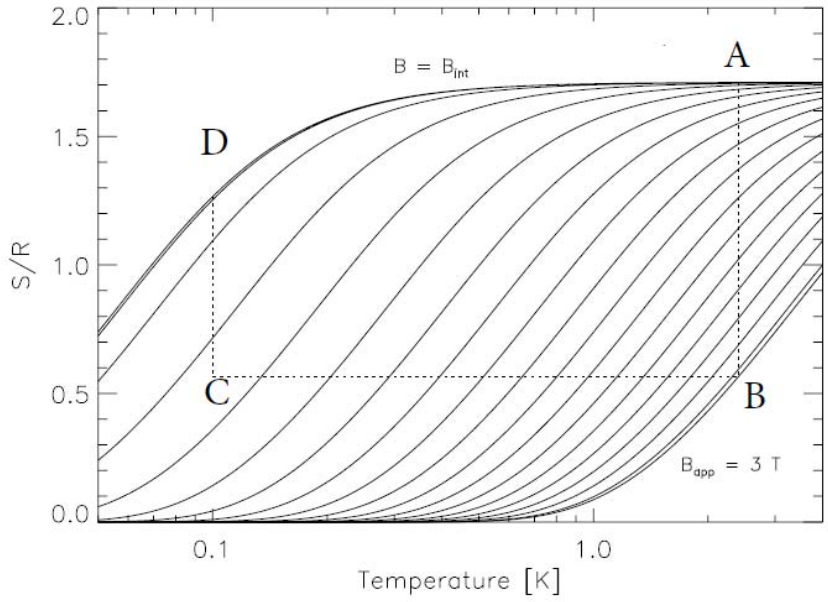

Figure 3 – Theoretical reduced entropy of FAA, a paramagnetic salt plotted against temperature, with lines of applied magnetic field from 0 T to 3 T. *An adiabatic demagnetization refrigeration cycle is indicated by the dotted lines. [10]*

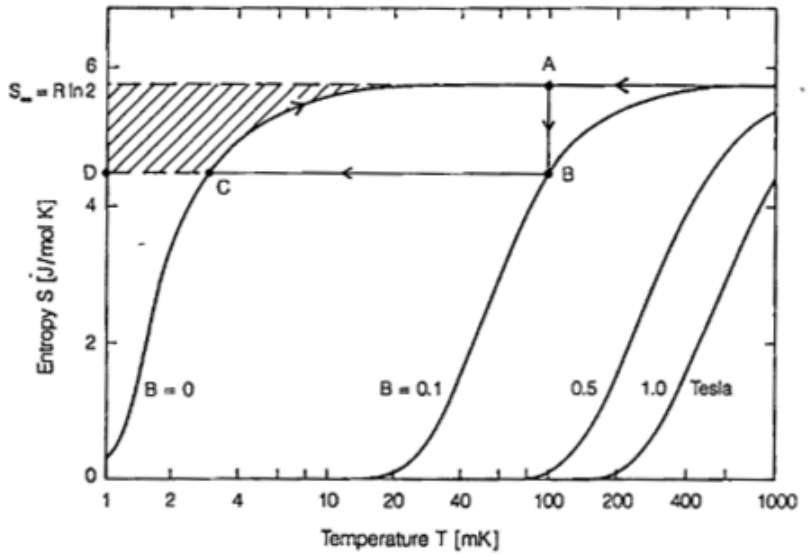

Figure 4 – Theoretical reduced entropy of CMN, a paramagnetic salt plotted against temperature, with lines of applied magnetic field from 0 T to 1 T. *The starting temperature is lower than in Figure 3, < 100 mK. The cycle begins in the same manner, with application of a magnetic field while the ADR is in thermal contact with a heat sink (path AB). At B the thermal contact with the heat sink is broken, the magnetic field is reduced, and the ADR cools adiabatically (isentropically) along path BC. The end of the cycle is different than in Figure 3. Here the magnetic field is reduced to 0 T, and the ADR then warms along the curve of 0 T. The lowest temperature here is about 2 mK [9].*

Pobell, writing in 1995, consigned the ADR to history. "For the last 15 years it has not been much used, because it has been replaced by the 3He-4He dilution refrigerator which has the substantial advantage of being a continuous refrigeration method" [9]. But a rennaissance in development and use of ADRs has since occurred with the development of space-based low temperature X-ray and infrared bolometers. The detection power of these bolometers is a strong function of temperature of a heat sink they contain, with a major difference between a 1K heat sink and one at 100mK [11]. Advances in NbTi superconducting wire made possible low current high field magnets required by ADRs. This and the solid state character of the ADR have made them useful for operation in space [12].

For this thesis, the points of interest in the ADR cooling cycle are points A and B in Figure 3 and Figure 4. These are the points where contact is first made, and then broken between the ADR and a heat sink, and where the heat switch comes into play.

1.2 Heat Switches in the ADR cycle

1.2.1 Types of ADR Heat Switches

At the start of the ADR cycle there must be thermal contact between the paramagnetic salt and a thermal reservoir. But when the applied magnetic field has reached its maximum, a brief time has been allowed for the system to reach thermal equilibrium, and the adiabatic demagnetization is about to commence (point B in Figure 3 and Figure 4), thermal contact between the salt and the thermal reservoir must be broken. A device is required that provides a thermal link between salt and sink, breaks it, and re-establishes it. This is the heat switch.

The switch must have a mounting structure that does not itself communicate thermal energy between salt and sink nor generate heat during its own operation in amounts significant relative to the heat budget of the cryogenic system. The friction of moving parts, or from gripping and releasing, or heat from electrical connections or eddy currents are all of concern. The heat switch must work reliably for thousands of cycles under vacuum, and for space operations be small in mass and volume, able to operate in microgravity or under acceleration, and able to survive vibration during launch.

Review articles by P Kittel [13] and Shirron and DiPirro [14] trace the development of ADR heat switches from Giauque to the present designs. As they relate, in Giauque's experimental ADR it was sufficient to have the heat of magnetization transferred through helium exchange gas to a surrounding dewar containing pumped liquid helium. At point B in the cycle

(Figure 3, Figure 4) the exchange gas was removed by an external vacuum pump, thermally isolating the paramagnetic salt from the heat sink. The gas gap heat switch (GGHS), developed in the 1980's, uses this same principle but in a more compact form with decreased pump out time, and less residual gas pressure. In the GGHS warm and cold ends with large surface areas are separated by a small gap. Typical designs involve copper arranged in concentric cylinders or interleaved fingers with the smallest gap possible that can be fabricated with necessary resistance to vibration. In the ON state a gas with relatively low thermal conductance fills the chamber. In the OFF state the gas is pumped out to a reservoir, or adsorbed by a getter. The low thermal conductance of this gas is required as some residual gas will remain in the chamber in the OFF state. Hermetic gas containment is essential and a design challenge. Gas leakage may be expected over time and limits operating life. The lowest operating temperature is about 0.2 K as the saturated vapor pressure of helium is too low to provide enough conduction at any temperature lower than that.

Figure 5 – Active gas gap heat switch. *Interleaved fingers with the smallest gaps possible are required needing precise fabrication. Vibration during launch to space poses a design challenge. Photograph by Photograph by Amir Jahromi, NASA.*

The superconducting heat switch (SCHS) uses a different principle. Some pure metals have the property that at a critical low temperature T_c they become electrical superconductors

and while in that state are poor thermal conductors. But if at a temperature below T_c they are subjected to a magnetic field, they are forced into their normal electrical conducting state and at that same temperature become good thermal conductors. So at a suitable temperature an applied magnetic field can convert a piece of such a metal from a low to high thermal conductor. At temperatures below 0.5 K five metals have a ratio of normal state thermal conduction to superconducting state thermal conduction of above 100. These are zinc, aluminum, indium, tin, and lead. So the SCHS is useful where the warm end temperature is 0.5 K or lower. High thermal conductance copper is bonded to the ends of the superconductor. Care is required that the applied magnetic field not induce eddy currents in the copper. There is a small release of heat in transitioning from normal to electrically superconducting states. But the switch is rugged, and can also function as a structural member.

Mechanical switches are also in use. They have the advantage that in the OFF state there is a physical separation between surfaces and the possibility of zero OFF state conduction. With the gas gap switch in the OFF state there is still some residual heat- conducting gas. The superconducting switch has some conduction through its metal in the OFF state. But because the mechanical switches must make and break contact multiple times at very low temperatures without the benefit of vacuum grease or indium foil between surfaces, they are more massive and require more structure to keep them stable while contacting and releasing. This can result in structural parts that bridge the thermal gap and no full physical thermal separation in the OFF state. In addition, for actuation they require more in the way of feed-throughs from warmer areas outside the system, whether hydraulic or mechanical. These add parasitic heat loads.

1.2.2 Active and Passive Heat Switches

All of the heat switches described so far may be called ‘active.’ Some external activation is required – pumping of a gas, application of a magnetic field, starting a hydraulic or mechanical actuator. Activation introduces another possible failure mode. For a ground-based system a heat switch failure requires a time consuming round trip between high vacuum and low temperature to standard temperature and pressure. For space-based machines a heat switch failure cannot be fixed and ends the mission. ‘Passive’ heat switches are therefore highly desirable. These would be heat switches specific to ADR operating temperatures that take advantage of some natural fact to activate the switch under desired conditions with no external action required.

A passive heat switch suitable for the ADR cycle is the passive gas gap heat switch (PGGHS), developed by DiPirro, Shirron, Tuttle, and Canavan[15]. At the end of the heat switch connected to the paramagnetic salt, and so usually the cold end, is placed a getter that adsorbs gas from the gap between warm and cold end when the temperature of the cold end falls to a certain temperature. The adsorption of the gas produces a vacuum between the warm and cold ends placing the switch in the OFF state. If the required OFF state temperature is known, the gas and getter can be ‘tuned’ so that when the cold end reaches a critical value the switch turns ON or OFF. PGGHSs have been demonstrated at operating temperatures equal to 0.2, 1.0, 1.3, 4.2, 5.2, 11, and 13K. “The gas type, dosage, and getter type and surface area are determined by calculating the residual pressure such that the mean free path of the gas is as long or longer than the separation between metal plates when the switch temperature is at its turn-off point.” [15] This can be accomplished within a relatively narrow pressure by taking advantage of the fact mentioned earlier in the discussion of the limits of evaporative cooling, that at low temperatures gas pressure has an exponential dependence on temperature. The problem with

evaporative cooling was that at low temperatures a large change in pressure yields only a small change in temperature. But here where a narrow range of temperature change is wanted for the switch's OFF/ON transition, a small change in temperature is all that is required for a large change in pressure. With the proper getter and gas the switch can be tuned to adsorb gas, and so transition between OFF and ON in a narrow temperature range [15]. Getters of solid hydrogen or charcoal are used with helium gas. Design difficulties encountered include manufacturing switch containers that are impermeable to helium at room temperature and have low thermal conductivity at low temperature. Titanium foil glued to Vespel polymer has been tried, but at room temperature the Vespel can absorb water that contaminates a getter, and the gluing process is difficult. Ti 15-3-3-3 cylinders were also machined with wall thickness of 0.11 mm (length 70 mm, diameter 21 mm), using electrical discharge machining. These design complexities are in addition to all those present with the active GGHS already described. But passive operation and the capacity to tune the switch to a range of ON/OFF temperature needs are positive features.

Figure 6 – Passive gas gap heat switch. *The grey circle on the center photograph is a sintered stainless steel cylinder used as the getter. Photograph by Amir Jahromi, NASA***.**

1.2.3 Switching Ratio

A useful way to compare the performance of these different types of heat switches is the 'Switching Ratio'. In the designs described the thermal connection between paramagnetic salt and heat sink cannot be completely broken. There remains some thermal contact by conduction through the structures holding the salt and switch in place, or through residual exchange gas. Rather than thinking of there being a complete break in thermal contact between salt and switch from point B in the refrigeration cycle and forward (Figure 3, Figure 4), it has proven useful to have a ratio that relates the ON state when the salt and sink are thermally connected (switch is open) with the OFF state when the salt and sink are more or less thermally isolated, when the switch is open.

One such switching ratio is the ON/OFF thermal conductance ratio:

$$SR_k = \frac{k_{on}}{k_{off}} \tag{1.7}$$

Another is the heat flow ratio:

$$SR_q = \frac{\dot{q}_{on}}{\dot{q}_{off}} \tag{1.8}$$

The thermal conductance ratio allows a general evaluation of a heat switch principle and the thermal properties of materials used without reference to a specific design. The heat flow ratio, by contrast, can evaluate an actual switch in the system in which it will be used [13].

1.3 Liquid Helium

1.3.1 Superfluid helium; the two-fluid model; the superleak

The normal boiling point of helium is 4.2 K. As helium is cooled below this temperature it initially behaves as a Newtonian fluid. But starting at 2.172 K liquid helium undergoes a second phase transition and exhibits unusual properties. This dividing temperature is denoted T_λ because of the resemblance to the Greek letter lambda of the plot of specific heat vs. temperature of helium below its normal boiling point. Liquid helium above T_λ is called He I, below He II. There is no latent heat or specific volume change at the 'lambda' transition.

Several macro-scale features of the phase change were discovered in the first half of the 20th century and may be plainly seen in the films by Leitner and by Allen. [16][17][18][19].

When liquid helium boils He I displays vigorous nucleate boiling, as with water or nitrogen. But once cooled through T_λ the nucleate boiling suddenly ceases. Evaporation continues at the surface, but no bubbles are visible. The thermal conductivity of He II is so great that heat is conducted through the bulk liquid before there is time for a bubble of rising vapor to form. The thermal conductivity of He II is as high as 100 kW/m-K, much higher than copper at room temperature. It resists, however, easy quantification, as it varies sometimes with the cube root of the temperature gradient , sometimes with the gradient, depending on the intensity of the heat flow and the shape or diameter of the channel [20][21].

He II obtains the name "superfluid" from the observation that it will flow through a capillary packed with a fine powder that does not allow passage of any other liquid, no matter how low that liquid's viscosity. Not clamped by viscous forces, the superfluid helium flows through the pores in the packed powder. In flow through small capillaries the resistance of superfluid helium to flow is less than the margin of error of experiment – is effectively zero. This was confirmed using a rotating torus cooled below T_λ then brought to rest. A constant angular velocity of He II in the torus was observed for hours and the drop in viscosity with cooling through T_λ was found to be at least eleven orders of magnitude. When viscosity is measured in this way helium II has no viscosity [2].

But in an experiment with an oscillating disk, viscosity in helium II is plainly visible. In Leitner's film this is shown with an induction motor that causes a cylinder that is within a glass-walled tank of helium II to rotate. Above the cylinder is visible a wooden four-armed vane floating in the helium above the rotating cylinder. After a few seconds the vane begins to rotate, clearly caused by some viscosity within the helium as fluid above the cylinder itself starts to rotate.

Does helium II have viscosity or not? This depends on the mode of observation. This contradiction is effectively modeled by the 'two-fluid model' and the notion that superfluid helium exhibits quantum phenomenon on a macro scale.

The two-fluid model describes helium II *as if* it were a mixture of two different fluids, one with normal viscosity, the other with no viscosity. In fact this is not so, in the sense that no individual atom of helium in a container of II helium is identifiably either normal or superfluid – all atoms would appear identical in this respect. Nevertheless the model accurately predicts much of the behavior of II helium. The model has it that the density, ρ, is

$$\rho = \rho_n + \rho_s \tag{1.9}$$

with *n* and *s* designating 'normal' and 'superfluid'. The density fraction of each type depends on temperature (Figure 7). There is an additional postulate, that the superfluid component has no entropy.

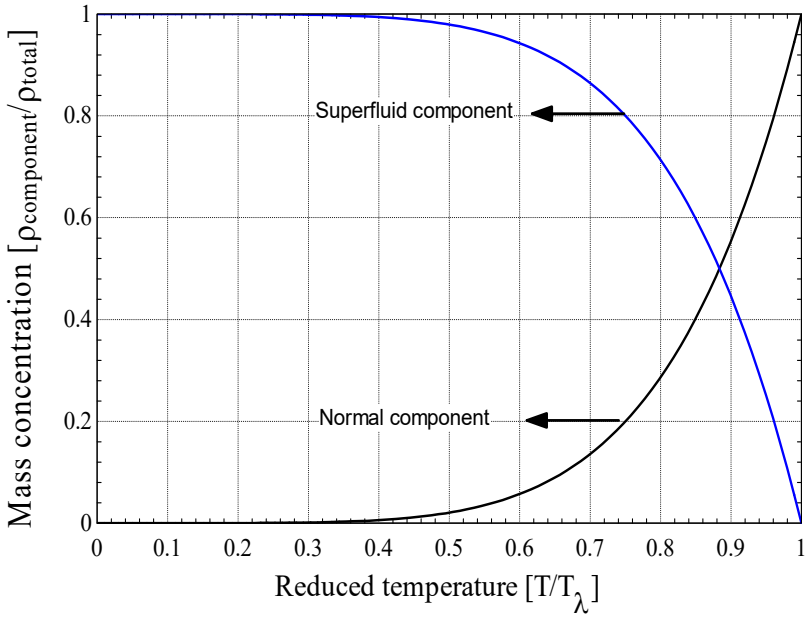

Figure 7 – Relative mass concentrations of normal and superfluid components in 4He below T_λ. [22]

Helium II has unusual heat and mass transport properties. Following the two-fluid model, "… if a temperature gradient is maintained in liquid helium II… [then] ρ_s atoms flow from the cold region to the hot, are there raised in energy to ρ_n levels, and a balancing flow of ρ_n atoms returns to the cold region…Thus it is possible to have a countercurrent flow of the two phases in the liquid without giving rise to a macroscopic current…" [23]. A barrier composed of a packed fine powder impermeable to any liquid that has any viscosity has been given the unfortunate name "superleak". If two chambers both below T_λ and containing helium II are connected with a superleak and one chamber is warmed, superfluid helium will pass through the superleak into the warmer chamber. But as that superfluid is warmed and some of it returns to the normal state, normal fluid cannot flow back through the superleak into the cooler chamber. So if a small opening is made in the warmer chamber displaced normal fluid will spout through the opening. This is the 'fountain effect' which may be seen in the films cited [16, 18]. If the channel between the warmer and colder chambers is not a superleak, superfluid helium will flow toward the warmer end, and normal helium will form a counter-flow back to the cooler chamber. It is possible to establish an equilibrium state between the two chambers with a temperature difference between the two. The superfluid component flows toward the heat, the normal away from the heat. This 'thermo-mechanical' effect has been used for pumping liquid helium.

It is important to add that with this counter-flow there is a 'critical velocity' of normal fluid relative to superfluid at which vortices will form in the helium II, disturbing the very high thermal conductivity of helium II. This critical velocity varies with capillary internal diameter and is relevant to the heat diode presented in this thesis. It will be discussed further in the next section [2].

1.3.2 ^{3}He, ^{4}He, Mixtures; the 'heat flush' effect

There are two stable isotopes of helium. ^{4}He occurs in trace amounts in the atmosphere, and is largely obtained from natural gas deposits. Its presence in earth's atmosphere is replenished by radioactive decay of elements in earth's crust. A lighter isotope, ^{3}He, was discovered in the 1930's. In natural gas deposits it occurs at only 0.14 ppm and must be produced using nuclear reactor waste or byproducts of hydrogen bomb materials. It is perhaps ten times more abundant on the surface of the moon.

Both isotopes of helium experience a very weak intermolecular binding force (Van der Waals bonds) and because of small molar volume have a relatively high zero-point energy. As a result helium is the only substance that remains a liquid under saturated vapor pressure as T approaches 0 K, and both isotopes have the lowest boiling points and critical points of any substance. Of particular interest for this thesis, ^{3}He in its normal state is a poor heat conductor [2].

In an experiment performed in 1947, Lane, Fairbank, Aldrich, and Nier set out to investigate what would happen if a small amount of 3He were added to 4He. They described the two fluid model, then posed a question. "Just prior to the war, L. Onsager advanced the hypothesis that He^3 atoms might be expected to participate in the ρ_n flow but not in the ρ_s type flow because of the different kind of statistics obeyed by He^3 and He^4 atoms" [23]. Previous experiments had led to ambiguous results. They set out to test this notion explicitly.

Their apparatus consisted of a cryostat dewar that containing a glass bulb immersed in liquid helium. The bulb could be heated with a filament. The bulb exited to a capillary that

ultimately led out of the cryostat so that concentrations of $^3He/^4He$ could be measured with a mass spectrometer as the helium evaporated (Figure 6).

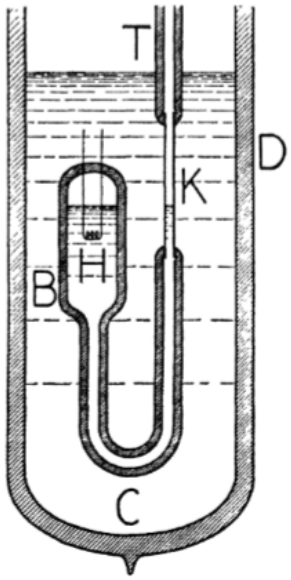

Figure 8 – Schematic drawing of the cryostat used to demonstrate the 'heat flush' effect. *Thick glass-walled bulb B containing a heater H is immersed in a bath of liquid helium. Isotopic content of helium exiting 1.5 mm diameter capillary C is measured at point K* [29].

With the dewar cooled to 2.01 K, the application of a small current to the heater resulted in an increase of ^3He at point K in the figure by a factor of several hundred with a very small temperature gradient. The authors named this phenomenon 'heat flush' and described it as follows:

"We found that a temperature gradient in bulk liquid helium II exerts a ponderamotive force on He^3 atoms dissolved in the liquid, such that the latter travel in the direction of the heat flow. In these experiments we were able to raise the concentration of the He^3, at the surface of the liquid subjected to the temperature gradient, by a factor of several hundred with very small temperature gradients" [23].

1.3.3 Turbulence in Superfluid Helium

The superfluid component of helium II has no viscosity, and so if placed in a cylinder and spun it may reasonably be expected to stand still, with only the normal component rotating. But an experiment conducted by D.V. Osborne in 1950 with such a cylinder (referred to in several articles as a 'bucket') showed that when the velocity of the periphery of the rotating cylinder was above 35 cm/sec the superfluid portion did not stand still, but participated in the rotation of the fluid. [24]

The previous year C.J. Gorter and J.H. Mellink, in an article giving a comprehensive review of research on superfluid helium up to 1949, had proposed a force of "mutual friction" between superfluid and normal components. This 'Gorter-Mellink force' varies with temperature and is proportional to the cube of the relative velocity of normal and superfluid velocities, also called the 'counter-flow velocity', $(v_n - v_s)^3$ [25]. The mutual friction force was experimentally shown to exist by W.F. Vinen in 1957 and shown by him to be the basis of 'quantum turbulence' [26].

As some portion of the superfluid exceeds a critical velocity it returns to its normal state and forms a core for a vortex in which this normal fluid is surrounded by a vortex of superfluid. These superfluid vortices are "quantized".

> "Suppose that the superfluid at absolute zero is characterized by a stationary rotational flow pattern with flow velocity $\mathbf{v_s}$. In a quantum-mechanical description of the super-fluid, this flow pattern can be described by a single well-defined wave function $\boldsymbol{\psi}$ extending over *mac*roscopic spatial dimensions. One expects this wave function to have the form $\psi = e^{i\varphi}\psi_0$, where ψ_0 is the ground-

state wave function of the fluid at rest and where φ is a phase factor whose gradient is related to the flow velocity $\mathbf{v_s}$. The condition that ψ be single-valued leads to the requirement that φ change by an integral multiple of 2π in going around any closed path …

$$\oint \boldsymbol{p} \cdot d\boldsymbol{l} = m \oint \boldsymbol{v_s} \cdot d\boldsymbol{l} = hN \qquad [1.10],$$

where **p** is the momentum associated with a helium atom of mass *m* moving with the flow velocity v_s, *h* is Planck's constant and *N* is any integer. The application of quantum mechanics to superfluid helium thus leads to the expectation of quantization on a *mac*roscopic scale, the "circulation" κ defined by

$$\kappa \equiv \oint \boldsymbol{v_s} \cdot d\boldsymbol{l} \qquad [1.11]…$$

quantized in units of

$$\kappa_0 = {}^{h}/_{m} = 0.997 \cdot 10^{-3}\ cm^2 sec^{-1} \qquad [1.12].$$

The simplest situation is one of cylindrical symmetry. In this case (2) becomes $\kappa = v_s(2\pi r)$ where *r* denotes the distance from the symmetry axis and v_s the circumferential component of v_s . Thus

$$v_s = {}^{\kappa}/_{2\pi r} \qquad [1.13]"$$

Note that vortex lines may be curved, may close in on themselves, or even form rings [27] .

In a rotating bucket of helium II these vortices appear regularly spaced and distinct, with an axis of rotation parallel to that of the bucket. These are "unlike eddies in ordinary fluids, which are continuous and can have arbitrary size, shape, and strength" [28].

These quantized vortices can become entangled causing 'quantum turbulence.' The growth rate of these tangles has been found to be proportional to the cube of the counter-flow velocity $(v_n - v_s)^3$; that is, related to the Gorter-Mellink mutual friction force [29]. Such vortices occur in the thermal counter-flow when there is a temperature gradient in liquid helium. As described above, when a container of helium II is given a temperature gradient, the normal fluid flows away from the heat source while the superfluid flows toward the heat source. "In a

simple one-dimensional case (e.g. counterflow through an insulated channel with a heater at one end), the normal fluid velocity is related to the magnitude of the heat flux q as

$$v_n = \frac{q}{\rho s T} \qquad [1.14]$$

where T denotes the fluid temperature and s its specific entropy. The corresponding theoretical superfluid velocity $v_s = v_n \rho_n / \rho_s$ is easily obtained by conservation of mass. As the heat flux increases, the counter-flow velocity $v_{ns} = v_n - v_s$ increases accordingly and turbulence can develop in both fluid components. Superfluid turbulence manifests as a tangle of quantized vortex lines …"[30].

Superfluid vortices can also be formed by acceleration of charged particles in superfluid helium at temperatures between 0.6 K and 0.28 K. Research in this mode of superfluid vortex formation led to the only size estimate of the core radius of these vortices, about 0.1 nm [27].

Significant for this thesis, "Vinen showed that a turbulent vortex tangle can be generated in the laboratory by applying a heat flux to helium II"[28].

1.3.4 Imaging of vortices in superfluid helium

Vortices in superfluid helium have been imaged using several techniques. In 1979 E.J. Yarmchuk, M.J.V. Gordon and R.E. Packard used a photographic technique to image the ends of quantized vortex line in a rotating bucket of superfluid helium. Each vortex had an electron trapped in its core. These electrons were extracted, imaged on a phosphor screen, then by fiber optics brought to room temperature, amplified, and captured on a frame of film. The images show patterns of regularly spaced dots [31]. In 2006 G.P. Bewley, D.P. Lathrop and K.R. Sreenivasan photographed quantized vortices directly in arbitrary 3D configurations by infusing liquid helium II with a mist of small particles of solid hydrogen and photographing a thin laser-

illuminated sheet. In one image the particles may be seen tracing fluid motion and forming branching filaments. When the helium container was rotated, the hydrogen particles appear in regularly spaced vertical lines – a 'front view' of the vortices whose ends ('top view') were seen by Yarmchuk et al.(Figure 9) [32].

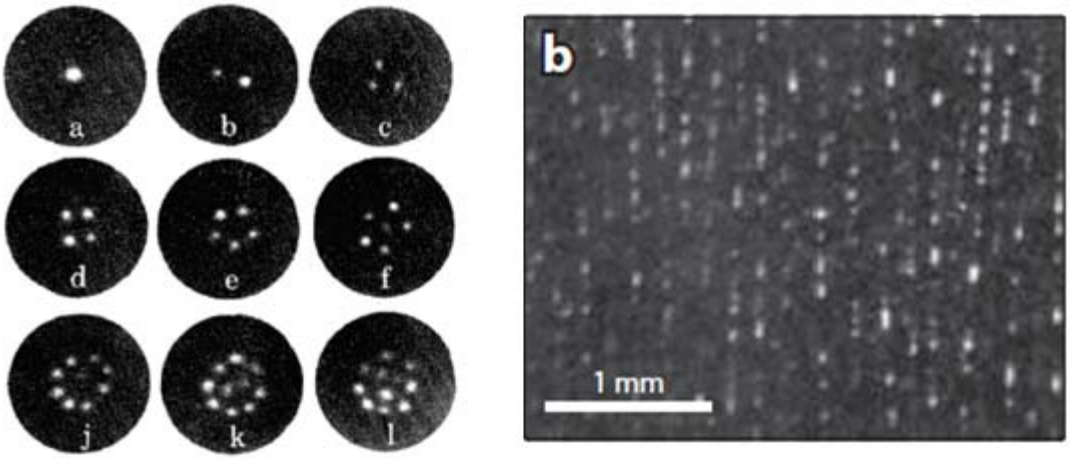

Figure 9 -- Quantized vortices In liquid helium viewed end- on (left) **[31]** ***and from the side(right)*** **[32].**

Two techniques have been used to visualize normal and superfluid motion in thermal counter-flow. W. Guo, M. LaMantia, D. Lathrop and S.W. Van Sciver have developed techniques they call 'particle image velocimetry (PIV) ' and 'laser-induced fluorescence imaging technique.' The former uses micron sized particles; the latter uses angstrom-sized He_2^* triplet state excited molecules. In PIV particles in the liquid helium reflect light from a laser sheet that is trained on the flow field and are imaged. The micron-sized particles proved too dense, however, to resolve details of quantum turbulence. The excited He_2^* triplet molecules form bubbles in liquid helium with a radius of about 0.6 nm and can be used as tracers. A femtosecond laser pulse excites these triplets so that they emit detectable fluorescent photons [33].

Recent research on imaging superfluid vortices has used rotating superfluid helium droplets with added dopants such as xenon or hydrogen that are attracted to vortex cores by hydrodynamics. These vortices are imaged using "transmission electron microscopy (TEM) and ultrafast in situ light scattering using X-ray free-electron lasers (XRELs) and femtosecond high-order harmonic generation (HHG) light sources (Figure 10) [34].

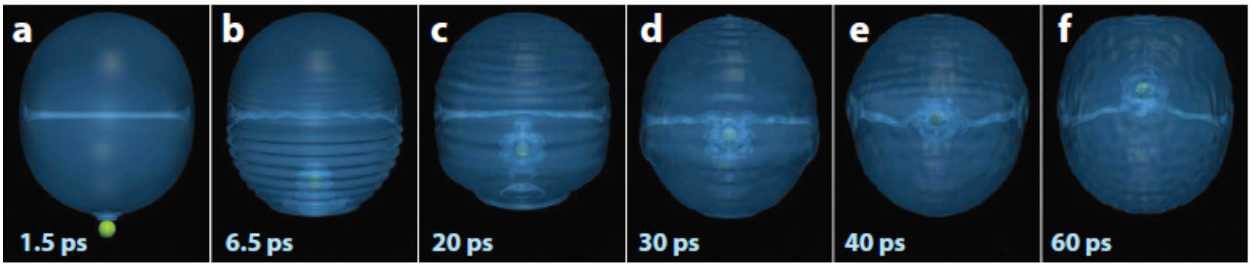

Figure 10 – "Capture of an argon (Ar) atom by a vortex in a ^{4}He droplet containing 1000 atoms." *The argon atom (green) intersects with a single vortex (horizontal line in the center of the droplet). The atom is trapped in the vortex and sets it oscillating [34].*

1.4 The ^{3}He/ ^{4}He Diode Heat Switch

In 1956, C.D. Fulton, C.F. Hwang, W.M. Fairbank and M.M. Vilas successfully built and tested a "thermal rectifier or automatic heat switch" using a weak solution of ^{3}He in ^{4}He. It was designed for use in an ADR. It is a passive switch and may be characterized as a diode – all heat will flow through it is almost entirely in one direction only [35].

The authors note that at 1.5 K the addition of as little as five parts per thousand of ^{3}He to ^{4}He converts the helium from a 'superconductor' of heat to having about the thermal conductivity of stainless steel. They also note the heat flush effect – that below the lambda point (2.17 K) ^{3}He "does not move with the superfluid, but can be flushed by the normal fluid component of the liquid helium to the cold end of the container when a temperature gradient is

impressed across the He^3 – He^4 solution." Putting these two facts together, their heat switch (Figure 11) consists of a small copper volume (10 - 20 mm^3) connected by a steel capillary (ID .04 cm to .15 cm) to a larger copper volume (a few hundred mm^3). In Figure 11 (left) the copper volumes are called "copper end pieces". The volume is filled with a weak solution of ^{3}He (0.1% to 0.2%) in ^{4}He.

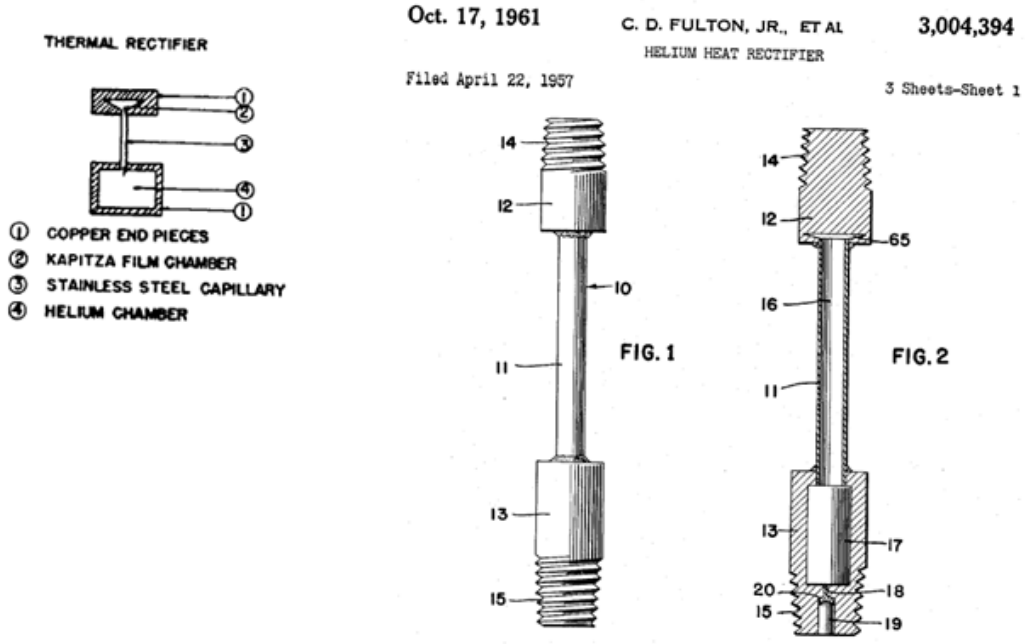

Figure 11 -- The ^{3}He / ^{4}He Diode Heat Switch shown as a schematic (left) [35] and as drawn for a US patent filing in 1957 (right) [36]. The bottom of the extreme right hand drawing shows parts for charging the switch with a mixture of ^{3}He and ^{4}He.

In operation, the small volume is placed in contact with the ADR cold head. The larger volume is placed in contact with a heat sink. Referring to Figure 11, (left), the inventor's explained that when the top of the switch,2, is colder, the ^{3}He is flushed to the cold end of the capillary and into this small volume. The ^{3}He forms an insulating layer in the capillary just outside the cold volume through which the heat can pass only with difficulty. "When the bottom end of the switch (the large volume 4) is the colder, heat flush drives most of the He^3 into

this large volume leaving practically pure He^4 in the stainless steel capillary. Under these conditions the switch is a very excellent conductor of heat. The ratio of conductivity [switching ratio] in the two directions has been observed to exceed 10,000 to 1 at a temperature of 1° [1K] and above…" [35].

During the 1990's Prof. Dan McCammon of the UW – Madison Department of Physics became acquainted with the ^3He / ^4He Diode Heat Switch. He had been photocopying an article on a different topic from the 1958 UW Madison Cryogenics Conference Proceedings cited earlier in this section. Photocopying from the Proceedings which were in a physical book format, Prof. McCammon noticed on the page facing the end of the article he had been copying the end of the article on the Heat Diode. He then read that article, and went on to incorporate the switch into his design for the Astro-E X-ray spectrometer instrument to be used with an ADR for space-based X-ray astronomy research. He built a number of diodes with varying capillary lengths and ^3He concentrations. But though they worked as required for his design, he noted that when ΔT between warm and cold ends of his system rose above about 1.3K, the OFF state heat flux rose by orders of magnitude. As a result the switching ratio collapsed and the diode ceased to function. As the anomaly could not be explained decisively, NASA required that he use a different type of heat switch [37].

Figure 12 shows experimental data from McCammon's diodes showing data points for OFF state heat flux. For this data the cold end is at 50 mK, so the plotted warm end temperature is effectively the ΔT across the diode. Aaron Schmidt, in a BS thesis from MIT written in correspondence with Prof. McCammon [38] added theoretical lines to McCammon's plot that estimate heat flux in a column of pure ^4He. These approximate an ON state at several temperatures and allow computation of a switching ratio. Relative to the slope of the ^4He lines all

the OFF state configurations of length, diameter, and concentration jump up around 1.3 K. Some seem to start this jump at a lower temperature, though no data below 1.3 K is shown. It is the unexpected change in OFF state heat flux, then, that drives the collapse of the switching ratio and the failure of the diode around ΔT of 1.3 K.

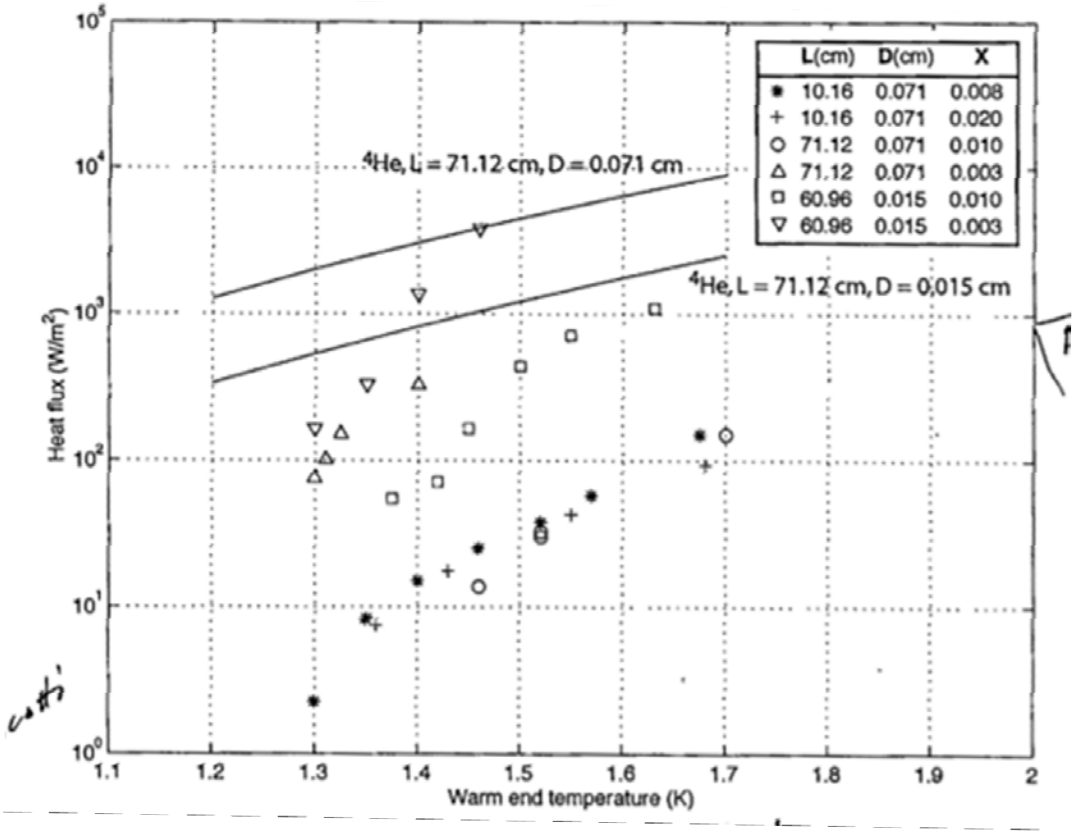

Figure 12 -- Heat flux in ^{3}He /^{4}He heat diodes. *Empirical data from D. McCammon, theoretical lines for ^{4}He from A. Schmidt. Steel capillaries have varying lengths, inner diameters and ^{3}He concentrations. The cold end temperature is fixed at 50 mK. Noting the log scale on the y-axis, for all the tested switches the switching ratio falls by orders of magnitude as the warm end temperature goes above 1.3 K, that is when ΔT goes above about 1.3 K. [37, 38]*

F.K. Miller has suggested that the reason for the OFF state failure of the diode above some value of ΔT is that at sufficiently large ΔT the relative velocities of the superfluid fraction ρ_s and the normal fluid fraction ρ_n reach the two-fluid model critical velocity (Figure 13). The ^{3}He atoms entrained in the normal fraction of the ^{4}He then become cores of vortices which

become entangled, creating turbulence. As a result, ^{3}He is no longer concentrated in the capillary near the small volume of the switch to form a thermally insulating plug (the OFF state). Instead it is diffused through the capillary. The conductivity of the capillary rises to a point that the switching ratio collapses.

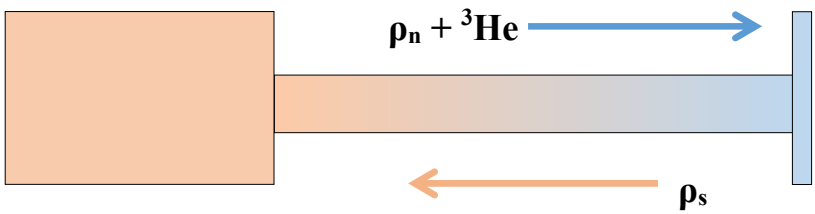

Figure 13 – OFF state counter-flow. *In the OFF state normal fluid ^{4}He flushes ^{3}He toward the cold end of the diode. The ^{3}He is a poor thermal conductor and so blocks thermal flow. Normal fluid flows toward the warm end. At the cold end some normal fluid changes to the superfluid state and flows back toward the warm end. At the warm end some superfluid changes to the normal state and counter-flows back toward the cold end. Miller theorizes that when ΔT is greater than some critical value – here evidently 1.3 K – the counter-flow exceeds the critical velocity and vortices form leading to turbulence and the dispersion of the ^{3}He through the capillary. Thermal conductivity in the capillary rises and the switching ratio collapses.*

Miller's remedy is to alter the flow of liquid helium in the heat diode such that the fluid does not exceed the critical velocity, even as ΔT rises above 1.3K. To accomplish this, a second capillary between the two end volumes is added. The second capillary is a superleak packed with a fine powder (e.g. jewelers' rouge, Fe_2O_3) so that only the inviscid superfluid component of the liquid helium can flow through the pores in it, not the normal component or the ^{3}He which are clamped by viscous forces. Superfluid velocity is inversely proportional to capillary diameter. The pore diameters in the superleak are orders of magnitude less than the open capillary diameter so the superleak will provide the path of least resistance for superfluid.

As a result in there will be no counter-flow in the non-superleak capillary. Instead there will be a circulation of superfluid through the diode (Figure 14).

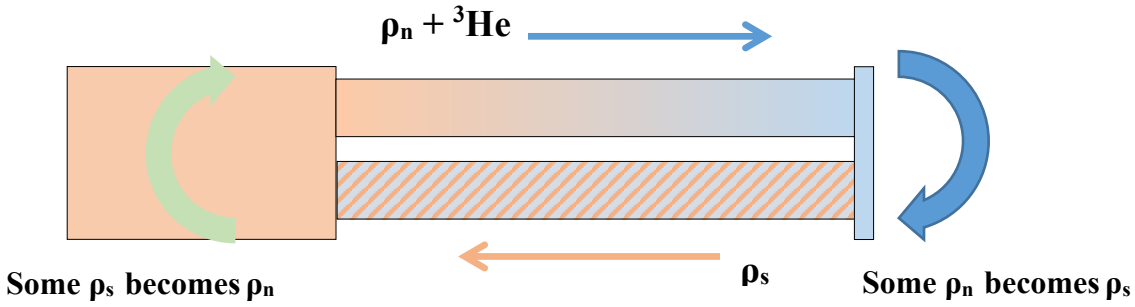

Figure 14 – OFF state with a superleak capillary added. *No counter-flow, instead circulation of superfluid. Only superfluid can flow through the superleak. Superfluid velocity is inversely proportional to capillary diameter. The pores in the superleak have much smaller diameters than that of the entire other capillary. So the superleak provides the path of least resistance for the superfluid. The entire superfluid flow will be in the directions indicated, in circulation, with no counter-flow In the first capillary. The critical velocity will not be exceeded, no vortices will form and the diode will continue to function for $\Delta T > 1.3$ K.*

Because the superleak is the path of least resistance for the superfluid this should be the case in both OFF and ON states. No vortices should form, the ^{3}He 'plug' should stay in place. The diode should then function with $\Delta T > 1.3$ K. It is assumed that the heat flow through the superleak capillary will be small and not interfere with a useful switching ratio. Conduction through the steel is small; the jewelers' rouge particles have large contact resistances; and the pure superfluid carries no entropy.

1.5 Scope of this thesis

The scope of this thesis the construction of a heat diode along the lines of that made by Fulton, Hwang, Fairbank, and Vilas and modified by McCammon with the addition of a second capillary acting as a superleak, with sufficient background information; writing a computer model of the original diode without a superleak, in order to verify the prediction that the original switch should continue to function with $\Delta T > 1.3$ K; and preparation of an experiment to demonstrate whether the improved diode will function as predicted. A detailed account of the fabrication of a superleak in a small-diameter capillary is included as no such account could be found in any published source.

2 Computer Model

2.1 The model

A computer model has been written using EES to explore the functioning of the original Fulton, Hwang, Fairbank, and Vilas heat diode as modified by McCammon. That switch fails to operate properly when ΔT, the temperature difference between cold end and warm end (T_c and T_h), is greater than about 1.3 K. With ΔT above that point the OFF state conductance rises rapidly causing the switching ratio to collapse (Figure 12). This was an unexpected experimental finding. The improved two- capillary heat diode is expected not to have this problem. OFF state conductance with $\Delta T > 1.3$ K is expected to be unaffected by quantum turbulence and so continue low, preserving a high switching ratio. The model is designed to predict how the diode *should* continue to function if the expected quantum turbulence can be prevented by addition of a second capillary that is a superleak.

The model consists of a numerical analysis of conditions in the ordinary non-superleak capillary including ^{3}He concentration x, temperature T, and heat flux q. The user can vary capillary length L and inner diameter ID, initial ^{3}He concentration, size of the large and small helium volumes, and the end temperatures of the large and small volumes T_h and T_c (where they are in thermal contact with the ADR or heat sink). In this thesis the large and small volumes containing helium and located at either end of the capillaries will be called 'large and small volumes', 'end volumes', 'reservoirs', or in some places 'copper end volumes' or 'copper reservoirs' as in the version of the diode built for this thesis they are made of copper, the capillaries of stainless steel.

In this numerical model the end volumes and capillary are divided with N nodes delimiting N-1=S slices. The slices include the large and small volumes. N can also be varied by the program user.

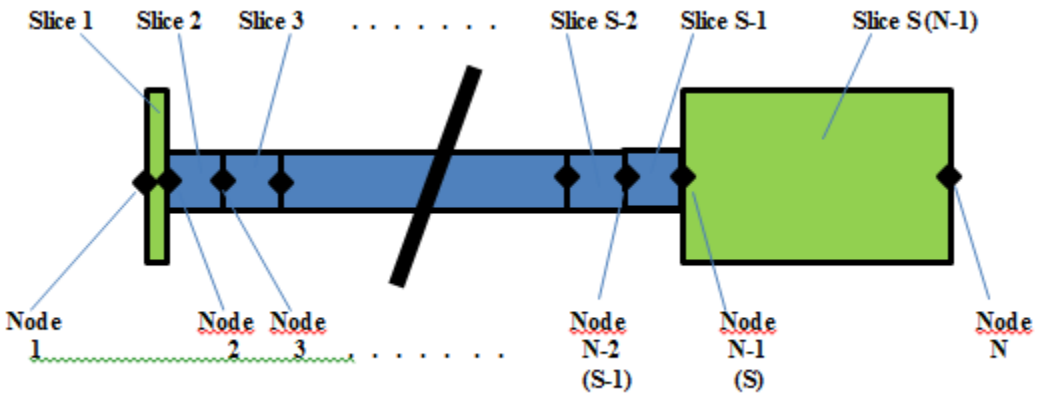

Figure 15 – Schematic drawing showing the division of end volumes and capillary into nodes and slices. *There are a total of N nodes and N-1 slices. Slice N-1 is also designated slice S. Node 1 and slice 1 are always at the warm end of the diode.*

Node 1 is always fixed at T_h. So the first slice S_1 is always the warm end. Similarly the last Node, N, is always fixed at T_c so that the last slice, S_{N-1} also designated S, is always the cold end. To convert from ON state (large end volume cold, small end volume warm) to OFF state (large end volume warm, small end volume cold) the user comments out one of the following sections, in effect designating either the large or small end volume as the warm or cold one Figure 14).

```
"ON, THAT IS HIGH CONDUCTIVITY -- Large end volume cold, small end volume warm."
vol_res_cold = vol_large
vol_res_hot = vol_small

"OFF, THAT IS LOW CONDUCTIVITY -- Large end volume warm, small end volume cold."
vol_res_hot = vol_large
vol_res_cold = vol_small
```

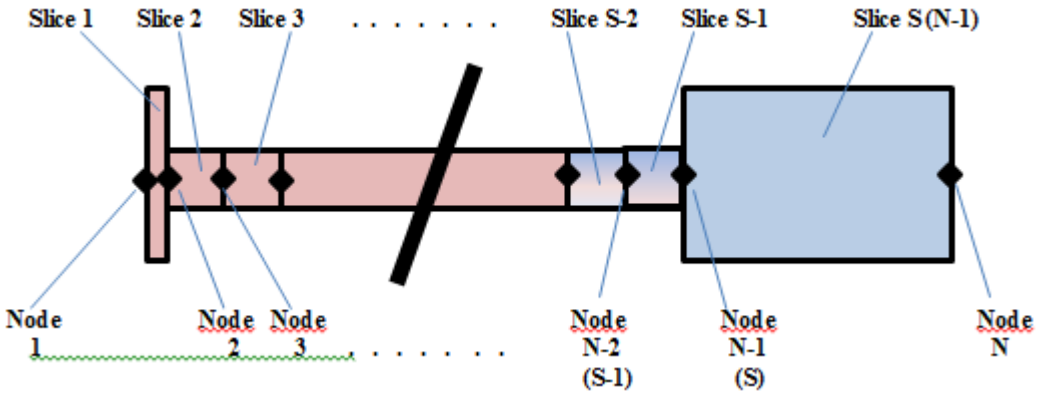

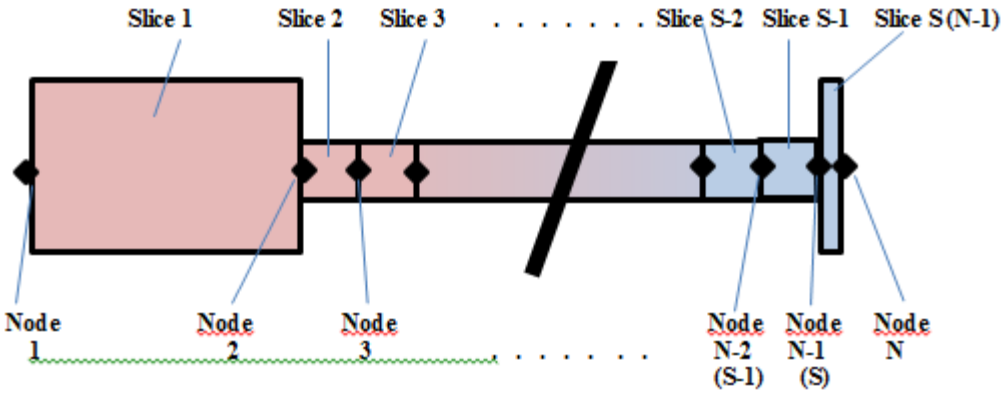

Figure 16 -- Schematic drawing showing (above) ON state and (below) OFF state with numbering of nodes and slices.

Prof. McCammon provided engineering drawings for the diode his lab built in the 1990's along with data plots describing the performance of his diodes. In particular this computer model sets out to describe the experimental results of one of McCammon's diodes, with L = 10.16 cm (4 in), ID= 0.071 cm and large and small volumes with dimensions McCammon specified. The diode built for this thesis uses approximately the same dimensions.

In mixtures of ^{3}He and ^{4}He with low concentrations ^{3}He ($x < .20$) thermal conductivity is a strong a function of ^{3}He concentration. For this thesis a relationship between conductivity and concentration has been used supplied by Franklin K. Miller,

$$k(x) = .00145\, x^{-1.167} \tag{2.1}$$

where conductivity k is in W/m-K and is a function of concentration of ^{3}He x in units of mole ^{3}He / mole ^{3}He ^{4}He solution.

When chemical potential is constant the ^{3}He concentration x and temperature T in any one slice of the capillary can be related to the adjacent slice by the equation

$$x_2 = x_1 \frac{T_1}{T_2} + \frac{1}{RT_2}\left[BT^4 + AT^{3/2}e^{-\Delta_1/T} + Ce^{-\Delta_2/T}\right]\Big|_{T_2}^{T_1} \tag{2.2}$$

with the fit parameters

A = 23.2 [J/mol-K^(3/2)]
B = .00675 [J/mol-K^4]
C = 500 [J/mol]
Δ_1 = 8.65[K]
Δ_1 = 15.7[K]
R = 8.314 [J/mol-K] (gas constant) [39].

The temperatures at node 1 and node N are set by the user, as is the overall volume of the system (large and small end volumes and the capillary) and the total ^{3}He concentration. Nodes are established at the ends of the two end volumes away from the capillaries (N_1 and N_N). Nodes are established evenly spaced the length of the capillary (N_2 to N_{N-1}). Using Equation (2.2) and an energy balance for each node, the relationship between temperature and concentration is established for all N nodes. S = N-1.

```
x[N] = x[S] * (T[S]/T[N]) +   (1/(R*T[N])) *( (B*T[S]^4 + (A*T[S]^(3/2)) *(exp(-delta_1/T[S])) + C*exp(-
delta_2/T[S]) ) - (B*T[N]^4 + (A*T[N]^(3/2)) *(exp(-delta_1/T[N])) + C*exp(-delta_2/T[N]) )  )
"molar concentration of He3 at node N"

Duplicate j =2, S
x[j] = x[j-1] * (T[j-1]/T[j]) +   (1/(R*T[j])) *( (B*T[j-1]^4 + (A*T[j-1]^(3/2)) *(exp(-delta_1/T[j-1])) + C*exp(-
delta_2/T[j-1]) ) - (B*T[j]^4 + (A*T[j]^(3/2)) *(exp(-delta_1/T[j])) + C*exp(-delta_2/T[j]) ) )

(((T[j-1] - T[j]) * ((kx(average(x[j-1],x[j])))) * A_c) / delta_y )     + (((T[j+1] - T[j]) * ((kx(average(x[j+1],x[j]))))
* A_c)   / delta_y)= 0

End                                                    "This loop sets the He3 concentration at every
node except Node 1 and Node N, based on the variation of conductivity with concentration."
```

Numerical data, however, is not yet available, as the conductivity k depends on concentration, the concentration at each node depends on that of the previous node, and the concentration for N_1 is not yet set.

An empirical relationship has been established between specific molar volume of ^{3}He in ^{3}He - ^{4}He solution, v, (units of m^3 ^{3}He-^{4}He solution/mole ^{3}He) and concentration of ^{3}He, x,

$$v = \frac{E}{x} + F + Gx^2 \tag{2.3}$$

with fit parameters

```
E = 27.58 [cm^3/mole] * convert(cm^3/mol, m^3/mol)
F = 7.60 [cm^3/mole] * convert(cm^3/mol, m^3/mol)
G = 1.65 [cm^3/mole] * convert(cm^3/mol, m^3/mol) [39]
```

The initial concentration of helium for the entire system x_{ini} has been set, the volume of the system is known, so the number of moles of ^{3}He in the entire system can be determined. The sum of the number of moles of ^{3}He in each slice must total to the initial total number of moles of ^{3}He. With this information Equation 2.3 may be used to now establish the ^{3}He specific molar volume v and hence the ^{3}He molar concentration x at node N_1 (whether at the large or small volume), node N at the opposite end of the diode, and through the capillary.

```
v_ini = ((E/x_ini) + F + G*x_ini^2)   "Specific molar volume of He3; that is, volume of He3-He4 solution
that contains one mol of He3 with He3 molar concentration (x_ini) set at 'concentration'; Radebaugh
Eq(5)[40]"

vol_tot /v_ini = n3_tot                                   "Determine total number of moles of He3 in
system with given molar concentration of He3."
```

```
v[1] = ( E/x[1]) + F +G*x[1] ^2                    "Radebaugh eq(5)[40].  This line in the program determines the concentration at node [1], the hot end reservoir"

vol_res_hot/ ((v[1]+v[2])/2) = n3_slice[1]          "number of moles of He3 in hot reservoir -- average the molar concentration at nodes [1[ and [2] to estimate He3 molar concentration in slice [1], the hot reservoir"
vol_slice[1] = vol_res_hot

vol_slice[S] = vol_res_cold
v[S] =  E/x[S] + F +G*x[S] ^2
v[N] = E/x[N] + F +G*x[N] ^2
vol_res_cold/ (( v[N-1] + v[N])/2) = n3_slice[N-1]          "number of moles of He3 in cold reservoir -- average the molar concentration at nodes [N] and [N-1] to estimate He3 molar concentration in slice [S= N-1], the cold end reservoir"
{vol_res_cold/  v[S] = n3_slice[S]}

"Establish the number of moles of He3 in each slice of the capillary from slice [2] (the hot end of the capillary)  to slice [S-1]  (the cold end of the capillary), exclusive of the reservoirs."

Duplicate i = 2, S-1                                "note, N-2 = S-1"

vol_slice[i] = vol_cap/(S-2)
v[i] = E/x[i] + F +G*x[i] ^2
vol_slice[i]/ ((v[i] + v[i+1])/2) = n3_slice[i]

{vol_slice[i]/ v[i] = n3_slice[i]}
End

sum(n3_slice[1..S]) = n3_tot                        "the sum of the number of moles of He3 in all the slices -- hot end reservoir, capillary, cold end reservoir -- must equal the total number of moles of He3 defined above to be in the capillary and reservoirs"
```

To determine the heat flow in the ON or OFF states the end volumes and capillary were described as a resistance network, with the effective resistance, R_{eff} taking all the resistances in series. For the capillary, it was divided into S-2 equal lengths – again S, the number of slices in the entire system including the end volumes is one less than N, the total number of nodes. So the capillary contains S-2 equal lengths, denoted for this part of the EES model as Δ_y.

$$R = \frac{L}{kA_c} \tag{2.4}$$

and

$$k_i = \frac{k_i + k_{i+1}}{2} \tag{2.5}$$

that is conductivity for the resistance for each slice is evaluated with the average of the conductivities at the nodes at either end of that slice. The resistances for the two end volumes are evaluated separately. In the EES code given here their actual lengths and cross-sectional areas from the switch built for this thesis are employed.

The heat flow in W is denoted by $\dot{q}$, either $\dot{q}_{HC}$ ('hot large, cold small') for the OFF state; or $\dot{q}_{CH}$ ('cold large, hot small') for the ON state.

$$\dot{q} = \frac{\Delta T}{R_{eff}} \tag{2.6}$$

The heat flux in W/m^2, denoted by q, is found by dividing the heat flow by the cross sectional area of the capillary.

```
"Resistance Network"

Duplicate i = 1, S
ky[i] = kx(x[i]) * 1[W/m-K]                                   "conductivity (k, W/m-K], at each node, units
added; so this is k as a function of location, y, the y-axis moves along the capillary away from the initial
hot end"
dT[i] = (T[i+1] - T[i])                                       "define dT as the change in temperature from
node to node along the y-axis, moving away from the initial hot end"
R[i] = delta_y/ (A_c * ( (ky[i] + ky[i+1]) / 2 ) )

End

"Small volume"
L_sv = .004[in] * convert(in,m)                               "length of small volume -- that is, its depth"
ID_sv = .593[in] * convert(in,m)                              "ID of small volume"
Ac_sv = (pi/4) * ID_sv^2                                      "cross-sectional area of small volume"

"Large volume"
L_Lv = 0.415[in] * convert(in,m)                              "length of large volume -- that is, its depth"
ID_Lv = .4685[in] * convert(in,m)                             "ID of large volume"
Ac_Lv = (pi/4) * ID_Lv^2                                      "cross- sectional area of large volume"

R_small = L_sv/ (Ac_sv *( (ky[1] + ky[2]) / 2) )              "small volume"
```

```
R_large = L_Lv/ (Ac_Lv *( (ky[N] + ky[N-1]) / 2) )          "large volume"

ky[N] = kx(x[N]) * 1[W/m-K]                                  "units added"


"Reservoirs and capillary, 'all' -- this includes all slices (both reservoirs plus capillary); ignore conductance of copper end volumes  containing helium as the helium conduction is so much larger than that of copper"

R_eff_all = sum(R[2..UU]) +  R_small + R_large               "R_effective goes from the first slice in the capillary (slice [2]) one slice to another slice through the last slice in the capillary (slice UU = S-1).  The large and small volume helium resistances are then added."
q_dot_HCall= (T[1]  - T[N]) / R_eff_all                      "Q_dot uses the temperatures from node 1, where the hot end volume contacts the ADR cold finger or the heat sink to node N, where the cold volume makes similar contact."
q_OFF = q_dot_HCall/A_c                                      "Heat flux, q_dot_HC normalized for cross-sectional area"
```

It is possible to select any section of the capillary for analysis. For example, with 1000 nodes (N = 1000) one may consider the capillary from node 880 to 980 (node 1 is always at the warm end) by writing

```
".88N to .98N"

R_eff_88%to98% = sum(R[HH8..II8])                            "HH = .8N, HH8 = .88N; II 8 denotes .98N."
q_dot_HC88%to98%= (T[HH8]  - T[II81]) / R_eff_88%to98%  "II81 denotes node .88N + 1 so the nodes enclose the slices."
q_OFF[6] = q_dot_HC88%to98%/A_c                              "Heat flux, q_dot_HC normalized for cross-sectional area"
```

The switching ratio for the capillary – all or part – is found by using Equation 1.8, with either heat flow or heat flux.

The model has the important difficulty that when the distance between T_h and T_c is varied, or when the number of nodes N is varied when greater than about 200, EES requires resetting some guess values. Experience has shown that the difficulties are usually with guesses for temperature

T, concentration x, and specific molar volume v. When N has been changed, usually resetting guesses for these three variables between the former N and new N suffices. When resetting T_h and T_c the guess values T must be reset for the entire capillary. In general in the ON state 95% of the capillary is within .12K of T_h while in the OFF state temperature falls at a steady rate through the entire capillary. As a practical measure it is simple to save versions of the model in ON state and OFF state with a range of values of N, T_h and T_c.

2.2 Results

The best test of the model will be when the two-capillary diode is tested. If it is correct that the diode fails with $\Delta T > 1.3$ K because of turbulence and the second superleak capillary remedies this, the model should predict the two-capillary diode's performance. This should include OFF state heat flux that remains low and has only small and smooth changes, and switching ratios on the order of 10^3 or greater. In addition the model should predict plausible distributions of temperature and ^{3}He concentration in the capillary in both ON and OFF states.

Also, the information supplied by Prof. McCammon about his experiments with diodes of various configurations (Figure 12) includes one data point that the model might be tested against. The main concern of the data in Figure 12 is to display the diode failures – when and how much the OFF state diverges from the expected, jumping up and so collapsing the switching ratio. But the trailing data point, (Figure 12, lower left) may plausibly represent OFF state data not yet disturbed by turbulence. As such the model should predict it

"Before the numerical solution can be used with confidence, it is necessary to verify its accuracy. The first step in this process is to ensure that the mesh is adequately refined. […] the

solution becomes smoother and represents the actual temperature distribution better as the number of nodes is increased" [41].

The model will only run to 1275 nodes before reaching the limit for the number of variables available in EES. By plotting heat flux vs. nodes and fitting the resulting curves as limbs of a downwardly opening parabola it is possible to determine where the slope becomes 0 (Figure 17). This is something of a 'rough and ready' procedure for estimating convergence. By this method the OFF state model should converge at about 1500 nodes. The ON state convergence varies with temperature, converging between 3600 and 4000 nodes.

Using the fit equations so obtained, the value for number of nodes where the slope reaches 0 is used as the x-value to solve the fit equation for Heat Flux (y).

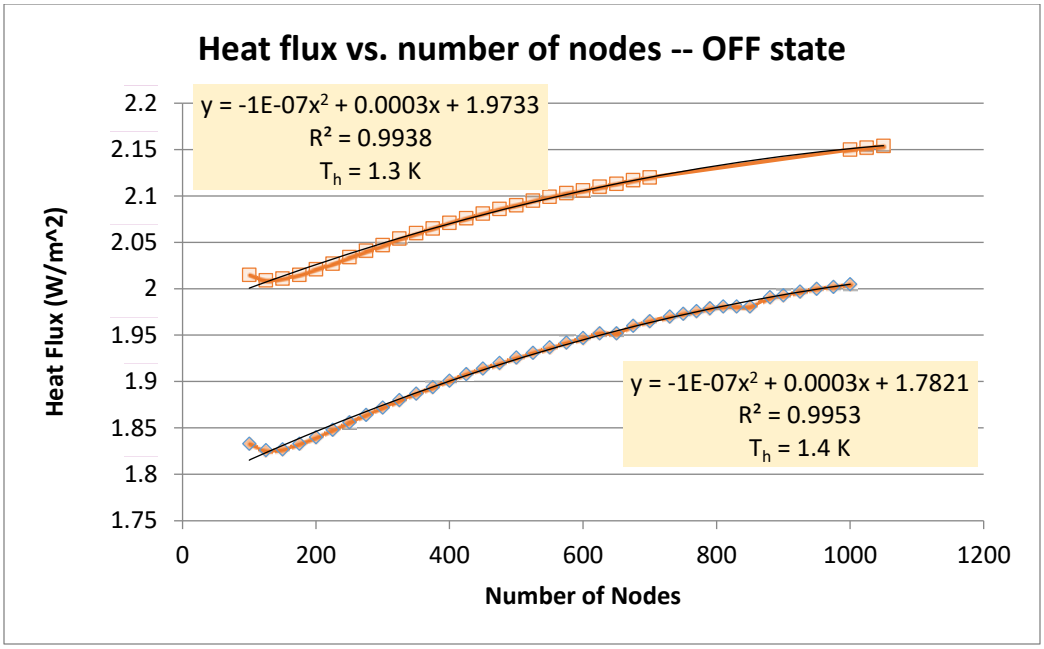

Figure 17a -- OFF state heat flux is predicted by extrapolating from results with increasing numbers of nodes up to 1000. *With T_c 50 mK and T_h either 1.3K or 1.4 K convergence is predicted around node 1500.*

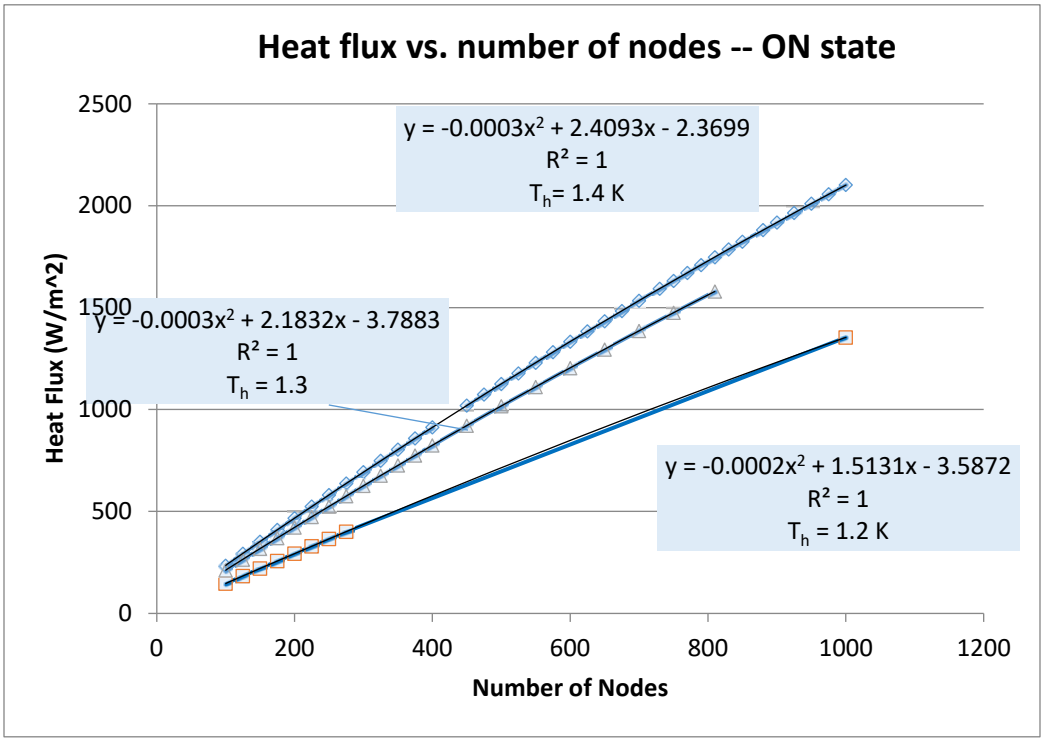

Figure 17b -- ON state heat flux is predicted by extrapolating from results with increasing numbers of nodes up to 1000. *With T_c 50 mK and T_h at 1.2K, 1.3K, or 1.4 K convergence is predicted between nodes 3600 and 4000.*

With this procedure, for the 'trailing' data point in Figure 10 the model agrees with the observed within 10% difference (Table 2-1).

Table 2-1 McCammon's experimental vs. EES predicted Off state heat flux

T_h (K)	Experimental (W/m^2) (Heat Diode, *x* .008, L 10.16 cm, ID .071 cm)	Predicted (W/m^2) (Heat Diode, *x* .008, L 10.16 cm, ID .071 cm)
1.3	2.37	2.20 (1500 nodes extrapolation)

In addition, varying ΔT from 1.0 K to 1.6 K, the model's OFF state heat flux prediction does not vary by more than 10%, changing only in small smooth steps (Table 2-2).

Table 2-2 Predicted OFF state Heat Flux with varying ΔT, extrapolated to 1000 nodes

T_h (K)	q (W/m^2)
1.0	2.16
1.2	2.25
1.3	2.15
1.4	2.01
1.5	1.87
1.6	1.82

To calculate a switching ratio at the same point, predicting that at T_h = 1.3 K the model will converge at 3640 nodes (Figure 17b), and the resulting switching ratio is 1805, a plausible number. "The ratio of conductivity in two directions has been observed to exceed 10,000 to 1 at a temperature of 1° and above, although this ratio is a function of the temperature difference across the switch" [35,36].

The model returns reasonable results for distribution of temperature and helium concentration within the column. For temperature, in the ON state most of the ^{3}He is flushed into the large cold reservoir; the capillary has high conductivity and most of the column is at T_h. In the OFF state ^{3}He is flushed toward the small reservoir, too small to contain it, and remains in the capillary, impairing conduction; temperature falls gradually through the entire capillary

length. For ^{3}He concentration, In the ON state (top) most of the ^{3}He is flushed into the large cold reservoir. Compared with the OFF state (bottom) relatively little remains in the capillary. In the OFF state the concentration of ^{3}He in the right hand two-fifths increases with rising warm end temperature, predicting that the diode should have a switching ratio that increases steadily with ΔT.

Figures 18 and 19 agree well with similar plots produced in Schmidt's model [38].

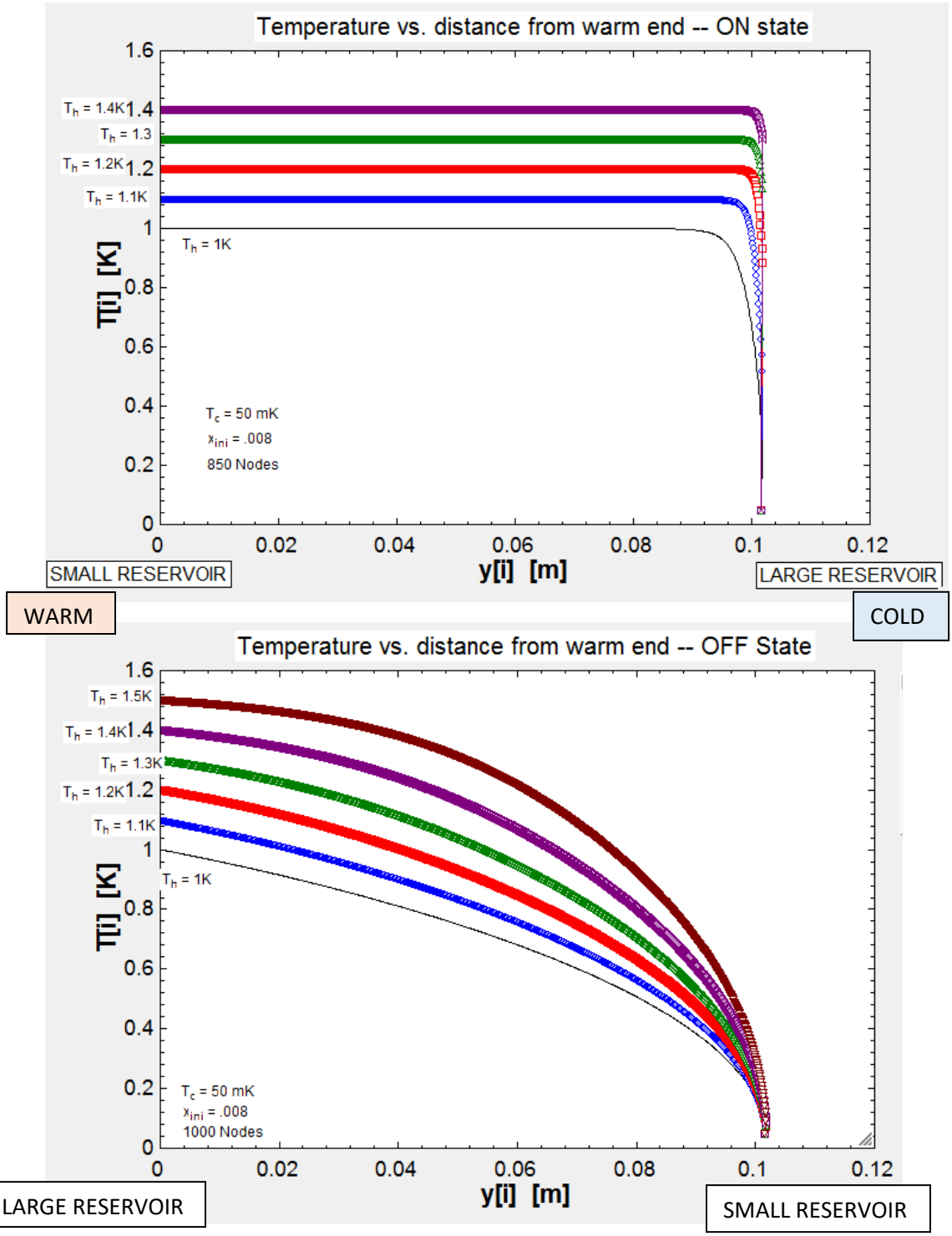

Figure 18 -- EES model prediction for temperature in the capillary. *In the ON state (top) most of the 3He is flushed into the large cold reservoir ; the capillary enjoys high conductivity and most of the column is at T_h. In the OFF state (bottom) 3He is flushed toward the small reservoir, too small to contain it, and remains in the capillary, impairing conduction; temperature falls gradually through the entire capillary length. Note that on these plots the distance is shown left to right from the warm end. The physical end volumes are reversed between the two plots.*

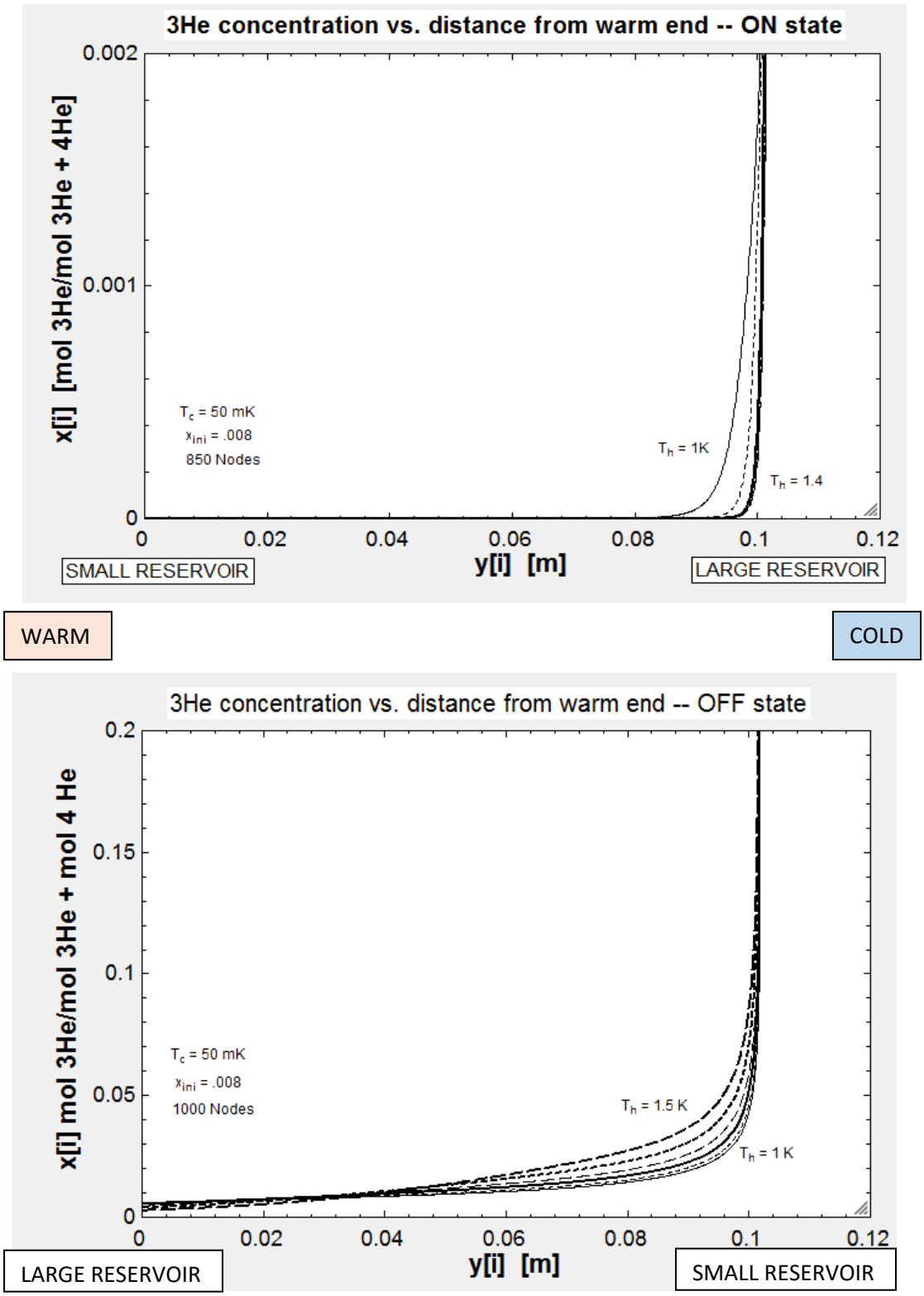

Figure 19 -- EES model prediction for 3He concentration in the capillary. *In the ON state (top) most of the 3He is flushed into the large cold reservoir. Compared with the OFF state (bottom) relatively little remains in the capillary. In the OFF state the concentration of 3He in the right hand two-fifths increases with rising warm end temperature, predicting that the diode should have a switching ratio that increases steadily with ΔT.*

3 DESIGN AND FABRICATION OF A TWO- CAPILLARY DIODE HEAT SWITCH

3.1 Copper end pieces and steel capillary

A two-capillary heat diode was fabricated. Dimensions were selected for the large and small volumes and capillaries to approximate those used by D. McCammon. From his capillary lengths the shortest was selected (10.16 cm = 4 in). For the superleak it seemed likely to be easier to pack a fine powder into a 4 inch capillary than into a 28 inch one. The diameter was selected to match the 'trailing edge' point in Figure 12, 0.071 cm. The ^{3}He concentration for that data point will also be used, 0.008.

The design described by drawings from D. McCammon required silver brazing skills beyond those the author could acquire in the time available. A modified version of the end volumes, but with the same interior spaces, was produced instead (Figure 20).

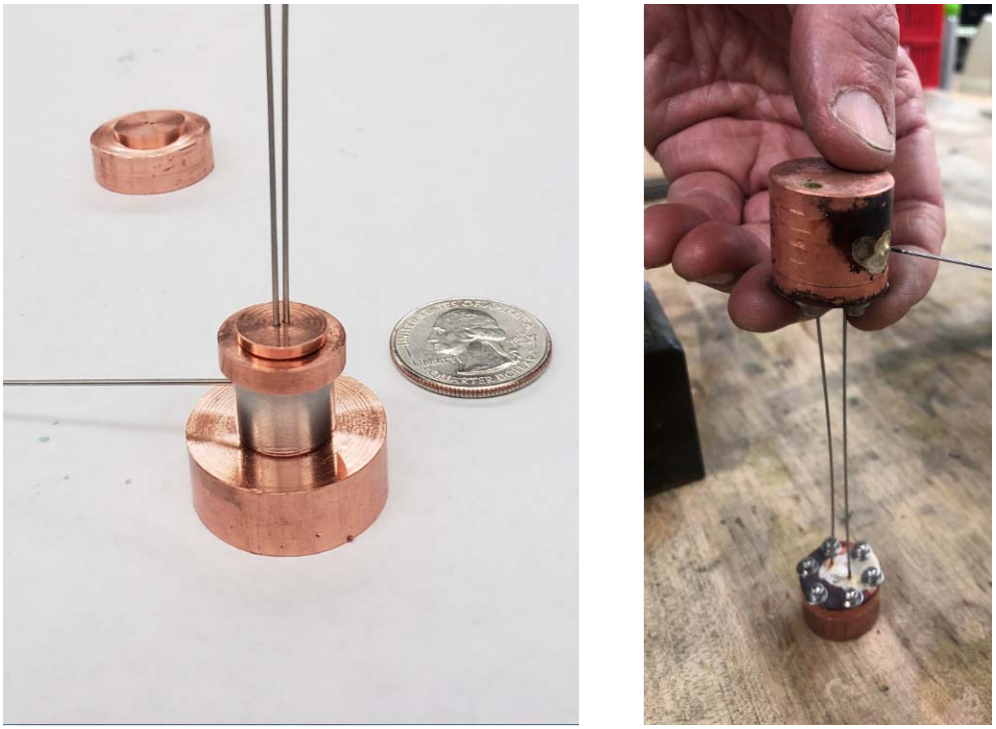

Figure 20 – The two-capillary heat diode*. Left: Parts of the two-capillary diode following McCammon's drawings before unsuccessful brazing. The upper volume rests in the background. Right: Modified design, completed. In both images a fill line capillary enters the large end volume. Photographs by Lindsey Thomas and Yanan Wang.*

The end volumes were machined from ETP copper cylinders. Both bottom and top volumes were formed in the same manner. A copper cylinder was cut into two cylinders. One of them was machined so that it had a raised cylinder in its center surrounded by a flat rim (Figure 21, left). The other piece was milled so that it had a hollow cylinder within it with a diameter that would exactly receive the raised center of the first piece when pressed in by hand. The diameters differed by .002". Six evenly spaced holes were drilled through the rims of these mated parts. In one of the pair the holes were tapped and steel helicoils were placed in the threaded holes. An indium wire ring (.04" diameter indium wire) was looped around the raised center and the two parts were pressed together by hand, then screwed together with stainless steel screws to form a vacuum seal. Just before this was done all surfaces that would contact the indium wire were dipped in "The Works" Toilet Bowl Cleaner (9.5% HCl) for about 60 seconds, sprayed with distilled water, and scrubbed with Scotch Brite. A Belleville washer was placed on each screw to ensure continued sealing when the diode is cooled to very low temperatures (Figure 21, right). The dimensions of the resulting end volumes to contain the liquid helium are given in Table 3-1.

Table 3-1 Dimensions of the interior space of the end volumes

	Diameter (in)	Length (in)	Volume (in^3)
Large volume	0.4685	0.345	0.0595
Small volume	0.593	0.004	0.0011

A hole in the bottom piece of the large volume was drilled and tapped and threaded with a helicoil insert. It will be used to attach the switch with a stainless steel screw to a 1K heat sink. In the top piece of the small volume three similar holes were made to affix copper wires to attach it to an ADR cold plate.

Figure 21 – Each end volume was formed from two pieces of milled ETP copper that were fitted together*. One piece has a raised center (left), its mate a milled hollow. An indium wire was looped to form a vacuum seal (left). The two mated pieces were pressed together by hand, then screwed down in six places (right). Belleville washers ensure continued sealing at low temperatures. Photographs by Yanan Wang.*

The ratio of large to small volume is similar to that used by McCammon, about 50. This is important since as the large volume: small volume ratio diminishes, at some unknown lower value the switching ratio will decline at any ΔT. It is known that whatever large:small ratio McCammon employed will allow the diode to work successfully.

To form the small volume with a thickness of only 0.004" the height of the raised rim and the depth of the matching milled-out space were made the same. Then as the two parts were screwed together a feeler gage was used to control the thickness of the gap. After the first tightening of the screws 24 hours were allowed for the indium to flow before the final tightening.

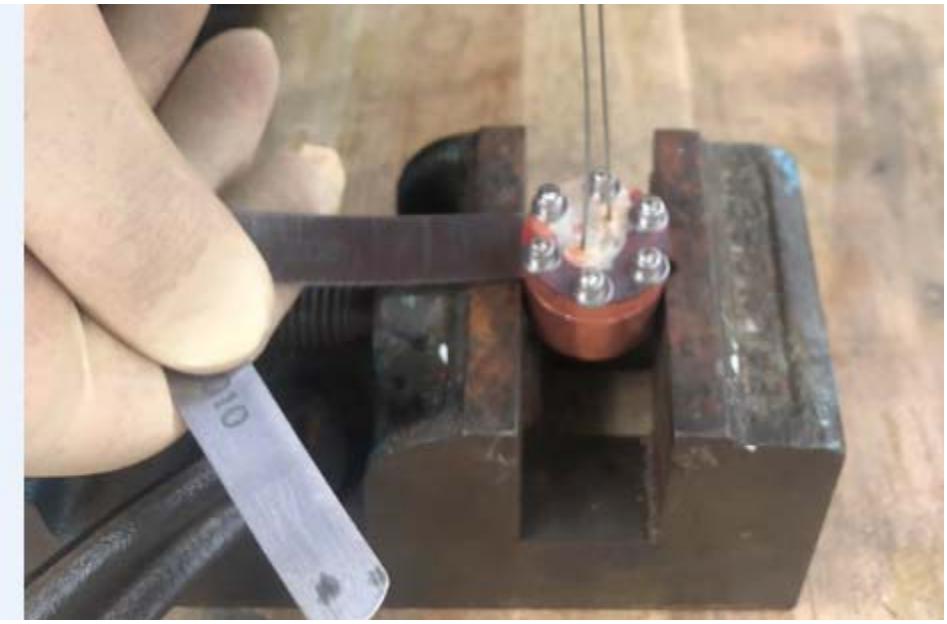

Figure 22 – Obtaining the .004" chamber thickness of the small volume*. A feeler gage was used with tightening of the screws over the indium seal. Photograph by Yanan Wang.*

The stainless steel capillary used by McCammon was specified with OD .031", ID .027" . Capillary tubing was obtained from Eagle Stainless Tube and Fabrication, Franklin, MA, with the same wall thickness, but OD .032", ID .028". The thin walls are desirable to minimize parasitic conduction in the switch beside the helium.

To complete this exposition, it should be noted that the thin-walled capillary could be readily cut with a wire cutter, and the resulting pinched end restored to roundness by gentle squeeze of a pliers followed by insertion of stiff steel music wire (diameter .025").

3.2 Silver Brazing

The capillaries and fill line were attached to the copper end pieces by silver brazing using Safety-Silv 45 alloy. Attaching the thin-walled steel capillaries (wall thickness .002") to the much larger copper pieces required finding the right temperature and shielding the steel parts from applied flame while heating the copper. Several combinations of acetylene torch, propane torch, and MAP gas were tried. The successful combination involved shielding the steel from direct application of heat with a woven calcium silicate strip while applying MAP gas from beneath the copper part (Figure 23; cf. Figure 21, right).

Figure 23 – Silver brazing required protecting the thin-walled steel capillaries from direct heat. *MAP gas was applied from below the calcium silicate cloth, silver brazing above. Al foil holds wet paper in contact with the capillaries to dissipate heat. Photograph by Yanan Wang.*

3.3 The Superleak -- Literature review; filter material selection; construction

3.3.1 Literature Review

Superleaks made from powder-filled tubes have been in experimental use for eighty years but the literature is not explicit on the details of how to construct one. Nevertheless a review of literature provided ideas for how to proceed and raised several issues. These include selection of a superleak powder, selection of a particle size, and ensuring uniform packing in an opaque capillary.

Allen and Misener in their early work on superfluid helium provide a good starting place. "During the course of the experiments on the flow through very fine capillaries, measurements were made on the flow through a tube packed with fine powder. The tube had a bore of 3 mm. and a wall thickness of 3 mm. A length of 10 cm was tightly packed with jewellers' rouge. The process of packing consisted in pouring in successive small quantities of the rouge and tamping it down each time with a steel rod. Before the powder-filled tube was forced through it, both to remove the air from the interstices in the powder…"[42].

Jewelers' rouge (Fe_2O_3) is a sticky red powder that adheres to every surface and is difficult to remove even with soap, abrasives, or acetone. It does not pour readily. In a photomicrograph of jeweler's rouge particles that are several microns in average diameter the particles appear covered with protrusions and jagged edges [43]. It might be possible with a 3 mm diameter aperture to insert a funnel, fill it with jeweler's rouge, and tamp it down with a steel rod inserted through the funnel. But for the capillary used in this thesis with an inner diameter of .028" (0.71 mm) pouring the rouge was not practical.

Two papers with relatively small diameter superleak capillary IDs (2mm, 2.5 mm respectively) mention jewellers' rouge superleaks without fabrication details. "... [A] german

silver tube *B* (28 mm long, 2 mm diameter) filled with a very fine Fe2O3 powder" [44]. "The two sections of the capillary were tightly packed with jewellers' rouge… The rouge was held in position by small pluge of cotton-wool at each end…" [45].

A review article on superfluid helium in porous media states "Traditional materials for porous media studies have been the fine grained powders such as lampblack (soot), jeweler's rouge, and the different grades of industrial abrasive powders…These materials have found frequent use as superfluid filters where the superfluid is free to flow through the filter while impurities such as ^{3}He atoms and the normal fluid excitations are clamped by viscous forces within the pores of the filter" [46]. Again, no fabrication details.

One article mentions a detailed packing procedure designed to ensure a constant packing fraction in a vessel with 6 mm ID, using Al_2O_3 1μ powder "…pressed in six cumulative layers… At each completion of a layer, pressing pressure was adjusted such that the packing fraction remained constant…The homogeneity and absence of large cracks were checked by an X-ray tomography technique with resolution of 11 μm" [47]. This helpfully raises the issue that there must be a way to ensure uniform internal packing in an opaque capillary.

A succinct article reviews using various powdered rocks for superleak filler, but with no fabrication details [48].

One article was found mentioning a superleak with a 0.7 mm ID capillary. "The superleak is made by compressing the powder in a chamber (0.7 mm in diameter and 1 cm long), drilled in a brass block, with a powder filled entrance on each side in order to restrict the critical effects to the narrow part of the superleak"[49]. The diagram gives some idea of how the

capillary was filled, but lacks detail. For example, did the ends need to be plugged initially? How was uniformity of packing ensured in an opaque object?

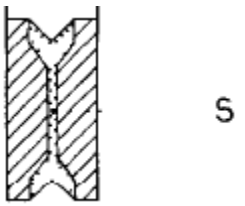

Figure 24 – A narrow capillary (0.7 mm) drilled in a brass block for a superleak [49].

Three of the same authors show another set of superleaks filled with jewelers' rouge, again with an initial funnel-like opening apparently drilled into a solid object. The material used for the capillaries is not mentioned. "The apparatus consists mainly of two superleaks, L_1 and L_2, 6 and 40 cm long respectively and 0.1 cm in diameter"[50].

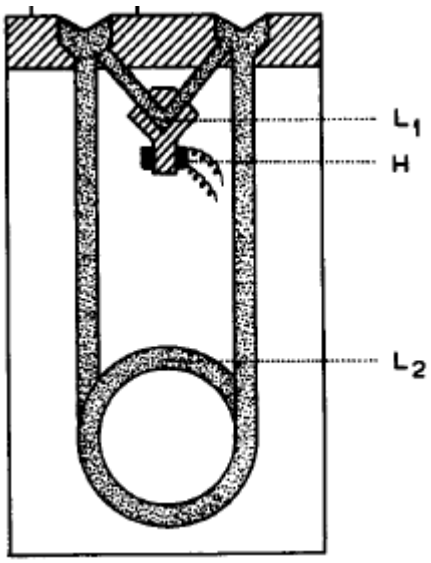

Figure 25 – Superleaks 1 mm ID, 6 cm and 40 cm long. *No details are given as to how they were filled with jewelers' rouge [50].*

A procedure using ultrasound to help advance the particles into the capillary was investigated but seemed impractical for the few capillaries needed [51].

3.3.2 Filter material selection

Porous Vycor glass is now a superleak of choice, but it is not available in the small diameter required. [52]

As this thesis is primarily about the functioning of a heat diode rather than helium flow through porous materials, jewelers' rouge was selected for the filter as being the most-used substance found in the literature review. It was used by the original English and Dutch researchers in this area, and is mentioned in patents held by the US Atomic Energy Commission[53] and NASA[54] so appeared a conservative choice. It is notable that an article by Japanese authors [47] states that packed powder aluminum oxide ("PAP-SL", Al_2O_3) "is popular in the study of superfluid 4He…"

The articles cited in the literature review mention particle sizes < 1 μ. But the NASA patent just mentioned is explicit that particles of sizes between 10 μ and 15 μ are sufficient to filter out ^{3}He from superfluid ^{4}He. "… any micro-porous filter having a pore size which is effective to pass superfluid without passing impurities may be used. Given the concept of the present invention, only routine experimentation is required to determine operable filters. The iron oxide filter bed **21** [illustration in patent] employed in the foregoing example was prepared from London Optical Red Rouge i.e., particles having a size of about 10 – 15 microns… "[54].

Considerations of price, availability in a relatively small quantity, and safety led to selection of Atlantic Equipment Engineers 1-5 μ 99.9% pure at $12.15/lb. Finer particles were available at a much higher price (.05 μ at $31.00/1.25 g) but would have required use of respiratory protection with no obvious gain in filtering function for this application. The MCDS sheet provided by Atlantic did not require respiratory protection but did mention danger of long-term inhalation so that the fabrication of the superleak was done under a ventilation hood.

3.3.3 Construction

It is not possible to pour the jewelers' rouge powder into the .028" (0.71 mm) ID capillary for the heat diode. But powder could be placed into the capillary by placing a small powder-filled cup on its side, or a small mound of powder on a hard surface, and dipping the capillary into it, then tamping down the contents of the capillary with a stiff steel music wire having diameter slightly smaller than the capillary, as shown in Figure 26. Initially a second piece of music wire was inserted half way up the capillary to function as a 'blocking tool' so that the powder could be tamped against it. It was found that once a small amount of powder had been pressed into the capillary in this manner the 'blocking tool' could be removed and the powder would not be moved or made to fall out of the bottom of the capillary by subsequent tamping. This led to the conclusion that no cotton wadding or other coverings would be needed to keep the powder in place inside the superleak.

Figure 26 -- Filling a capillary with jewelers' rouge. *(Left) a capillary (ID .028") is pressed into a part of a cup containing the powder. Here the capillary is guided by a plastic tube also containing powder. (Center) The powder is about to be tamped in with the piece of music wire (OD 0.25") on the right. (Right) The powder is tamped in. Photographs by Lindsey Thomas.*

By this method a four inch capillary could be filled within several hours. Then, however, another student working for a time on this project using this method appeared to have filled the capillary in 30 minutes. The capillary was cut apart and numerous gaps were discovered. The stickiness of the powder had made it seem that that the opaque steel capillary was continuously filled, when in fact it was not. Without resorting to X-ray tomography a method was needed to ensure continuous and relatively uniform filling and tamping. A method was developed whereby two separate fabricators would follow exactly the same procedure for two or three capillaries, and weigh them before and after. If the results converged on about the same weight for the jeweler's rouge put into a capillary it seemed reasonable to conclude that it had been properly filled.

A fabricator would dip the end of a capillary into a mound of powder that was on a hard surface. The fabricator would take three dips, in each case touching the capillary to the hard surface; and would then tamp ten times. After ten or some fixed number of sets of this operation they would insert a music wire into the capillary and measure and record the distance filled. This process would be repeated until the capillary was completely filled – first one half, started off

with the ‘blocking tool’ in place, then the other half. In general it was found difficult to achieve a uniform result. Table 3-2 shows a typical set.

Table 3-2 Length of powder inserted into the superleak

Sets of dips/tamping	ΔL (in)
First Half	
10	.10
20	.22
30	.22
40	.32
50	.34
60	.52
Second Half	
10	.24
20	.28
30	.28
40	.28
50	,34
60	.32
70	.40

After numerous trials several 4” capillaries were produced with powder masses between 0.096 g and 0.119 g. Using the density for the powder listed by the manufacturer, 5.24 g/cm^3 ,yielded a packing fraction of about 0.5 which seems plausible. There may nevertheless be gaps within the superleak capillaries.

When tamping the powder, capillaries would frequently buckle and break – the tamping wire would often catch on a bit of powder inside the capillary. To prevent this the individual capillary, or the entire heat switch, was encased in a temporary support structure for the tamping operation. (Figure 27). Using a rotating motion while tamping also seemed to reduce bending stress on the capillary.

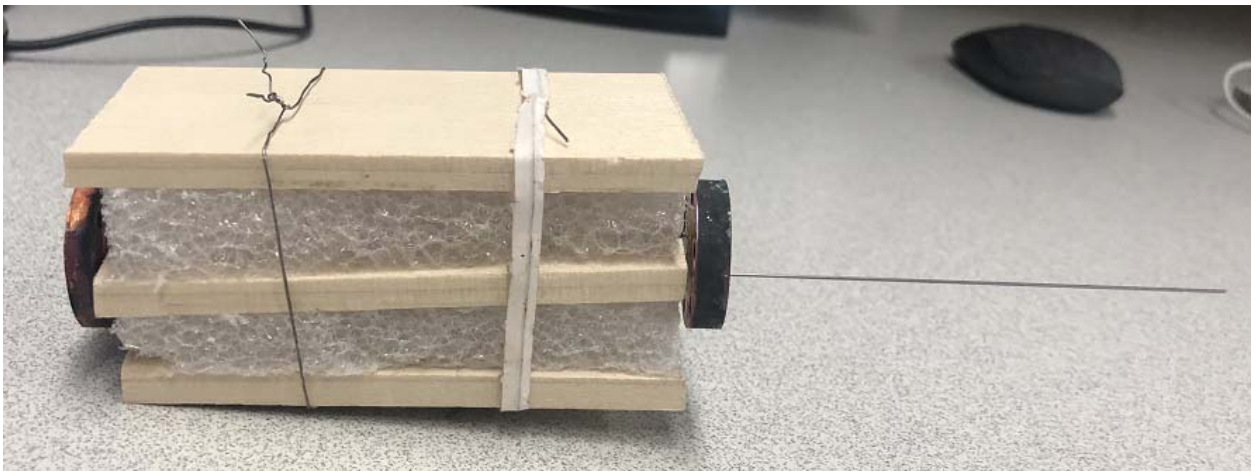

Figure 27 – Entire heat diode in temporary support structure*. Music wire was inserted into the non-superleak capillary to strengthen it. Earlier in the process while the superleak was being filled a piece of it protruded from the copper end piece, which was not yet sealed to its mating part. This protruding piece of capillary was the one dipped and tamped. Photograph by Yanan Wang.*

The jeweler's rouge was packed into the superleak capillary only after the capillaries and copper end pieces had been silver brazed together, but before the copper end pieces had been sealed to their respective mates. It would have been physically easier to fill the capillaries and then braze them. Photomicrographs were taken of capillary ends that had been packed with jeweler's rouge and then placed in an acetylene flame (Figure 28). It could not be established from these whether or not the brazing temperatures would seal the pores and render the superleak useless. So the less convenient order of steps was selected, brazing then filling.

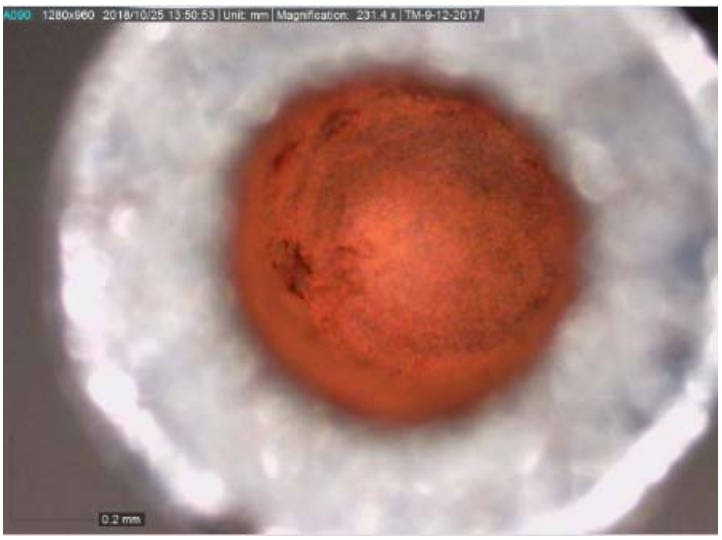

Figure 28 -- Steel capillary (ID .028") filled with jewelers' rouge and heated in an acetylene torch flame, magnified 230 x.

3.4 Leak Testing

An ASM 142 leak tester was used in 'sniffing' mode. Several versions of the silver brazed and fully assembled switch failed to pass leak testing. In all cases there was a small black patch of about ¼ in length on one of the capillaries near a braze joint. But when the technique described in Section 3.2 was used, and a final slight soldering with 50-50 Pb-Sn solder was used to coat 1" on one of the capillaries near the joint, all four junctions of capillary to copper (Figure 21) resulted in no measured change from a background reading of 2.0×10^{-10}. Indium gasket joints between the mated end piece copper cylinders remained at a background reading of 4.0×10^{-9}. A bubble of helium was puffed on each test spot using a hypodermic needle.

4 EXPERIMENTAL METHODS

4.1 Description of the 1K Facility

The two-capillary heat diode will be tested in the 1K facility at the UW – Madison Solar Energy Laboratory. The facility is described in detail by its designer and builder Amir Jahromi. [55] [56]. A dewar is pumped to a low vacuum by a turbomolecular pump backed by a dry diaphragm pump. A Cryomech pulse tube model 410 cryocooler cools two stages, one to 30 K, the second to 4 K. Inside the dewar a custom-built copper 1 K pot works on an open cycle. The cryocooler brings the 1 K pot to a sufficiently low temperature that it can function as an evaporative cooler for liquid helium (Section 1.1). An external rotary vane pump pulls on the 1K pot keeping the pressure sufficiently low to keep it at about 1.4 K. The 1 K pot is attached to a 1K plate which serves as a station for experiments (Figure 29).

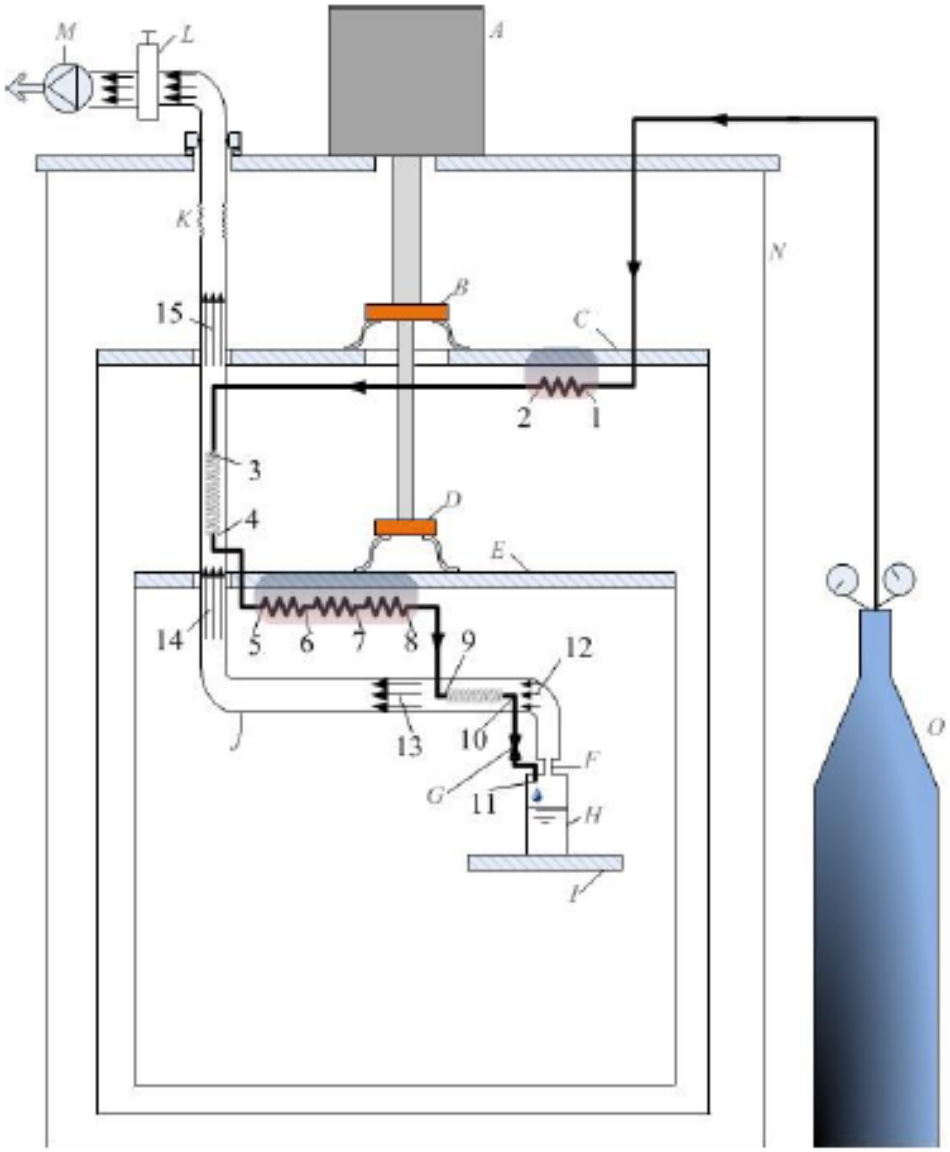

Figure 26. An overall schematic of our 1 Kelvin facility (Helium is traced by numbers, Components are labeled by letters, HX: Heat Exchange(r)); *A*: PT-410 Cryomech cryocooler equipped with vibration isolator, *B*: Cryocooler's 1st stage HX, *C*:1st stage HX platform and shield assembly connected to *B* via heat straps [16], *D*: 2nd stage HX, *E*: 2nd stage HX platform and shield assembly connected to *D* via heat straps, *F*: Superfluid film killer, *G*: Capillary (fixed J-T valve), *H*:Copper 1 Kelvin pot, *I*: 1Kelvin plate, *J*: evacuated exhaust line, *K*: bellows, *L*: Vacuum isolation valve, *M*: SogeVac SV 25-B rotary vane vacuum pump, *N*: Dewar, *O*: Helium reservoir equipped with a 2 stage pressure regulator.

Figure 29 -- An overall schematic of the 1K facility. *Note H (1K pot), I (1K platform) and M (rotary vane pump) [56].*

4.1.1 Pump Sizing

The volume of gas the rotary vane pump can remove per unit of time (pump speed) is directly related to the temperature in the pot (Figure 28).

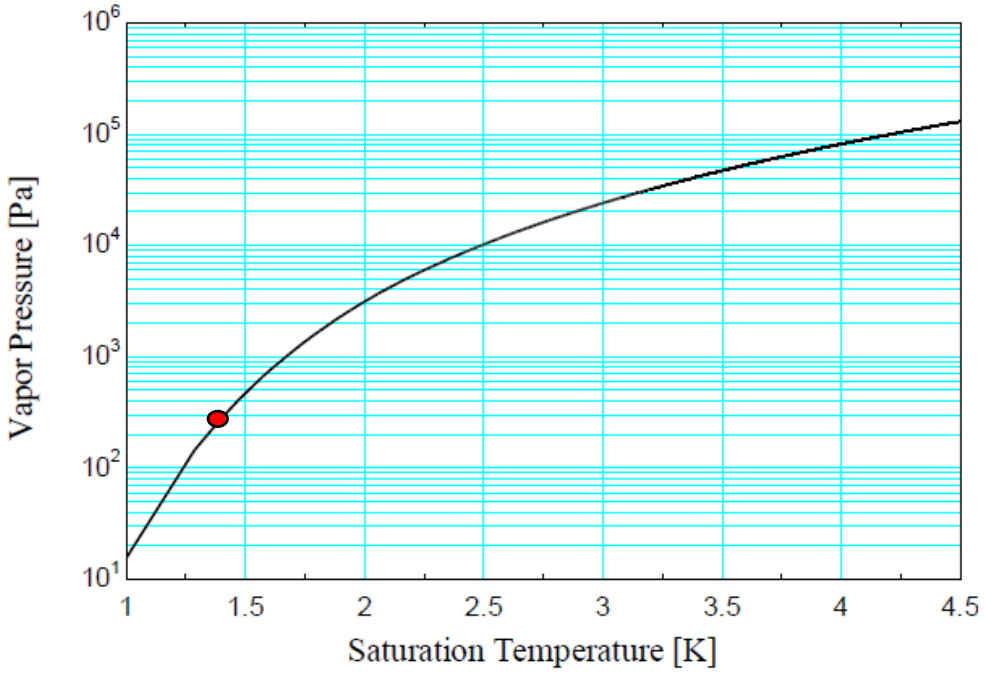

Figure 30 – Helium vapor pressure vs. temperature. *To achieve a saturation pressure of 1.4K a vapor pressure of 120 Pa is required. Adapted from [55]*

Helium reaches the rotary vane pump at room temperature so the volumetric flow rate of helium at the rotary vane pump is determined by

$$\dot{V} = \frac{\dot{m}}{\rho} \tag{4.1}$$

where $\dot{V}$ is the volumetric flow rate of helium at the pump, ρ is the density of helium at room temperature and pressure (0.3933 kg/m^3) and $\dot{m}$ is the flow rate for the system, fixed by the design at 7 x 10^{-6} kg/s. The pump speed as related to pressure is determined by [57]

$$S = S_{max}\left(1 - \frac{P_u}{P}\right) \tag{4.2}$$

where S and S_{max} are speed, and maximum speed, P_u is ultimate pressure. S_{max} and P_u are specified by the pump manufacturer.

The original SogeVac SV 25-B rotary vane pump motor had burned out from long use (Figure 2xx, M). It has been replaced with an Alcatel 2063 rotary vane pump which should provide adequate pumping capacity when in good operating condition. To achieve a saturation temperature of 1.4 K a vapor pressure around 120 Pa is required. A comparison of specifications and pump curves for the two pumps are shown in Table 4-1 and Figure (31).

Table 4-1 Rotary Vane Pump Speed and Pressure Comparison

	Ultimate pressure	Maximum speed
SogeVac SV-25B	50 Pa	25 m^3/hr (27.5 m^3/hr for He)
Alcatel 2063	0.021 Pa	85 m^3/hr (50 cfm)

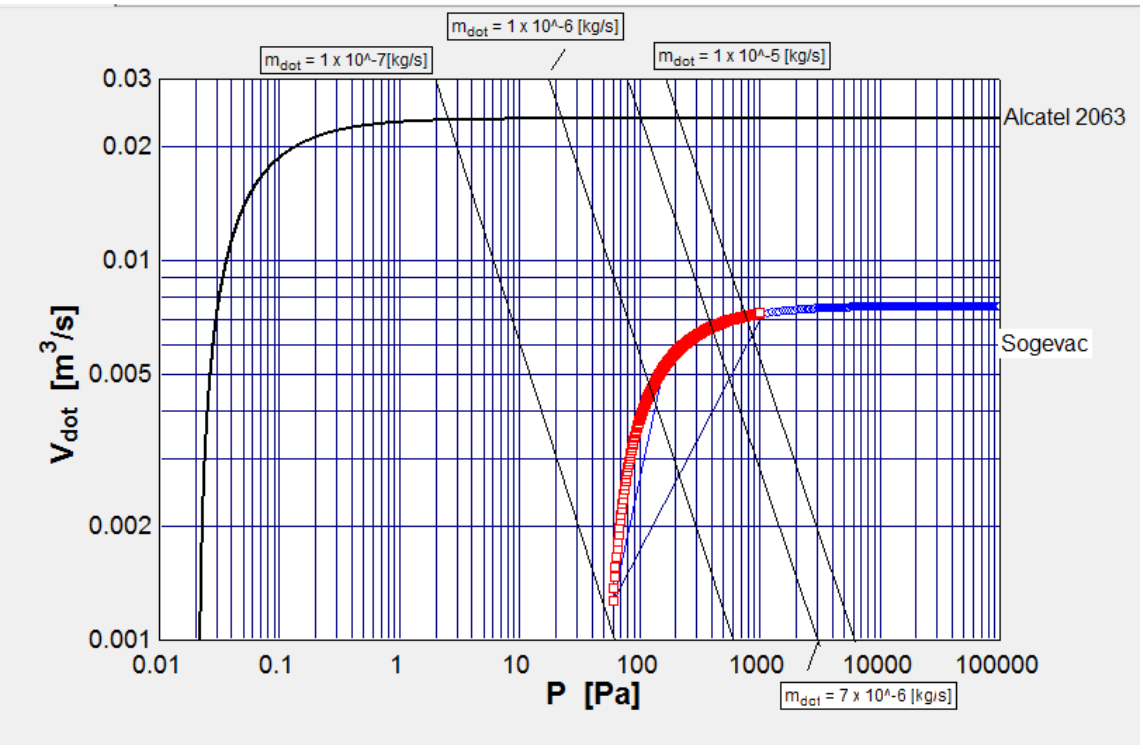

Figure 31--Pump speed vs. pressure. *The system operates at a mass flow rate of 7 x 10^{-6} kg/s, well within the capacity of the Alcatel 2063 pump as specified by the manufacturer.*

4.3 Thermometry and instrumentation

The 1K facility has two 44 Cryo-con temperature controllers that function as temperature monitors. Each provides four channel readings. They can also function as temperature controllers to operate heater loops for a platform within the dewar. Four Lakeshore DT-470 silicon diode temperature sensors (with accuracy of ± 1K at temperatures < 100 K) and two Cernox 1030 sensors (accurate to ± 25 mK at temperatures < 77 K) with minimum temperature 1.4 K are at present wired to the controllers. A Cernox 1030 sensor with a minimum temperature of 0.3 K (marked X57246) is also wired in. Available for use from the Physics Department is a Lakeshore GR-200A-30 germanium resistor thermometer calibrated to 50 mK.

Wires run into the dewar for heaters, thermometers, and the superconducting magnet for the ADR. Voltage and current are read, and can be controlled by a Keithly 2440 Source Meter. A maximum of 5 amps current and/or 30 volts can be provided. In one mode of operation the unit provides current and measures voltage. In the other it supplies voltage and measures current.

4.3 The ADR

4.3.1 Description

An ADR was loaned by Prof. Peter Timbie, UW – Madison Physics Department, for use in this experiment. It was built by Timbie in the 1990's for flight in a balloon borne telescope with a sister unit designed for the Space Infrared Telescope Facility (SIRTF) [58]. It was designed to be bolted to a cold plate inside a dewar and connected to a heat sink by an electromechanical heat switch. It has been mounted to the 1K plate in our 1K facility. The two-

capillary heat diode will take the place of the electromechanical heat switch, and will be placed between the ADR cold plate and the ADR thermal bus that is in turn attached to the 1K plate.

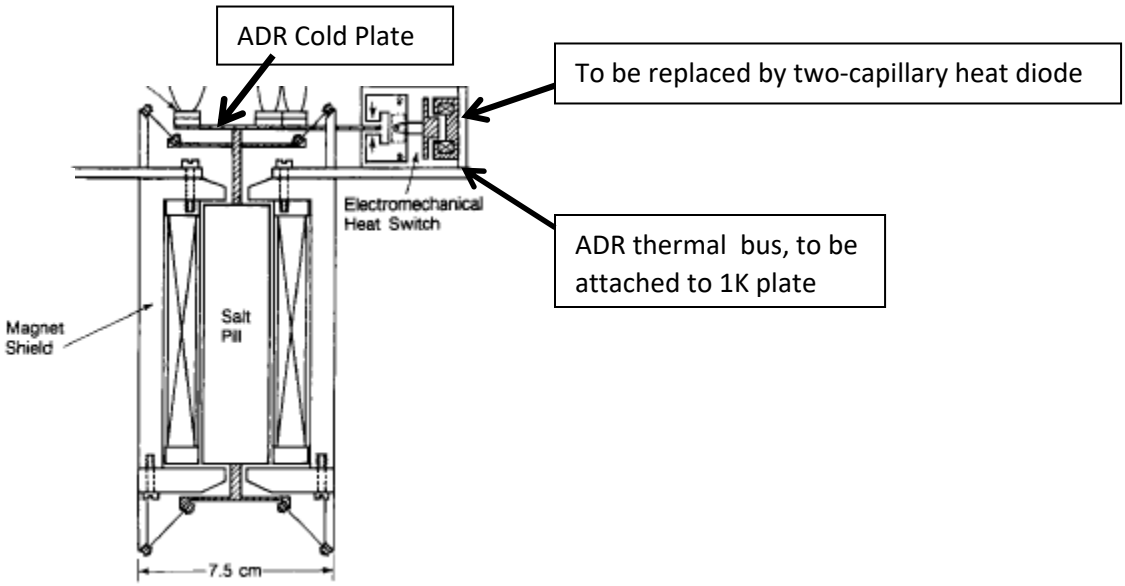

Figure 32 – Flight prototype ADR. *Parts of scientific instruments mounted on the ADR cold plate (top of the image) have been cropped. The length of the entire assembly is 22.9 cm (9"). Adapted from [58].*

The ADR paramagnetic salt pill is FAA. It was grown around 200 gold wires which are silver soldered to a copper post that goes to the cold plate to ensure good thermal contact between the salt and the cold plate. The copper post and copper thermal bus are also gold plated. The salt pill is sealed into a steel canister by stainless steel end caps held by epoxy to prevent dehydration of the salt pill. The hydrate in the FAA crystal provides essential physical separation between iron ions in the paramagnet which will not function if dehydrated. Tensioned Kevlar cords suspend the salt canister within the magnet without touching it. They are designed for the vibration of balloon flight and space launch [58][10].

To fit the ADR in the dewar a bracket assembly was made. A notched copper plate that goes around a steel support in the existing 1K facility was screwed to the copper 1K plate through existing holes. Steel helicoils were placed in the threaded holes in the 1K plate to support the stainless steel screws. A machined brass block functions as a clamp to hold the ADR thermal bus to the notched copper plate. The ADR weighs 5.9 kg (13 lb).

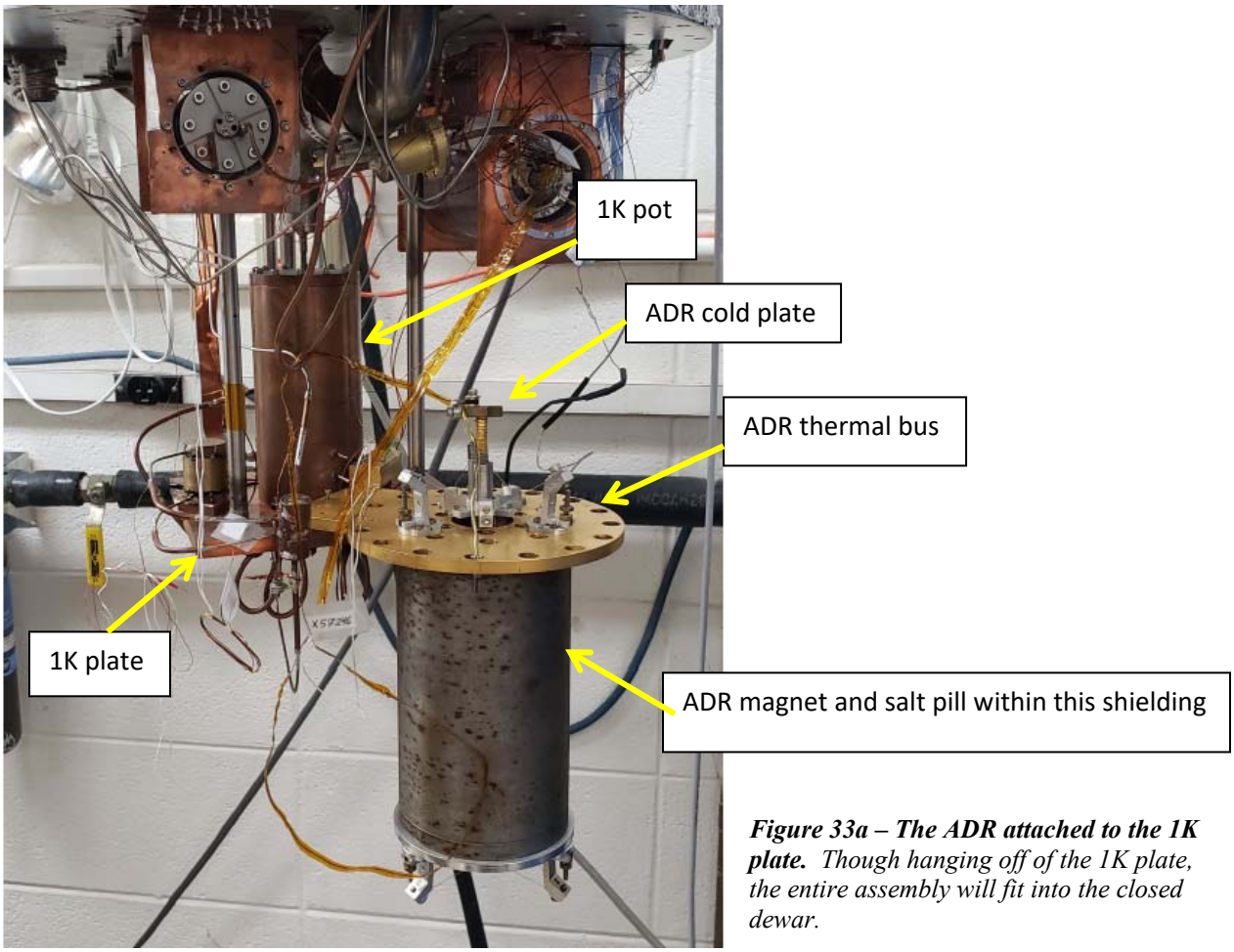

Figure 33a – The ADR attached to the 1K plate. *Though hanging off of the 1K plate, the entire assembly will fit into the closed dewar.*

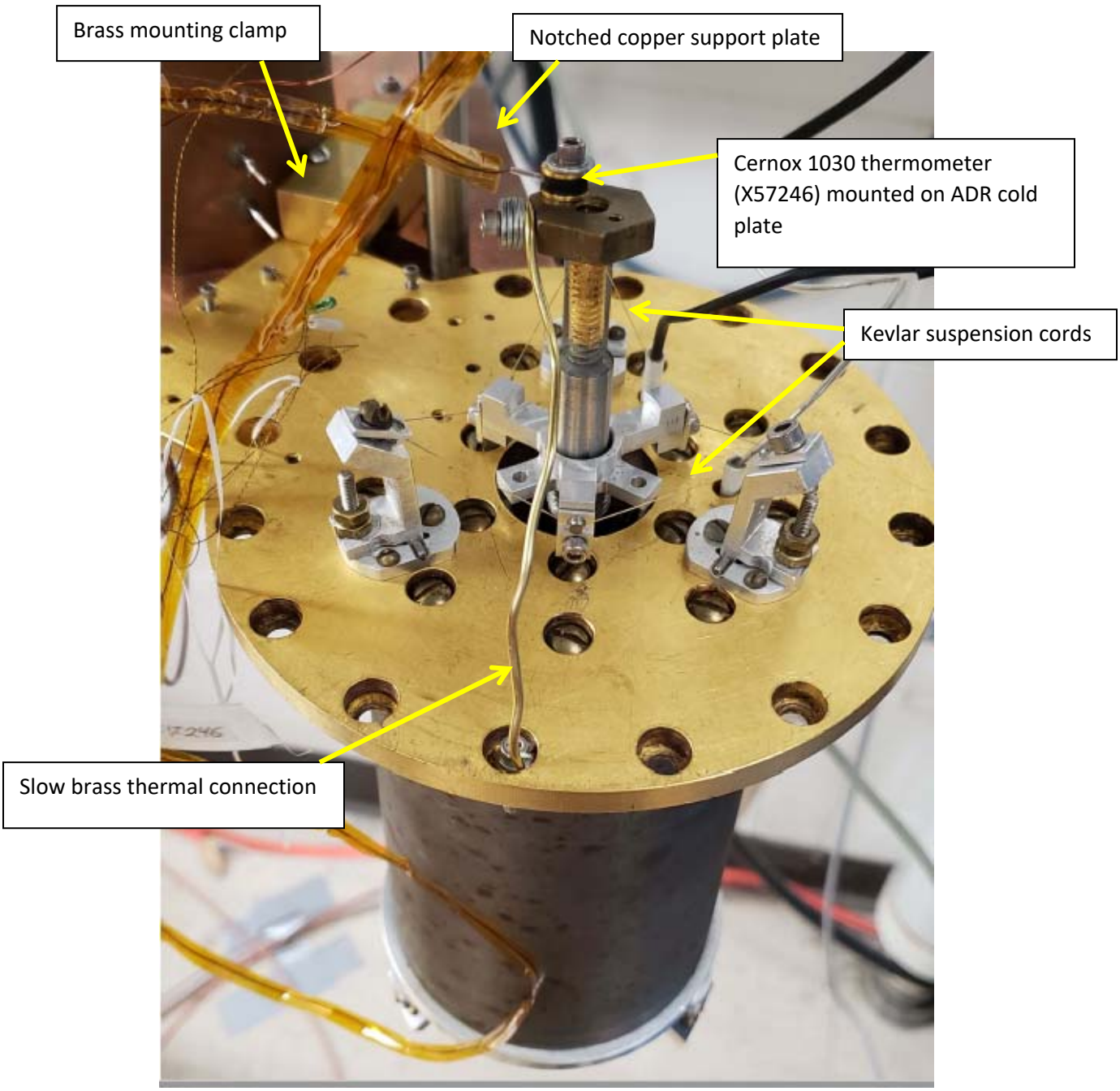

Figure 33b – ADR attached to the 1K plate (close up). *Photographs by Jennifer Detlor.*

4.3.2 Validation of ADR function

For this ADR to function the FAA salt pill must remain sealed in its steel canister. But its canister shows corrosion on the outside and so there was doubt that it would function. The most direct test would be to run it. Timbie applied 8 A current to the ADR magnet to get a magnetic field of 3 T. The 1K facility has a maximum current of 5 A yielding five-eigths that magnetic field, 1.9 T. Using Figure 3, at 1.4 K the change in *S/R* for a change in magnetic field from 0 T to 1.9 T is 1.3. Using the relation

$$q = mT\Delta S \tag{4.3}$$

it was calculated that the energy absorbed by the FAA pill during magnetization to 1.9 T is 3.8 J.

```
R = 8.314[kj/kmol-K]                                  "universal gas constant"
MW_FAA_mass = 482.25 [kg/kmol]                        "molecular weight of FAA"
R_FAA = R/MW_FAA_mass                                 "gas constant for FAA"
T_hot = 1.4[K]                                        "temperature of cold plate -- modify after
running an actual cool-down with the Alcatel 2063 pump"
B_field = (5/8) * 3[T]                                "B field we will generate using 5 Amps; Timbie
used 8 amps"
deltaS\R = 1.3                                        "read from Figure 3"
deltaS = R_FAA * deltaS\R                             "delta S at 1.4 K for this magnetic field"
mass_FAA = .12 [kg]                                   "mass of FAA "
q_absorbed = mass_FAA*T_hot*deltaS*convert(kJ,J)      "ADR's mass of FAA absorbs about 3.8 J when
brought to 1.9 T isothermically at 1.4 K."
```

Upon magnetization the ADR was expected to rise in temperature to between 5K and 6K [10]. Wanting a minimum ten minute time for the ADR temperature to fall, wire diameters and values of thermal conductivity for a slow thermal connection were tried in order to select a material. A brass wire, diameter .065” (Figure 33b) was selected as having a thermal conductivity at the temperatures required around 40 W/m-K [9].

```
q = (3.8[J]/600[s])                                   "ten minutes for the FAA to release 3.8 J"
L = 3[in] * convert(in, m)                            "length of link"
D = .065[in] * convert(in, m)                         "diameter of brass wire"
A = (pi/4) * D^2                                      "cross sectional area"
```

delta_T = 5[K]	"temperature would fall from 5K or 6 K to < 1K"
q = (delta_T * k * A) / L	"solve for desired thermal conductivity"

Wth the slow thermal connection the ADR was mounted inside the dewar with its thermal bus in contact with the 1 K plate which was to function as a heat sink. A Cernox 1030 thermometer sensitive to 0.3 K was mounted on the ADR cold plate (Figure 33b). The dewar was cooled to 1.5 K and the magnet was energized. The rate of magnetization – that is the rate at which the current was ramped – goes according to

$$V = L\frac{dI}{dt} \tag{4.4}$$

where L, the inductance of the magnet is constant, in this case 15 Henrys. The voltage was raised in slow steps, first by increments of 0.5 V, then 0.7 to control the rate of current and magnetic field increase. In thirteen minutes the current reached its maximum of 5.25 A and the temperature stood at 6.89 K. The ADR was to be allowed to cool through the brass wire to 1.8 K before demagnetization. In five hours the temperature had fallen only to 3.86 K; in 20 hours only to 2.4 K. It was remagnetized with 5.25 A and again the FAA was left to cool from a high temperature, of 3.08 K. In eleven hours it fell to 2.39K. It was then slowly demagnetized and now its temperature began to fall more rapidly. Within two hours it had fallen as low as 0.620 K, the lowest temperature it reached. The FAA crystal canister was intact and the ADR was shown to be functional.

4.4 Gas mixing to charge the heat diode

The amount of ^{3}He to be mixed with ^{4}He at room temperature was determined. To do this it was first necessary to determine the volume within the diode, its fill line, and other lines

within the dewar that will be filled with $^{3}He/\ ^{4}He$ liquid mixture when cooled to liquid helium temperatures.

The 1K facility has one helium line running through the 1K pot for evaporative cooling (Figure 29) and a second line to provide a loop of liquid helium inside the dewar to be used for experiments (Figure 34).

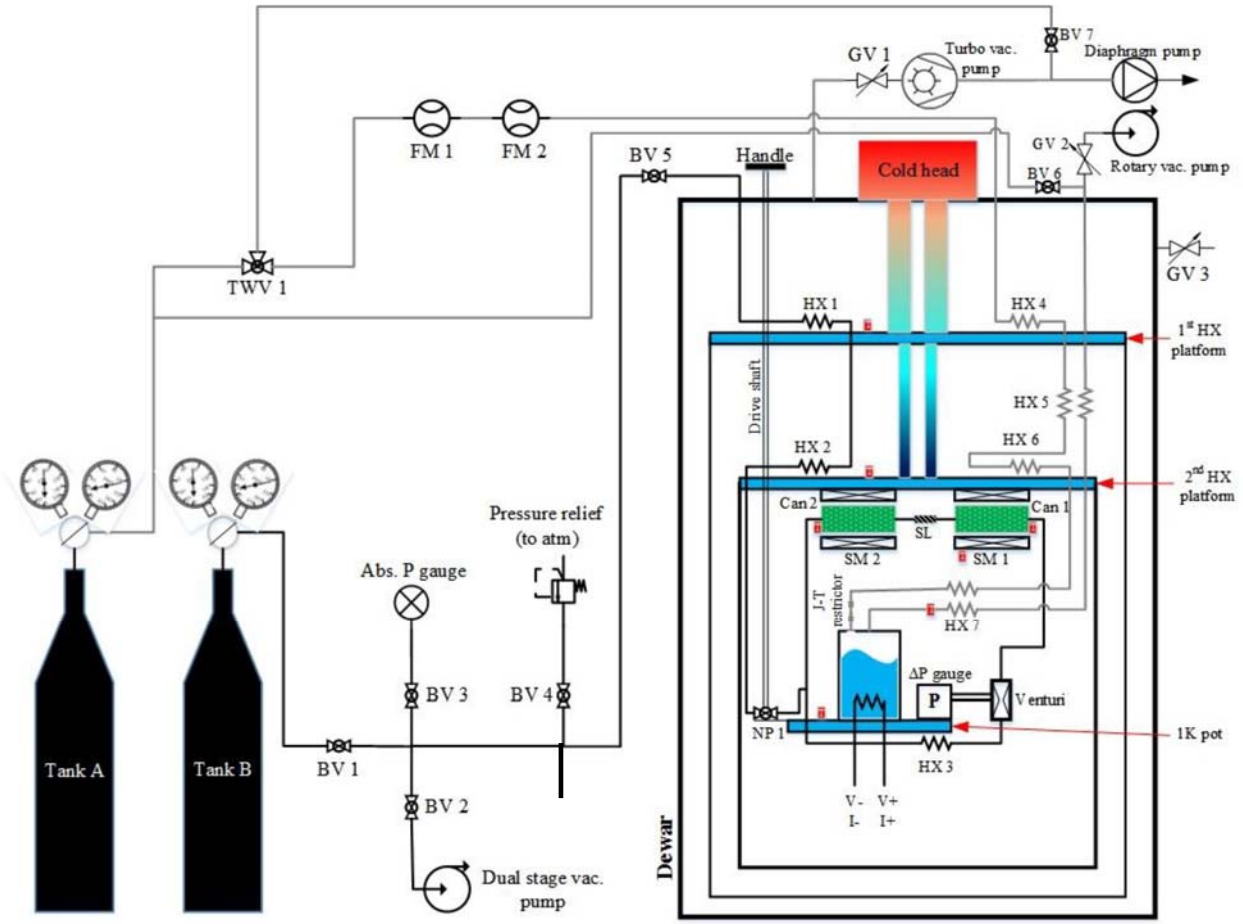

Figure 34 – Schematic of the 1K facility including two helium lines. *The line from Tank A runs through the 1K pot for evaporative cooling (Figure 29). The line from Tank B feeds a loop for experiments, This loop may be seen running to the right from valve NP 1 which appears on this schematic at the lower left of the innermost section of the dewar [56].*

Figure 35 shows a detail of the inside of the dewar with a schematic drawing of the placement of the ADR, heat diode, and helium fill line. Looking at Figure 34, the helium feed loop exiting NP 1 to the right and running counterclockwise through HX 3, the Venturi tube, Can 1, and Can 2 (in green) will be closed off between NP 1 and Can 2 and between HX 3 and the Venturi tube. The fill line capillary from the heat diode (Figure 20, right, top; Figure 21, right, bottom) will be attached to the right of HX3 (Figure 34, Figure 35). The volume to be considered will be the sum all the volumes connected to the heat diode that will be at liquid helium temperatures while the diode is being charged. The 2nd HX platform (Figure 34) will be kept at 4K by the Cryomech cryocooler, so the volumes to be summed are all those along the path from the diode back to the 2nd HX platform. These include the diode end volumes, its capillaries and fill line, HX 3 and the line to NP 1, NP 1 itself, and the line from NP1 to the 2nd HX platform. Though appearing on the schematic (Figure 34) as a straight line, this last part contains multiple lines of different diameters and many loops and turns. The estimated summed volume is 30 cm^3.

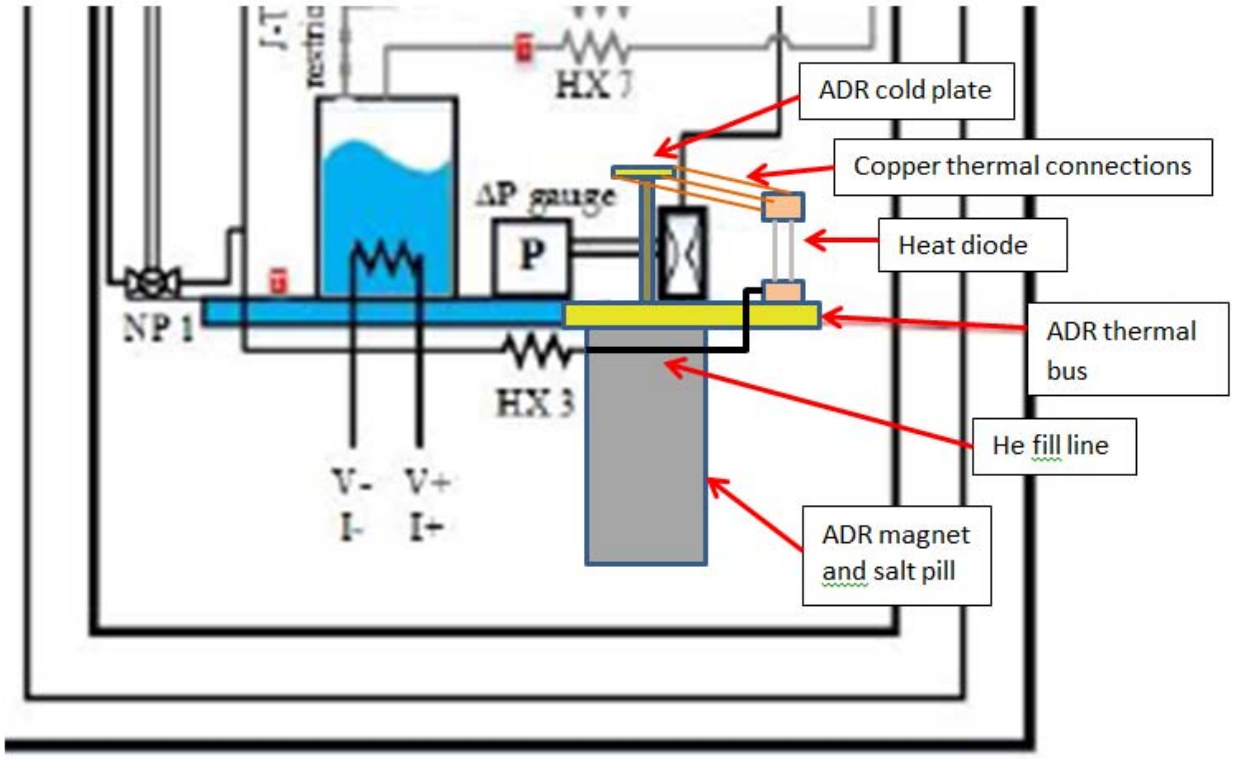

Figure 35 – Detail schematic of the interior of the innermost dewar with the ADR and heat diode installed. *The heat diode will be charged by the line that comes through valve NP 1 and HX 3.*

The density of helium is not a strong function of temperature below the lambda line, and it is necessary that the diode contain superfluid. So the number of moles of helium required to fill the summed volume at T_λ is computed. The density of helium at that temperature is multiplied by the summed volume and divided by the molecular weight.

```
mass_He_liq = density(Helium, T=T1, x=0)  * V_tot_He_liq  "mass of liquid helium in system from 4.2 K
to heat switch; model this as if it were at 2.177K for the entire length for conservative result"
MW=molarmass(Helium)                                      "molar mass of helium"
mol_He_liq = mass_He_liq/MW                               "number of moles of helium in system from 4.2 K
to heat switch; estimate will be on the high side"

V_cylinder = 3.5[liters] * convert (liters, m^3)          "total of all other volumes outside vacuum
system and above BV-5 are small compared to the cylinder so neglect them."

P_cylinder * V_cylinder = mol_He_liq * R# * T3            "pressue in cylinder for liquid helium alone --
ideal gas law -- estimate on the high side"
P_cylinder_psi = P_cylinder * convert(Pa, psi)            "pressure in cylinder for liquid helium alone, psi"
```

```
"Useful temperatures for this problem"
T1 = 2.177[K]                                   "T_lambda"
T2 = 3[K]
T3=4.2[K]
T4 = 295[K]       "room temperature"
```

The charging cylinder must contain that same number of moles of helium at room temperature (295 K). The final charging cylinder pressure must be 1 atm greater than the result, to ensure that when the gas is released from the charging cylinder it will fill the summed volume. Dalton's law of partial pressures is used to determine the pressure of ^{3}He and ^{4}He needed at the charging tank. Results are shown in Table 4-2.

```
P_tot = P_cylinder + 1[atm] * convert(atm, Pa)      "total pressure for charging system"
x_3He = .002                                        "percentage of helium 3"
x_4He = 1 - x_3He                                   "percentage of helium 4"
P_3He = x_3He * P_tot                               "charging pressure for 3He, Dalton's law of
partial pressures"
P_4He = x_4He * P_tot                               "charging pressure for 4He, Dalton's law of
partial pressures"

P_3He_psi = P_3He * convert(Pa, psi)                "charging pressure for 3He, psi"
P_4He_psi = P_4He * convert(Pa, psi)                "charging pressure for 4He, psi"
```

Table 4-2 Charging pressure for ^{3}He and ^{4}He

Fraction of ^{3}He	Charging pressure for ^{3}He	Charging pressure for ^{4}He
.008	1.01 psi	126 psi
.02	2.53 psi	124 psi

To carefully measure the required low pressure of ^{3}He when it is added to the charging tank, a Wallace and Tiernan pressure gauge that can read to fractions of 1 psi will be used. It will be attached above BV 3.

The helium isotopes will be mixed in a 20 cu. ft. steel cylinder (water capacity 3.5 liters) attached to a line entering the system below BV 4 (Figure 34). Stainless steel ¼" ID capillary with a male NPT connector was silver brazed to a CGA-540 brass nut and nipple to connect the mixing cylinder to the system. The ^{3}He will be admitted through a valve to be added above BV 4.

Once the diode is charged NP 1 will be closed, sealing in the helium mixture. NP 1 is a Swagelok SS-4BW-TW valve used to seal against superfluid helium. There is a feedthrough handle allowing the valve to be closed from outside the dewar.

4.5 Sizing a thermal link between the heat diode and the ADR cold plate

The physical placement of the ADR and heat diode in the dewar makes direct contact between the diode and the ADR cold plate impossible. A thermal link between them is required to allow rapid transmission of the ON state heat flow when ΔT across the switch is at its largest, for the purposes of this thesis when ΔT = 1.4K. This heat flow can be estimated using the EES model. At ΔT = 1.4K, curve fitting was applied to a plot of heat flux vs the number of nodes (Figure 17b) yielding

$$y = -.0003x^2 + 2.4093x - 2.3699 \tag{4.5}$$

with number of nodes x and heat flux y. Taking the first derivative and setting it equal to zero, it was estimated the EES equations for heat flux would converge at 4016 nodes. Placing that value for x into Equation (4.5) yields a heat flux of 4835 W/m^2. Multiplying by the capillary area gives a heat flow of about 1.9 mW.

The cross-sectional area of a connection between the heat diode and ADR cold plate was determined using the relation

$$q = \frac{kA_c\Delta T}{L} \tag{4.6}$$

with heat flux q (*J/s),* and for the thermal connection length L, cross-sectional area A_c, and conductivity k. The length between the diode and the cold plate is 4 in (10.16 cm) and ΔT is required to be 1.4K. Stainless steel was rejected (k on the order of 10^{-1} W/m-K) in favor of copper. Using RRR = 60 for unspecified bare ETP copper wire and using a NASA low temperature thermal conductance spreadsheet calculator provided by Franklin Miller gave an estimate for k for copper between 100 mK and 1.4 K to be between 66 W/m-K and 85 W/m-K. Using the lower of these values, a copper wire with diameter .065" would be sufficient. As the thermal connection between the wire and the cold plate and the diode will only be by a stainless steel screw holding the wire against the plate and diode a conservative approach was taken and three 14 gauge copper wires (diameter .0641") will be used.

```
y = -.0003*x^2 + 2.4093*x - 2.3699          "curve fitting equation, heat flux (y, W/m^2), nodes (x)"
x = 4016                                    "value of x for which dy/dx = 0, EES code presumed to
converge"

D_cap = .028[in] * convert(in, m)           "diameter of diode capillary"
A_cap = (pi/4) * D_cap^2                    "cross-sectional area of diode capillary"
q = y* A_cap                                "heat flow in Watts -- heat flux times capillary cross sectional
area"

k = 500[W/m-K]                              "conductivity of 100 RRR copper at 1K, from Pobell"
delta_T = 1.4[K]                            "temperature difference across heat switch"
L = 4[in] * convert(in, m)                  "length of thermal connection between diode and ADR cold
plate"

q = (delta_T * k * A_wire)/L                "determination of cross sectional area of thermal connection"

A_wire = (pi/4) * D_wire^2                  "diameter of thermal connection"

D_wire_in = D_wire * convert(m, in)         "diameter of thermal connection in inches"
```

4.6 Proof of concept experiment

A brief experiment can show that the two capillary heat diode with a superleak will continue to function as ΔT rises. The heat diode will be secured inside the dewar with the large volume attached to the ADR thermal bus which is in thermal contact with the 1K plate. The small volume will be connected with three copper wires (a 'fast' thermal connection) to the ADR cold plate. The heat diode will be charged. The dewar will be cooled down to 1.5 K or if possible 1.392 K, its nominal lower limit. The temperature difference between warm and cold ends of the diode will be slowly ramped up to test the diode in the OFF state. This means the large volume end, attached to the 1K plate, must be the warm end. The ADR will be magnetized, then cooled to a subkelvin temperature and held there. This will be as close as possible to 100 mK, but most likely higher than that as in the 1K facility the ADR cannot be magnetized all the way to 3 T, only to 1.9 T. The 1K plate will then be slowly heated, raising the temperature difference between the two ends of the diode, the warm end attached to the 1K plate, and the cold end linked to the ADR cold plate. The heat flow through the diode can then be 'backed out' using Equation (4.6). A 'benchmark' ΔT of, say, 1K will be set as time 0. The 1K plate will then be slowly heated and the rate of change of the ADR cold plate temperature relative to the rate of change of the 1K plate temperature will be monitored and recorded. If the improved diode is functioning as expected, the rate at which ΔT changes should stay constant between ΔT = 1.0K and ΔT = 1.4 K with no sudden jumps at 1.3 K or elsewhere. The conductance of the capillary in the OFF state can be calculated at a range of values of ΔT and plotted against ΔT to ensure that the results do not show the jump in heat flux found by McCammon with ΔT around 1.3 K (Figure 12). Again, considering Equation (4.6), if the OFF

state is functioning properly and undisturbed by vortices and turbulence, then *k, L,* and A_c remain constant and ΔT is directly proportional to the rate of heat flow through the diode in *J/s.* As the difference in temperature between the cold and warm ends of the diode is gradually and steadily changed, a sudden change in the rate of temperature change measured in the ADR cold plate around ΔT = 1.3 K would indicate that the addition of a superleak capillary has *not* solved the problem. The absence of such a jump – something like Table 2-2 -- would indicate that the improvement is successful. This would be a practical engineering application of the theory of quantum vortices.

5 CONCLUSIONS AND FUTURE WORK

The principles of operation of the single capillary ^{3}He/^{4}He have been explored. A numerical model of its functioning has been presented. An explanation has been posed for the failure of the single capillary ^{3}He/^{4}He heat diode with increasing ΔT between its warm and cold ends – that counter-flow in the ^{4}He exceeds the two-fluid critical velocity causing vortices and turbulence that disperse the ^{3}He, destroying its insulating function. A remedy has been suggested, the addition of a second capillary that is a superleak, to change the flow in the diode from counter-flow to circulation. Fabrication of such a switch has been described, with emphasis on making a superleak in a small diameter capillary. A diode has been made, and an experiment has been described to use the 1K facility to test the diode's functioning.

Next, the test needs to be performed.

After that, it is desirable to study in detail the parasitic heat load of the second capillary. In the thesis it is claimed that the heat transfer through the second capillary will be negligible relative to the OFF state conduction in the first capillary, as the second capillary has low thermal

conduction stainless steel, the jewelers' rouge particles which have high contact resistance, and superfluid helium which carries no entropy. But this needs to be verified experimentally. This can be done by fabricating a second diode identical to the first in which the superleak capillary has been sealed at either end with solder, eliminating the superleak effect but preserving more or less its thermal conductivity. This second 'dummy' switch can then be tested in the same manner as the first switch. This would be both to check the thermal conductivity through the second capillary, and to duplicate the one-capillary failure that McCammon encountered around $\Delta T = 1.3$ K.

REFERENCES

[1] P. Shirron, "Optimization strategies for single stage, multi-stage, and continuous ADRs," *Cryogenics,* vol.62, pp.140-149, 2014.

[2] C. Enss, and S. Hunklinger, Low-Temperature Physics, Berlin: Springer, 2010.

[3] F.K. Miller, "Helium", PowerPoint presentation in ME 566 Cryogenics, UW-Madison, spring 2016, slide 19

[4] K. Onnes, "On the Lowest Temperature Yet Obtained," *Transactions of the Faraday Society*, vol.18, p.173, December, 1922.

[5] G.K. White, Experimental Techniques in Low-Temperature Physics, 3rd edition, Oxford: Clarendon, 1979.

[6] W.F. Giauque, "A thermodynamic treatment of certain magnetic effects. A proposed method of producing temperatures considerably below 1° absolute," *Journal of the American Chemical Society* vol.49, pp.1864-1867, 1927.

[7] W.F. Giauque and G.P. MacDougall, *Physical Review*, vol. 43, p. 768, 1933.

[8] H.B.G. Casimir, Magnetism and Very Low Temperatures, Cambridge: Cambridge University Press 1940 p. 34.

[9] F. Pobell, Matter and Methods at Low Temperatures 2nd edition, Berlin: Springer, 1995; and notable for completeness and clarity, P. Wikus, E. Canavan, S.T. Heine, K. Matsumoto, T. Numazawa, "Magnetocaloric materials and the optimization of cooling power density,"*Cryogenics*, vol. 62, pp.150-162, 2014.

[10] G. Wilson, An Instrument and Technique for Measuring the Anisotropy in the Cosmic Microwave Background Radiation, Ph.D. Dissertation (unpublished), Brown University, 1998. Figure adapted from p.42

[11] A.E. Jahromi, Development of a 1K facility and modeling of a superfluid magnetic pump with no moving parts, Master's Thesis, University of Wisconsin – Madison, 2011 pp. 2-4. [Online] Available: http://sel.me.wisc.edu/publications-theses.shtml [Accessed August, 2019].

[12] P. Shirron, "Editorial," *Cryogenics*, vol. 62, p.129, 2014.

[13] P. Kittel, "Heat switch limitations on multi-stage magnetic refrigerators," *AIP Conference Proceedings*, vol. 613, pp. 1167-1174, 2002.

[14] M.J. DiPirro and P. Shirron, "Heat switches for ADRs," *Cryogenics*, vol. 62, pp. 172-176, 2014.

[15] M.J. DiPirro, P. Shirron, J.G. Tuttle, E.R. Canavan, **"**Design and test of passively operated Heat switches for 0.2 to 15 K,". *Adv Cryog Eng A*, vol. 49, pp. 436-42, 2004.

[16] Liquid Helium II: The Superfluid (film), Prod. Alfred Leitner, Perf. Alfred Leitner, Audiovisual Center, Michigan State University (1965) [Online]. Available: http://www.alfredleitner.com/p/liquid-helium.html. [Accessed June 2019].

[17] J.C. Wheatley, **"**Liquid Helium II: The Superfluid (review)," *American Journal of Physics*, vol. 33, p.414, 1965.

[18] Superfluid Helium (film), Prod. J.F. Allen, Perf. J. F. Allen, St. Andrews University, Scotland (1972) [Online]. Available. https://www.youtube.com/watch?v=lEPc-rBMAuU . [Accessed June 2019. Allen was among the discoverers of superfluidity in 1938. For a review of the work and interactions of J.F. Allen, D. Misener, P. Kapitza, F. London, L. Tisza and L.D. Landau and others involved in the discovery of superfluidity and the development of the two-fluid model, against the background of politics in Europe and the Soviet Union, see S. Balibar, "The Discovery of Superfluidity," *Journal of Low Temperature Physics,* vol. 146, no. 516, pp. 441-470, March 2007.

[19] Wheatley, J.C. Superfluid Helium (review) *American Journal of Physics*, vol. 42, p.437, 1974.

[20] W.H. Keesom and B.F. Saris, "Further measurements on the heat conductivity of liquid helium II," *Physica*, vol. VII, no. 3, pp. 241- 252, March 1940.

[21] Wilks, J and Betts, D.S., *An Introduction to Liquid Helium, 2nd edition* Oxford (1987) 32-34.

[22] F.K. Miller PowerPoint, personal communication July, 2019.

[23] C.T. Lane, H.A. Fairbank, L.T.Aldrich, A.O. Nier, "He^3 Separation by a Heat Flux in Liquid Helium II," *Physical Review,* vol. 73, p. 256, 1948.

[24] D.V. Osborne, "The Rotation of Liquid Helium II", *Proc. Royal Soc. A,* vol. 63, p.909, 1950.

[25] C. J. Gorter and J. H. Mellink, "On the irreversible processes in liquid helium II," *Physica* , vol. XV, no. 3—4, May, 1949.

[26] W.F. Vinen, "Mutual friction in a heat current in liquid helium II," *Proc Roy Soc A* vol. 240, pp. 114–127, 1957.

[27] G.W. Rayfield, and F. Reif, "Quantized Vortex Rings in Superfluid Helium," *Physical Review* vol. 136 no. 5A, pp. A1194 – A1208, November 30, 1964**.**

[28] C.F. Barenghi, L. Skrbek, K.R. Sreenivasan, "Introduction to Quantum Turbulence," *Proceedings of the National Academy of Science*, vol. 111, suppl. 1, pp.4647 – 4652, March 25, 2014.

[29] E.B. Sonin, Dynamics of Quantised Vortices in Superfluids, Cambridge, 2016, pp. 346-347 summarizing Vinen's results.

[30] B. Mastracci, B. and W. Guo, "Exploration of thermal counterflow in He II using particle tracking velocimetry," *Physical Review Fluids* vol. 3, 063304, 2018.

[31] E. J. Varmchuk, M. J. V. Gordon and R.E. Packard, "Observation of Stationary Vortex Arrays in Rotating Superfluid Helium," *Physical Review Letters,* vol. 43, no. 3, p. 214-217, July 1979. Cited [34].

[32] G. P. Bewley, D. P. Lathrop, K. R. Sreenivasan, "Visualization of quantized vortices", *Nature,* vol. 441, June 1, 2006, cited in O. Gessner and A.F. Vilesov, op. cit.

[33] W. Guo, M. La Mantia, D.P. Lathrop, S.W. Van Sciver., "Visualization of two-fluid flows of superfluid helium-4," *PNAS* vol 111, suppl. 1, pp, 4653 – 4658, March 25, 2014.

[34] O. Gessner and A.F. Vilesov, ," Imaging Quantum Vortices in Superfluid Helium Droplets," *Annu. Ref. Phys. Chem* vol. 70, pp. 173-198, 2019

[35] C.D. Fulton, C.F. Hwang, W.M. Fairbank, J.M. Vilas, "He thermal rectifiers for magnetic cooling." University of Wisconsin Conference Proceedings, pp.221-223, 1958.

[36] C.D. Fulton and W.M. Fairbank, "Helium Heat Rectifier," US Patent 3004394 [Online]

Available:
https://patentimages.storage.googleapis.com/ad/e8/4e/12109f79f693b1/US3004394.pdf
[Accessed August, 2019].

[37] D. McCammon, personal communication, November, 2017.

[38] A.J. Schmidt, An Engineering Model for Superfluid Heat Diodes, BS Thesis Unpublished), Massachusetts Institute of Technology, 2002.

[39] F.K. Miller and J.G. Brisson, "A simple method for the analysis of sub-Kelvin refrigerators that use a dilute superfluid 3He - 4He mixture as a working fluid," *Cryogenics,* vol. 41, pp. 311-318, 2001.

[40] R. Radebaugh, "Thermodynamic Properties of He3-He4 Solutions with Applications to the He3-He4 Dilution Refrigerator", NBS Technical Note 362, Boulder, CO 1967, Eq(5).

[41] G. Nellis and S. Klein, Heat Transfer, Cambridge, 2009, pp. 52-53.

[42] J.F. Allen ad A.D. Misener, "The Properties of Flow of Liquid He II," *Proceedings of the Royal Society of London, Series A, Mathematical and Physical Sciences,* vol. 172, no. 951, pp. 467-491, Sep. 4, 1939.

[43] A.J. Strauss, The adsorbtion of helium on jeweler's rouge at liquid helium temperatures, Ph.D. Thesis (unpublished), University of Chicago, 1956.

[44] G.J.C. Bots and C.J. Gorter, "The Fountain Effect of Liquid Helium Below 1° K," *Physica*, vol XXII, pp.503-508, 1956.

[45] B.S. Chandrasekhar and K. Mendelssohn, "Superflow of Helium II through Compressed Powder," *Proceedings of the Royal Society of London. Series A, Mathematical and Physical Sciences,* vol. 218, No. 1132, pp.18-28, June 9, 1953.

[46] J.D. Reppy, "Superfluid Helium in Porous Media," *Journal of Low Temperature Physics*, vol. 87, nos. 3-4, p. 205 – 244, 1992

[47] A. Yamaguchi, N. Kamada, G. Motoyama, A. Sumiyama, Y. Aoki, Y. Okuda, M. Kubota· H. Kojima, "Recent Spin Pump Experiments on Superfluid 3He-Al," *Journal of Low Temperature Physics,* vol. 171, pp. 221-225, 2013

[48] J.M. Goldschvartz, A. Kollen, F. Mathu, and B.S. Blaisse, "On the possible application of rocks as superleaks," *Cryogenics*, pp.303-304., May, 1973.

[49] V.M. van Alphen, R. de Bruyn Ouboter, J.F. Olijhoek, K.W. Taconis, "The critical flow rate of superfluid helium through narrow pores," *Physica*, vol. 40, pp.490-496, 1969.

[50] V.M. van Alphen, R. de Bruyn Ouboter, K.W. Taconis, "Persistent superfluid flow in a circuit filled with jeweler [sic] rouge", *Physics Letters*, vol. 24A, no. 7, March 27, 1967.

[51] S. Matsusaka, M. Urakawa, and H Masuda, "Micro-feeding of fine powders using a capillary tube with ultrasonic vibration*," Journal of the Society of Powder Technology, Japan*, vol. 49(9), pp.658-662, 2012.

[52] A.E. Jahromi and F.K. Miller, "Construction and experimental validation of a simple, compact, resealable and reliable Vycor superleak assembly for use at low temperatures," *Review of Scientific Instruments*, vol. 87, 045112, 2016.

[53] J.L. McKinney and W.L. Taylor assignors to the US as represented by the US AEC (1969), "Apparatus and method of separation of helium isotopes," U.S. Patent 3421334 [Online] Available: https://patents.google.com/patent/US3192730A/en?oq=US+Patent++3%2c192%2c730+ [Accessed October 2017].

[54] J.E. Webb, Administrator of NASA, with respect to an invention of Alvin F. Hildebrandt, "Helium Refining by Superfluidity," U.S, Patent 3192730 [Online] Available: https://patentimages.storage.googleapis.com/16/95/4c/87bccd4ba38dcd/US3192730.pdf [Accessed October 2017].

[55] A.E. Jahromi, Development of a 1K facility and modeling of a superfluid magnetic pump with no moving parts, M.S. Thesis, University of Wisconsin – Madison, 2011 [Online] Available: http://sel.me.wisc.edu/publications-theses.shtml [Accessed August, 2019]. This provides an in-depth description.

[56] A.E. Jahromi, "Development of a Proof of Concept Low Temperature Superfluid Magnetic Pump with Applications", Ph.D. Thesis, University of Wisconsin – Madison, 2011 [Online] Available: http://sel.me.wisc.edu/publications-theses.shtml [Accessed August, 2019]. This provides a deeper description.

[57] J.F. O'Hanlon, A user's guide to vacuum technology, 3rd edition, John-Wilery, New York, 2003.

[58] P.T. Timbie, G.M. Bernstein and P.L. Richards, "Development of an adiabatic demagnetization refrigerator for SIRTF," *Cryogenics,* vol. 30, pp.271-275, March, 1990

APPENDIX A – EES CODE FOR ON STATE

"A 3He/4He Heat Switch for the temperatures < 2K

Kenneth Katz, University of Wisconsin - Madison
Department of Mechanical Engineering, Solar Energy Laboratory " "ON STATE"

"Unit error messages show when the code is run only because unit names were not added for all the many iterations of each unit as the number of nodes has been varied up and down while using this."

"This EES code models 3He concentration, temperature, and heat flux through a column of a weak (<5% molar) solution of liquid 3He in 4He. The user can vary concentration (x), end temperatures (T_h and T_c), inner diameter, length, and number of nodes used to model the column. As explained in the code annotations, solution heat conductivity (k) varies both with 3 He concentration and temperature.

To model the OFF state (pink highlighted section below) a large reservoir is established at the warm end. The model allows for this size to be changed relative to the cold end. To model the ON state (blue highlighted section below) a large reservoir is established at the cold end, whose size can also be varied.

The code is annotated with references to sources of data sets and equations for low temperature helium, and with explanations I used for myself as the project developed."

"Note: NODES and SLICES. The following variables are one per NODE with [1] at the hot end and [N] at the cold end: N, ky, T,v,x,y. The following variables are one per SLICE with [1] at the hot end and [S = N-1] at the cold end: S, dT, n3_slice, R, vol_slice.

N3_SLICE, the number of moles of He3 per slice, and in the reservoirs as they are defined as slices: for each slice, molar specific volume is defined at each node. To to determine the number of moles of He3 in each slice, we use vol_slice[i]/ ((v[i] + v[i+1])/2) = n3_slice[i] -- in words, for each slice we average the molar specific volume of the two nodes that are at either end of a given slice and use that average to determine the number of moles in a given slice.

RESISTANCE: for the resistance network, resistance is per slice, and is defined as R[i] = delta_y/ (A_c * ((ky[i] + ky[i+1]) / 2)) -- in words, for conductivity [k] in each slice we average the conductivity of the two nodes that are at either end of a given slice.

R_EFF goes by summing slices. Q_DOT goes by the temperature of the node at the hot side (LHS) of the hottest slice considered to the cold side (RHS) of the coldest slice considered."

$UpdateGuesses/A
$Unitsystem SI K Pa J mass deg

***Function* kx**(x)

"This function returns the thermal conductivity of Helium 3 (kx in [W/m-K]) as a function of concentration (x, [mol He3/ mol He3-He4 solution]). Conductivity kx [W/m-K] falls with increasing concentration."

kx := .00145 * x^(-1.167) "equation supplied by FK Miller"

End

"Fit Parameters -- from F K Miller and J G Brisson, 'A simple method for the analysis of sub-Kelvin refrigerators that use a dilute superfluid 3He - 4He mixture as a working fluid', Cryogenics 41 (2001) 311-318"

A = 23.2 [J/mol-K^(3/2)]
B = .00675 [J/mol-K^4]
C = 500 [J/mol]
Delta_1 = 8.65[K]
Delta_2 = 15.7[K]
R = 8.314 [J/mol-K]

"Moving from warmer to colder, the concentration of 3He (x, [mol He3/ mol He3-He4 solution]) increases and so conductivity (kx [W/m-K]) falls -- He3 is carried along from reservoir to capillary with the 'heat flush' from warm to cold, raising the concentration of He3 and so decreasing the conductivity of the solution in the capillary. The switch goes from on to off.

In general, moving along the capillary from warmer (x_1) to colder (x_2), x_2 = x_1 * (T_1/T_2) + (1/R*T_2) *((B*T_1^4 + (A*T_1^(3/2)) *(exp(-delta_1/T_1)) + C*exp(-delta_2/T_1)) - (B*T_2^4 + (A*T_2^(3/2)) *(exp(-delta_1/T_2)) + C*exp(-delta_2/T_2))).

which establishes x_2 based on x_1, T_1, and T_2 (Miller and Brisson 2001 p. 317, Eq (36)"

"Dimensions"

L = 10.16[cm] * **convert**(cm,m) "length of capillary; cf Schmidt Figure 5-2 p.39 after McCammon"
delta_y = L/(S-2) "capillary is divided into S-2 equal slices; the total number of slices includes the two volumes at either end of the capillary"

{D = 0.028[in] * convert(in,m) "inner diameter of built heat switch"}

D = .071[cm] * **convert**(cm,m) "inner diameter of capillary, cf Schmidt Figure 5-2 p.39 after McCammon"

A_c = (pi/4) * D^2 "cross-sectional area"

"Divide the capillary into some number of nodes and slices for analysis. Node 1 is at the (initial) hot end, Node N is at the (initial) cold end. Except for the extreme ends of the end volumes (node 1, node N) Nodes are equally spaced so that there is one less number of slices than nodes."

N =400
"number of nodes"
S = N-1 "number of slices"

T_h = 1.3 [K] "hot end temperature"
T_c = 0.05[K] "cold end temperature"

T[1] = T_h "node 1 is the hot end"
T[N] = T_c "node N is the cold end"

concentration = .008 "molar concentration of He3 in He3-He4 solution, cf Schmidt Figure 5-2 p.39 after McCammon"

"Establish He3 concentration at N nodes arrayed evenly spaced at intervals of delta_y = L/S from T_h to T_c"

x_ini = concentration "overall concentration of He3 in He3 - He4 solution"

x[N] = x[S] * (T[S]/T[N]) + (1/(R*T[N])) *((B*T[S]^4 + (A*T[S]^(3/2)) *(**exp**(-delta_1/T[S])) + C***exp**(-delta_2/T[S])) - (B*T[N]^4 + (A*T[N]^(3/2)) *(**exp**(-delta_1/T[N])) + C***exp**(-delta_2/T[N])))

Duplicate j =2, S
x[j] = x[j-1] * (T[j-1]/T[j]) + (1/(R*T[j])) *((B*T[j-1]^4 + (A*T[j-1]^(3/2)) *(**exp**(-delta_1/T[j-1])) + C***exp**(-delta_2/T[j-1])) - (B*T[j]^4 + (A*T[j]^(3/2)) *(**exp**(-delta_1/T[j])) + C***exp**(-delta_2/T[j])))

(((T[j-1] - T[j]) * ((**kx**(**average**(x[j-1],x[j])))) * A_c) / delta_y) + (((T[j+1] - T[j]) * ((**kx**(**average**(x[j+1],x[j])))) * A_c) / delta_y)= 0

End "This loop sets the He3 concentration at every node except Node 1 and Node N, based on the variation of conductivity with concentration."

"Variation of specific molar volume of He3 in He3-He4 solution (v [m^3 He3-He4 solution/mol He3]) with concentration of He3"

"Fit Parameters, from R Radebaugh, 'Thermodynamic Properties of He3-He4 Solutions with Applications to the He3-He4 Dilution Refrigerator', NBS Technical Note 362, Boulder, CO 1967, Eq(5)"

E = 27.58 [cm^3/mole] * **convert**(cm^3/mol, m^3/mol)
F = 7.60 [cm^3/mole] * **convert**(cm^3/mol, m^3/mol)
G = 1.65 [cm^3/mole] * **convert**(cm^3/mol, m^3/mol)
v_ini = ((E/x_ini) + F + G*x_ini^2) "specific molar volume of He3; that is, volume of He3-He4 solution that contains one mol of He3 with He3 molar concentration (x_ini) set at 'concentration'; Radebaugh 1967 Eq(5)"

vol_cap = A_c * L "volume of capillary"
vol_slice = vol_cap / (S-2) "divide capillary into S = N-1 slices of equal volume"

"Establish slice[1] as the hot end reservoir, and slice [S = N-1] as the cold end reservoir. The volume of the reservoirs can be set to any amount, including zero. Set the reservoir volumes as multiples of the volume of one capillary slice; or set the volume of the larger reservoir as a multiple of the volume of the smaller reservoir. The volume of the reservoirs will always be large relative to the volume a single slice of the capillary. So the volume of the capillary will actually be A_c*L minus the volume of two slices. But as the reservoirs are large relative to the capillary, neglect this fact in this model, for ease of computation. "

"Reservoir volumes -- Actual Built Heat Switch May, 2019"

D_small = 0.593[in] * **convert**(in,m) "diameter of small"
L_small = .0035[in] * **convert**(in,m) "length of small volume"
vol_small = pi*(D_small/2)^2 * L_small "volume of small volume"

vol_large = FACTOR * vol_small

FACTOR = 65.8 "actual volume of heat switch large volume relative to small volume"

"ON, THAT IS HIGH CONDUCTIVITY -- should be cold end large" "The program is switched from modeling ON state to OFF state by commenting in/out either the blue or red section here. It can, however, require much in the way of resetting guess values to make this change. The user is advised to retain copies of this program that are set to ON, OFF, various values of T_h or T_c, and higher or lower

values for N (number of nodes). In general as N is set higher, more adjusting of guess values is needed to change settings. The guess values that will most need resetting are T, x, and v.

vol_res_cold = vol_large
vol_res_hot = vol_small

{"OFF, THAT IS LOW CONDUCTIVITY -- should be hot end large"
vol_res_hot = vol_large
vol_res_cold = vol_small }

vol_tot = (S-2) * vol_slice + vol_res_hot + vol_res_cold "total volume, including (1) He3-He4 capillary, total of S-2 slices of equal volume; (2) volume of hot end reservoir set in multiples of; (3) volume of cold end reservoir; the device will contain only He3-He4 solution, and will be completely filled"

"Establish He3 molar volume and number of moles of He3 in S = N-1 volume slices. Again, slice [1] is the hot reservoir, slice [S = N-1] is the cold reservoir"

vol_tot /v_ini = n3_tot "determine total number of moles of He3 in system with molar concentration of He3= 0.05 or whatever value is selected for concentration"

v[1] = (E/x[1]) + F +G*x[1] ^2 "Radebaugh eq(5). This line in the program determines the concentration at node [1], the hot end reservoir"
{vol_res_hot/ v[1] = n3_slice[1] -- an alternative version}

vol_res_hot/ ((v[1]+v[2])/2) = n3_slice[1] "number of moles of He3 in hot reservoir -- average the molar concentration at nodes [1[and [2] to estimate He3 molar concentration in slice [1], the hot reservoir"
vol_slice[1] = vol_res_hot

vol_slice[S] = vol_res_cold
v[S] = E/x[S] + F +G*x[S] ^2
v[N] = E/x[N] + F +G*x[N] ^2
vol_res_cold/ ((v[N-1] + v[N])/2) = n3_slice[N-1] "number of moles of He3 in cold reservoir -- average the molar concentration at nodes [N] and [N-1] to estimate He3 molar concentration in slice [S= N-1], the cold end reservoir"
{vol_res_cold/ v[S] = n3_slice[S]}

"Establish the number of moles of He3 in each slice of the capillary from slice [2] (the hot end of the capillary) to slice [S-1] (the cold end of the capillary), exclusive of the reservoirs."

Duplicate i = 2, S-1 "note, N-2 = S-1"

vol_slice[i] = vol_cap/(S-2)
v[i] = E/x[i] + F +G*x[i] ^2
vol_slice[i]/ ((v[i] + v[i+1])/2) = n3_slice[i]

{vol_slice[i]/ v[i] = n3_slice[i]}
End

sum(n3_slice[1..S]) = n3_tot "the sum of the number of moles of He3 in all the slices -- hot end reservoir, capillary, cold end reservoir -- must equal the total number of moles of He3 defined above to be in the capillary and reservoirs"

"Plotting number of moles of He3, concentration, Temperature, or other variables against position in the capillary, slice 2 through S = N-1"

Duplicate i = 2, N-1 "Note, N-2 = S-1"

y[i] = i*delta_y "y[i] is the point in the capillary located i slice-widths from the hot end"

End

y[1] = 0
y[N] = L

"Resistance Network"

Duplicate i = 1, S
ky[i] = **kx**(x[i]) * 1[W/m-K] "conductivity (k, W/m-K], at each node, units added; so this is k as a function of location, y, the y-axis moves along the capillary away from the initial hot end"
dT[i] = (T[i+1] - T[i]) "define dTdy as the change in temperature from node to node along the y-axis, moving away from the initial hot end"
R[i] = delta_y/ (A_c * ((ky[i] + ky[i+1]) / 2))

End

"Small volume"
L_sv = .004[in] * **convert**(in,m) "length of small volume -- that is, its depth"
ID_sv = .593[in] * **convert**(in,m) "ID of small volume"
Ac_sv = (pi/4) * ID_sv^2 "cross-sectional area of small volume"

"Large volume"
L_Lv = 0.415[in] * **convert**(in,m) "length of large volume -- that is, its depth"
ID_Lv = .4685[in] * **convert**(in,m) "ID of large volume"
Ac_Lv = (pi/4) * ID_Lv^2 "cross- sectional area of large volume"

R_small = L_sv/ (Ac_sv *((ky[1] + ky[2]) / 2))
R_large = L_Lv/ (Ac_Lv *((ky[N] + ky[N-1]) / 2))

ky[N] = **kx**(x[N]) * 1[W/m-K]

"Determination of Heat Flux" "Any of the following can be commented in or out if information about subsections of the capillary are desired. For now only the last of the small sections below, covering the entire capillary, is commented in."

“The following substitutions provide a way to designate parts of the capillary within the ‘sum’ operator in the following.”
UU = S-1
{UU3 = S-3
OAA2 = .02*N
AA = 0.1 * N
AA2 = .12*N
AA21 = AA2+1
BB =0.2*N

```
BB1 = BB+1
CC = .3*N
DD = .4 * N
EE = .5 * N
FF = .6 * N
FF1 = FF + 1
GG = .7 * N
HH =0.8*N
HH1 = HH + 1
HH5 = .85*N

HH8 = .88 * N
II = 0.9*N
II1 = II +1
II5 = .95*N
II51 = II5+1
II8 = .98 *N
II81 = II8 + 1
JJ = N-2

"ON STATE, THAT IS HIGH CONDUCTIVITY -- cold end large.  For  q_dot_CH consider only some subset of capillary length, offset from both ends.  In all cases, R goes with slices, T goes with nodes.  So for slice 1 to 5, use R 1 through 5 AND T 1 through 5+1 = 6."

"slice 1 to slice 5"

R_eff_slice1to5 = sum(R[1..5])  + R_small
q_dot_CHslice1to5= (T[1]  - T[6]) / R_eff_slice1to5
q_ON[10] = q_dot_CHslice1to5/A_c                    "incorrectly normalized by A_c capillary -- must include A_c small volume; but this fact is included in R_small in R_eff, so multiply by A_c"


".02N to .12N"

R_eff_2%to12% = sum(R[OAA2..AA2])                   "slices from OAA2 = .02N to slice AA2 = .12N"
q_dot_CH2%to12%= (T[OAA2]  - T[AA21]) / R_eff_2%to12%   "temperatures from node OAA2 = .02N to node AA21 = .12N + 1"
q_ON[9] = q_dot_CH2%to12%/A_c

"slice S-3  to slice S, slice S is the last slice, the cold reservoir"

R_eff_Sminus3to3 = sum(R[UU3..S])  + R_large
q_dot_CHSminus3to3= (T[UU3]  - T[N]) / R_eff_Sminus3to3
q_ON[11] = q_dot_CHSminus3to3/A_c

".1 N to .2 N"

R_eff_10%to20% = sum(R[AA..BB])                     "R_effective goes from first slice in capillary (slice [2]) one slice to another slice through and including the large cold volume."
q_dot_CH10%to20%= (T[AA]  - T[BB1]) / R_eff_10%to20%   "Q_dot goes from the hot side (LHS) node of the hottest slice considered to the cold side (RHS) node of the coldest slice considered."
q_ON[14] = q_dot_CH10%to20%/A_c                     "Heat flux, q_dot_CH normalized for cross-sectional area"

".1 N to .6 N"
```

R_eff_10%to60% = sum(R[AA..HH]) "R_effective goes from first slice in capillary (slice [2]) one slice to another slice through and including the large cold volume."
q_dot_CH10%to60%= (T[AA] - T[HH1]) / R_eff_10%to60% "Q_dot goes from the hot side (LHS) node of the hottest slice considered to the cold side (RHS) node of the coldest slice considered."
q_ON[1] = q_dot_CH10%to60%/A_c "Heat flux, q_dot_CH normalized for cross-sectional area"

".1 N to .7 N"

R_eff_10%to70% = sum(R[AA..GG]) "R_effective goes from first slice in capillary (slice [2]) one slice to another slice through and including the large cold volume."
q_dot_CH10%to70%= (T[AA] - T[GG]) / R_eff_10%to70% "Q_dot goes from the hot side (LHS) node of the hottest slice considered to the cold side (RHS) node of the coldest slice considered."
q_ON_10%to70% = q_dot_CH10%to70%/A_c "Heat flux, q_dot_CH normalized for cross-sectional area"

".1 N to .8 N"

R_eff_10%to80% = sum(R[AA..HH]) "R_effective goes from first slice in capillary (slice [2]) one slice to another slice through and including the large cold volume."
q_dot_CH10%to80%= (T[AA] - T[HH1]) / R_eff_10%to80%
"Q_dot goes from the hot side (LHS) node of the hottest slice considered to the cold side (RHS) node of the coldest slice considered."
q_ON[2] = q_dot_CH10%to80%/A_c "Heat flux, q_dot_CH normalized for cross-sectional area"

".1 N to .9 N"

R_eff_10%to90% = sum(R[AA..II]) "R_effective goes from first slice in capillary (slice [2]) one slice to another slice through and including the large cold volume."
q_dot_CH10%to90%= (T[AA] - T[II]) / R_eff_10%to90% "Q_dot goes from the hot side (LHS) node of the hottest slice considered to the cold side (RHS) node of the coldest slice considered."
q_ON_10%to90% = q_dot_CH10%to90%/A_c "Heat flux, q_dot_CH normalized for cross-sectional area"

".1 N to end of column, give end of column temperature as T_c"

R_eff_10%tocolumnend = sum(R[AA..UU]) "R_effective goes from first slice in capillary (slice [2]) one slice to another slice through and including the large cold volume."
q_dot_CH10%tocolumnend= (T[AA] - T[S]) / R_eff_10%tocolumnend "Q_dot goes from the hot side (LHS) node of the hottest slice considered to the cold side (RHS) node of the coldest slice considered."
q_ON_10%tocolumnend = q_dot_CH10%tocolumnend/A_c "Heat flux, q_dot_CH normalized for cross-sectional area"

".2 N to .3 N"

R_eff_20%to30% = sum(R[BB..CC]) "R_effective goes from first slice in capillary (slice [2]) one slice to another slice through and including the large cold volume."
q_dot_CH20%to30%= (T[BB] - T[CC]) / R_eff_20%to30% "Q_dot goes from the hot side (LHS) node of the hottest slice considered to the cold side (RHS) node of the coldest slice considered."
q_ON_20%to30% = q_dot_CH20%to30%/A_c "Heat flux, q_dot_CH normalized for cross-sectional area"

".2 N to .4 N"

R_eff_20%to40% = sum(R[BB..DD]) "R_effective goes from first slice in capillary (slice [2]) one slice to another slice through and including the large cold volume."
q_dot_CH20%to40%= (T[BB] - T[DD]) / R_eff_20%to40% "Q_dot goes from the hot side (LHS) node of the hottest slice considered to the cold side (RHS) node of the coldest slice considered."
q_ON_20%to40% = q_dot_CH20%to40%/A_c "Heat flux, q_dot_CH normalized for cross-sectional area"

".2 N to .5 N"

R_eff_20%to50% = sum(R[BB..EE]) "R_effective goes from first slice in capillary (slice [2]) one slice to another slice through and including the large cold volume."
q_dot_CH20%to50%= (T[BB] - T[EE]) / R_eff_20%to50% "Q_dot goes from the hot side (LHS) node of the hottest slice considered to the cold side (RHS) node of the coldest slice considered."
q_ON_20%to50% = q_dot_CH20%to50%/A_c "Heat flux, q_dot_CH normalized for cross-sectional area"

".2 N to .6 N"

R_eff_20%to60% = sum(R[BB..FF]) "R_effective goes from first slice in capillary (slice [2]) one slice to another slice through and including the large cold volume."
q_dot_CH20%to60%= (T[BB] - T[FF]) / R_eff_20%to60%"Q_dot goes from the hot side (LHS) node of the hottest slice considered to the cold side (RHS) node of the coldest slice considered."
q_ON_20%to60% = q_dot_CH20%to60%/A_c "Heat flux, q_dot_CH normalized for cross-sectional area"

".2 N to .7 N"

R_eff_20%to70% = sum(R[BB..GG]) "R_effective goes from first slice in capillary (slice [2]) one slice to another slice through and including the large cold volume."
q_dot_CH20%to70%= (T[BB] - T[GG]) / R_eff_20%to70%"Q_dot goes from the hot side (LHS) node of the hottest slice considered to the cold side (RHS) node of the coldest slice considered."
q_ON_20%to70% = q_dot_CH20%to70%/A_c "Heat flux, q_dot_CH normalized for cross-sectional area"

".2 N to .8 N"

R_eff_20%to80% = sum(R[BB..HH]) "R_effective goes from first slice in capillary (slice [2]) one slice to another slice through and including the large cold volume."
q_dot_CH20%to80%= (T[BB] - T[HH1]) / R_eff_20%to80%
"Q_dot goes from the hot side (LHS) node of the hottest slice considered to the cold side (RHS) node of the coldest slice considered."
q_ON[3] = q_dot_CH20%to80%/A_c "Heat flux, q_dot_CH normalized for cross-sectional area"

".2 N to .9 N"

R_eff_20%to90% = sum(R[BB..II]) "R_effective goes from first slice in capillary (slice [2]) one slice to another slice through and including the large cold volume."
q_dot_CH20%to90%= (T[BB] - T[II1]) / R_eff_20%to90%
"Q_dot goes from the hot side (LHS) node of the hottest slice considered to the cold side (RHS) node of the coldest slice considered."
q_ON[13] = q_dot_CH20%to90%/A_c "Heat flux, q_dot_CH normalized for cross-sectional area"

".4 N to .6 N"

R_eff_40%to60% = sum(R[DD..FF])
q_dot_CH40%to60%= (T[DD] - T[FF1]) / R_eff_40%to60%
q_ON[4] = q_dot_CH40%to60%/A_c

".4 N to .9 N"

R_eff_40%to90% = sum(R[DD..II])
q_dot_CH40%to90%= (T[DD] - T[II1]) / R_eff_40%to90%
q_ON[12] = q_dot_CH40%to90%/A_c

".8N to .9N"

R_eff_80%to90% = sum(R[HH..II]) "R_effective goes from first slice in capillary (slice [2]) one slice to another slice through and including the large cold volume."
q_dot_CH80%to90%= (T[HH] - T[II1]) / R_eff_80%to90%
"Q_dot goes from the hot side (LHS) node of the hottest slice considered to the cold side (RHS) node of the coldest slice considered."
q_ON[8] = q_dot_CH80%to90%/A_c "Heat flux, q_dot_CH normalized for cross-sectional area"

".85N to .95N"

R_eff_85%to95% = sum(R[HH5..II5]) "R_effective goes from first slice in capillary (slice [2]) one slice to another slice through and including the large cold volume."
q_dot_CH85%to95%= (T[HH5] - T[II51]) / R_eff_85%to95% "Q_dot goes from the hot side (LHS) node of the hottest slice considered to the cold side (RHS) node of the coldest slice considered."
q_ON[7] = q_dot_CH85%to95%/A_c "Heat flux, q_dot_CH normalized for cross-sectional area"

".88N to .98N"

R_eff_88%to98% = sum(R[HH8..II8]) "R_effective goes from first slice in capillary (slice [2]) one slice to another slice through and including the large cold volume."
q_dot_CH88%to98%= (T[HH8] - T[II81]) / R_eff_88%to98% "Q_dot goes from the hot side (LHS) node of the hottest slice considered to the cold side (RHS) node of the coldest slice considered."
q_ON[6] = q_dot_CH88%to98%/A_c "Heat flux, q_dot_CH normalized for cross-sectional area"}

"reservoirs and columns, 'all' -- this includes all slices (both reservoirs plus capillary); ignore copper vessels containing helium as the helium conduction is so much larger than that of copper"

R_eff_all = **sum**(R[2..UU]) + R_small + R_large "R_effective goes from first slice in capillary (slice [2]) one slice to another slice through and including the large cold volume."
q_dot_CHall= (T[1] - T[N]) / R_eff_all "Q_dot goes from the hot side (LHS) node of the hottest slice considered to the cold side (RHS) node of the coldest slice considered."
q_ON_ALL = q_dot_CHall/A_c "Heat flux, q_dot_CH normalized for cross-sectional area"

APPENDIX B SOLIDWORKS DRAWINGS AND RENDERINGS

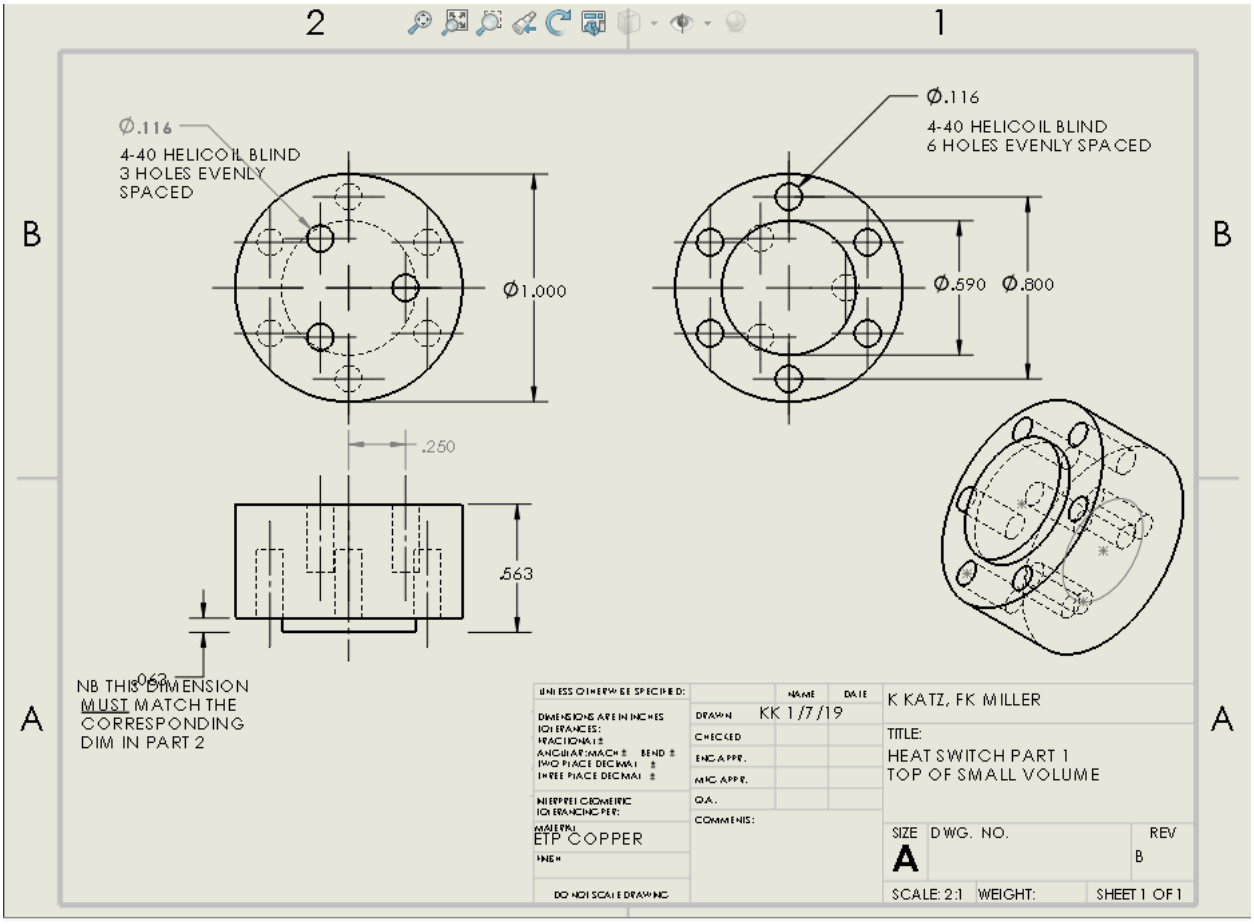

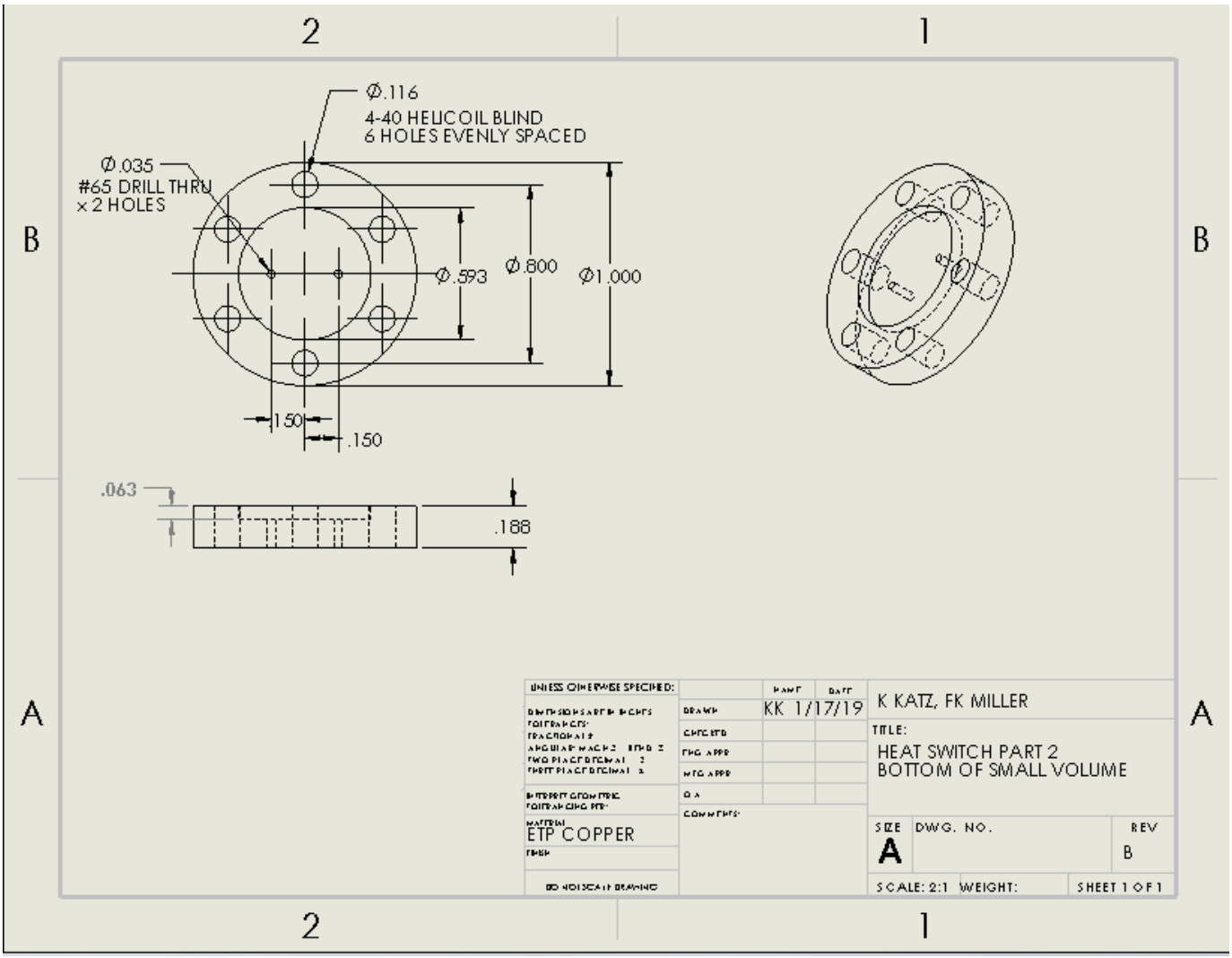
2
1
Ø.116
4-40 HELICOIL BLIND
6 HOLES EVENLY SPACED
Ø.035
#65 DRILL THRU
x 2 HOLES
Ø.593
Ø.800
Ø1.000
.150
.150
.063
.188
B
A
UNLESS OTHERWISE SPECIFIED:
NAME
DATE
DRAWN
KK 1/17/19
CHECKED
ENG APPR
MFG APPR
Q.A
COMMENTS:
MATERIAL
ETP COPPER
FINISH
DO NOT SCALE DRAWING
K KATZ, FK MILLER
TITLE:
HEAT SWITCH PART 2
BOTTOM OF SMALL VOLUME
SIZE
A
DWG. NO.
REV
B
SCALE: 2:1
WEIGHT:
SHEET 1 OF 1

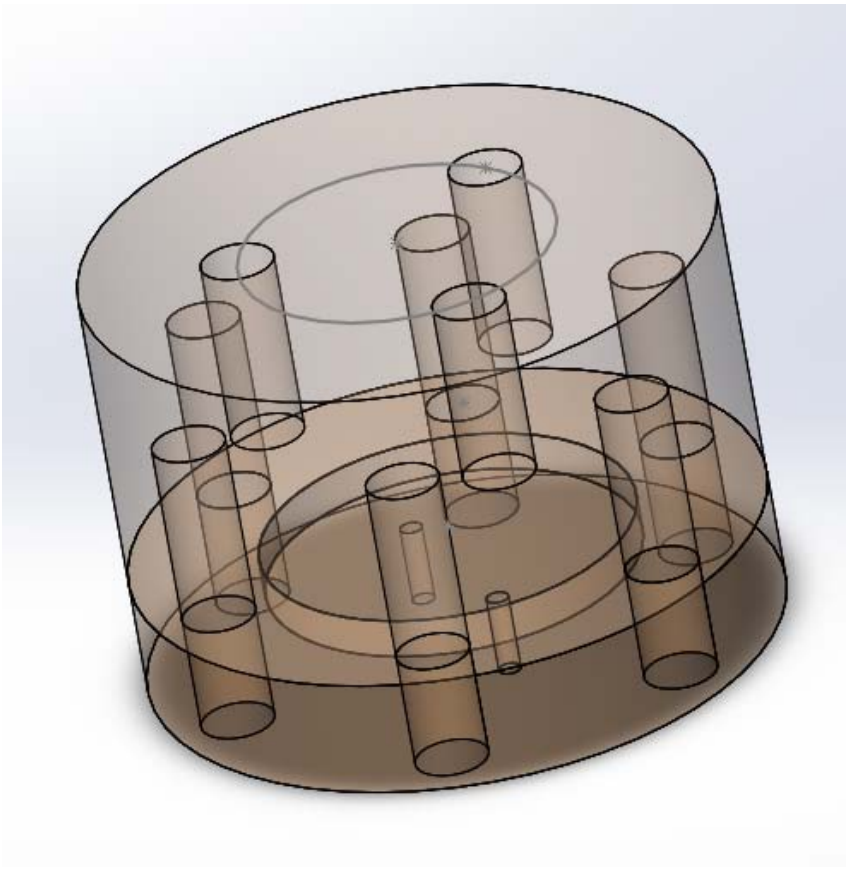

Part 1 is inserted into part 2. When the 6 screws joining them are tightened a feeler gauge is used to ensure that there is a space of .004” between them. This .004” space is the small end volume. The two steel capillaries enter the chamber through the two small holes at the bottom of this image.

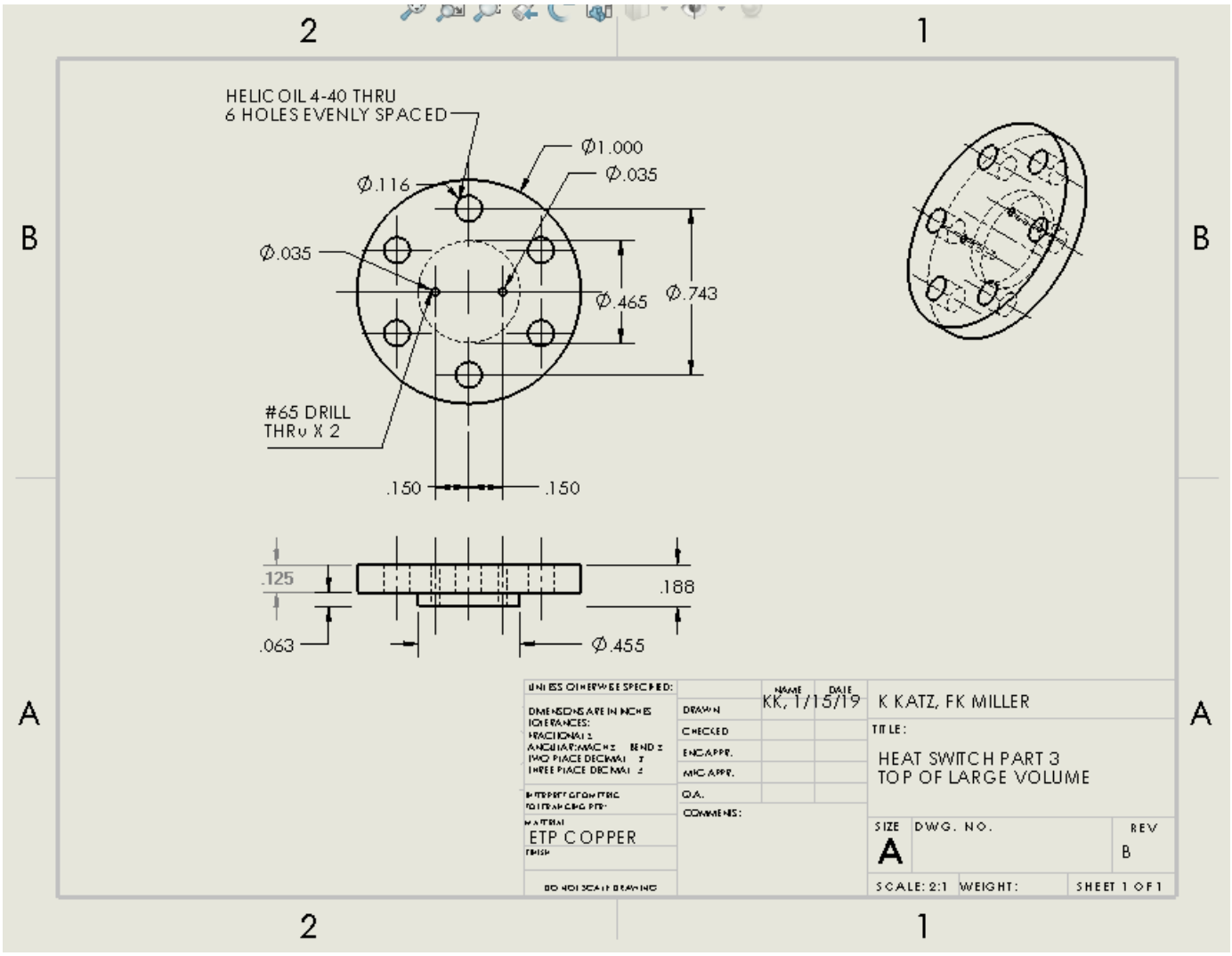
2
1
B
A
HELIC OIL 4-40 THRU
6 HOLES EVENLY SPACED
Ø1.000
Ø.035
Ø.116
Ø.035
Ø.465
Ø.743
#65 DRILL
THRU X 2
.150
.150
.125
.188
.063
Ø.455
UNLESS OTHERWISE SPECIFIED:
DIMENSIONS ARE IN INCHES
TOLERANCES:
FRACTIONAL ±
ANGULAR: MACH ± BEND ±
TWO PLACE DECIMAL ±
THREE PLACE DECIMAL ±
INTERPRET GEOMETRIC
TOLERANCING PER:
MATERIAL
ETP COPPER
FINISH
DO NOT SCALE DRAWING
NAME
DATE
DRAWN
KK, 1/15/19
CHECKED
ENG APPR.
MFG APPR.
Q.A.
COMMENTS:
K KATZ, FK MILLER
TITLE:
HEAT SWITCH PART 3
TOP OF LARGE VOLUME
SIZE
A
DWG. NO.
REV
B
SCALE: 2:1
WEIGHT:
SHEET 1 OF 1

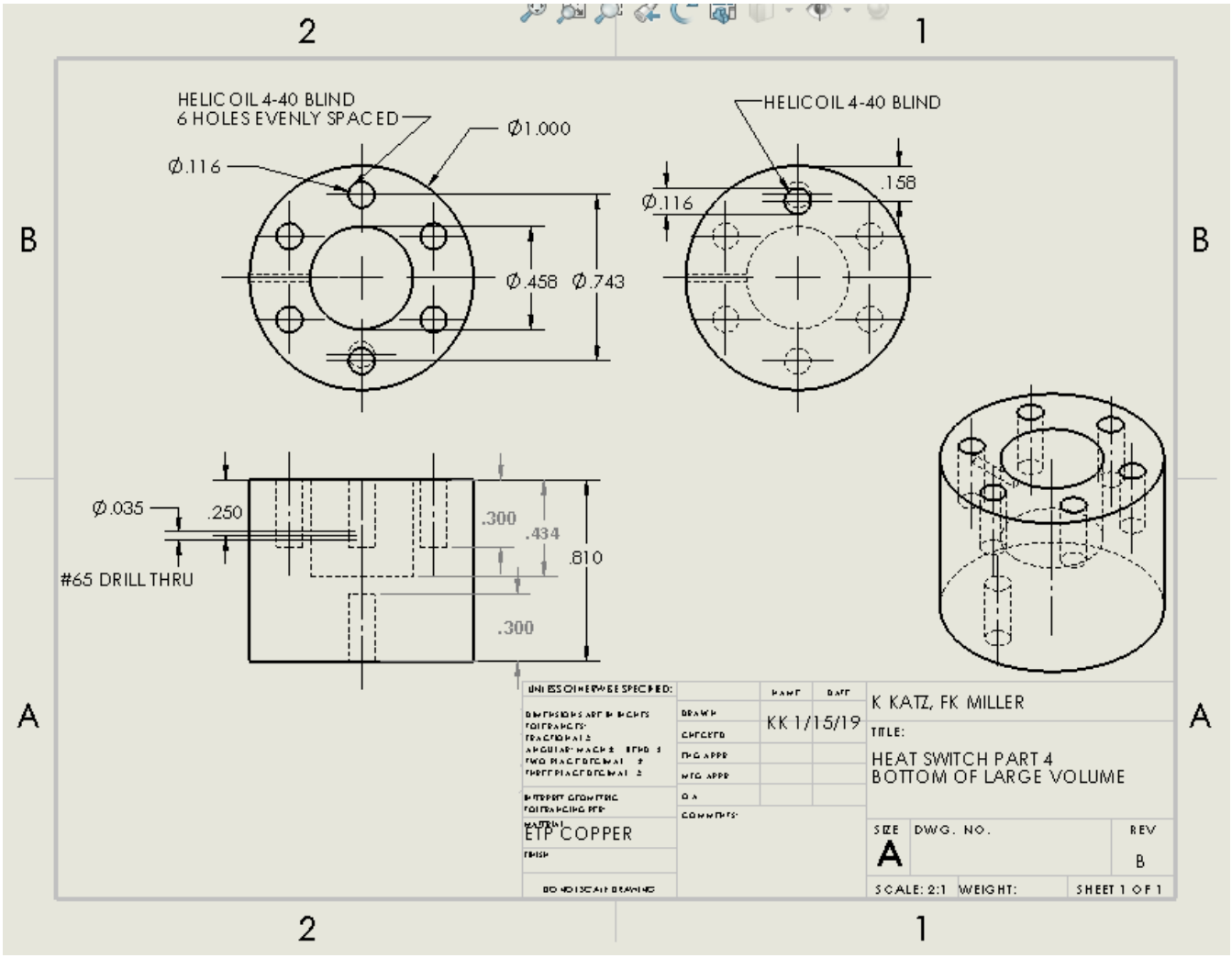
2
1
B
A
HELICOIL 4-40 BLIND
6 HOLES EVENLY SPACED
Ø1.000
Ø.116
Ø.458
Ø.743
HELICOIL 4-40 BLIND
Ø.116
.158
Ø.035
.250
#65 DRILL THRU
.300
.434
.810
.300
UNLESS OTHERWISE SPECIFIED:
NAME
DATE
DRAWN
KK 1/15/19
CHECKED
ENG APPR
MFG APPR
Q.A
COMMENTS:
MATERIAL
ETP COPPER
FINISH
DO NOT SCALE DRAWING
K KATZ, FK MILLER
TITLE:
HEAT SWITCH PART 4
BOTTOM OF LARGE VOLUME
SIZE
A
DWG. NO.
REV
B
SCALE: 2:1
WEIGHT:
SHEET 1 OF 1

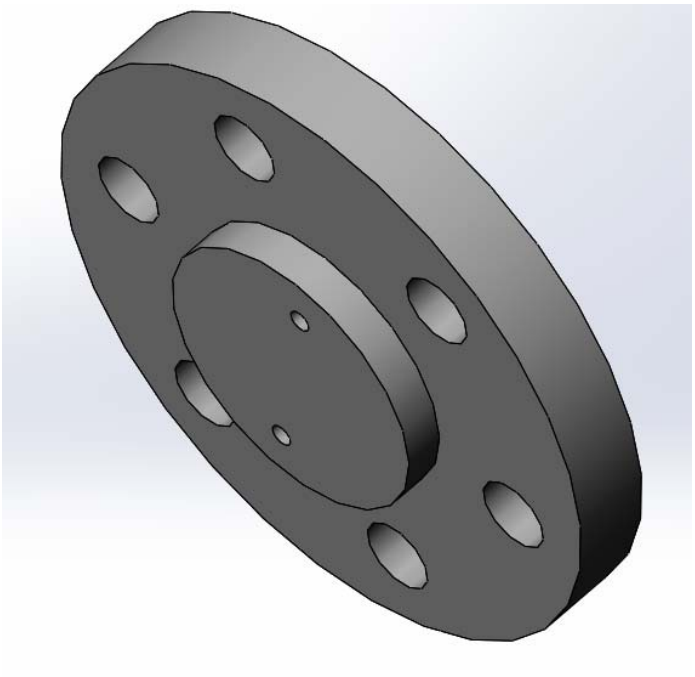

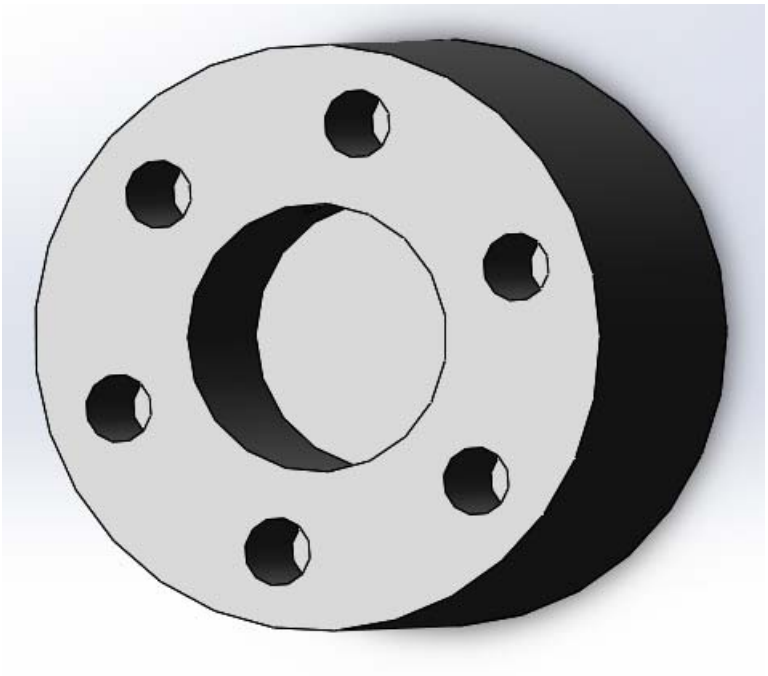

Part 3 (above) is inserted into Part 4 (below). The enclosed space is the large volume. The fill line comes through Part 4 to enter the large volume. The two steel capillaries enter the large volume through the two small holes in Part 3.